UNIVERSIDADE FEDERAL DO RIO GRANDE DO SUL
INSTITUTO DE FÍSICA

PROPRIEDADES TOPOLÓGICAS DE SISTEMAS CONDENSADOS DA CLASSE BDI

PEDRO BARBISAN WIDNICZCK

Dissertação apresentada como requisito parcial para a obtenção do título de Mestre em Física.
Orientador: Prof. Dr. Gerardo Guido Martínez Pino

PORTO ALEGRE, RS
2023

UNIVERSIDADE FEDERAL DO RIO GRANDE DO SUL
INSTITUTO DE FÍSICA

TOPOLOGICAL PROPERTIES OF BDI CLASS CONDENSED SYSTEMS

PEDRO BARBISAN WIDNICZCK

Dissertation presented in partial fulfilment of the requirements for the degree Master of Physics.
Advisor: Prof. Dr. Gerardo Guido Martínez Pino

PORTO ALEGRE, RS
2023

Agradecimento

Primeiramente gostaria de agradecer a minha família, mãe, pai, avós, avôs, tia, tio, primas, irmã; todos que participam ativamente da minha vida cotidiana, pois desde sempre me apoiaram a seguir a complicada 'vida acadêmica'. Mesmo com os muitos comentários do tipo "é dificil né", "Quando vai ter um emprego de verdade?" ou "Tem concurso chegando aí," nunca deixaram de apreciar meu interesse pelas ciências (mais específicamente pela física).

Seguindo na minha esfera pessoal, gostaria de agradecer aos meus amigos, aqueles que hoje em dia já não são tão próximos (como Bruno Maciel, João e outros), até os mais próximos como o recente mestre (apenas no que diz respeito ao mérito acadêmico, já que se olhar o padel, é frustração certa) Gustavo, Julio, Eduardo. Gostaria em especial de agradecer à Paula, pois durante todo o período do mestrado muitos foram os momentos de frustração, estresse e descontentamento.

Gostaria de agradecer aos professores do Instituto de Física, desde os que tive aula na graduação e também àqueles professores que se desdobraram durante o período da pandemia, quando terminei a graduação e iniciei meus estudos no mestrado. Além dos professores gostaria de agradecer ao meu orientador, Gerardo, primeiramente pelas discussões, conselhos e aulas durante todo período do curso.

Finalmente gostaria de agradecer ao CNPq pelo apoio financeiro para o desenvolvimento dessa dissertação.

Abstract

In this dissertation, topological properties of quantum mechanical non-interacting condensed matter systems are reviewed. Firstly, the formalism of the topological band theory is developed, by defining one of the principal quantities of topological quantum systems, the Berry geometric phase, to explore the geometrical features of such phase, like the Berry connection and curvature, with emphasis in two levels systems. In the next chapter, one of the simplest models of one dimensional topological insulators is explored, the Su-Schrieffer-Heeger (SSH) model. The non-unitary symmetry conditions are introduced and other models, derived from symmetry breaking processes, are presented. In the last chapter, the 1-D Kitaev p-wave superconductor model is studied and extended for long-range interactions (keeping the imposed symmetries valid). Topological properties are calculated. Topological phase diagrams are obtained, edge modes and fermion parity properties are discussed. **Key Words: Kitaev Chain, Majorana Fermions, Superconductivity, Long-Range, Topological Insulators, SSH Model**

Resumo

Na presente dissertação, as propriedades topológicas de sistemas quânticos da matéria condensada são revistas. Inicialmente, o formalismo da teoria de bandas topológicas é desenvolvido, desde a definição de uma das principais quantidades dos sistemas topológicos quânticos, a fase geométrica de Berry, até explorar quantidades geométricas derivadas, como a conexão e a curvatura de Berry, com ênfase em sistemas de dois níveis. Logo depois, no seguinte capítulo é descrito um dos mais simples modelos de isolantes topológicos em uma dimensão, o modelo Su-Schrieffer-Heeger (SSH). As condições sobre simetrias não-unitárias são introduzidas e outros modelos, derivados do procedimento de quebra dessas simetrias, são apresentados. No último capítulo, o modelo de Kitaev supercondutor 1-D de onda-p é estudado e extendido para interações de longo alcance (mantendo as simetrias impostas intactas). Diagramas de fases topologicas são obtidos, modos de Majorana nas bordas e as propriedades da paridade fermiônica são discutidos. **Palavras Chave: Cadeia de Kitaev, Férmions de Majorana, Supercondutividade, Longo Alcance, Isolantes topologicos, Modelo SSH**

Contents

List of Figures

Chapter 1

Introduction

Topological properties play a central role in condensed matter physics nowadays. This topological nature of effects was first obtained by Klaus von Klitzing (2), for the discovery of the integer quantum Hall effect. For this discovery, he won the 1985 Nobel Prize in Physics.

Since it was introduced, the topological behavior of matter has increased its importance. These properties are relevant to the description of superfluidity of a two-dimensional ^{3}He layer (3), semi-metals (4, 5), topological insulators, with a major contribution of all kinds of quantum Hall effects (integer, anomalous (6), fractional (7) and spin (8)) and for topological superconductivity, introduced later by Kitaev (9). All these systems are described by *symmetry-protected topological phases*. In an understandable language, this means that supposing that a system possesses some specific symmetry, say by tuning in the parameters, there will be novel phenomena, that is not predicted by one of the most successful theories in condensed matter physics, known as Landau Theory of symmetry breaking. The described phenomena are interesting in quantum systems and phases of matter when are quantized.

For insulating and superconductor systems, the topological behavior assures the presence of non-local states, localized at the edges, which cannot be 'deformed' into trivial ones. The occurrence of such behavior happens when translational symmetry, the symmetry that represents only the bulk properties of any system, is broken (some information of topological transitions can be achieved looking only in the translational invariant system, this encoded information computed only from bulk information is called *Bulk-Edge Correspondence* (10, 11)). Broken translational invariance is the same

as disregarding periodic boundary conditions, or putting disorder into the system, respecting symmetry conditions necessary to the existence of topological phases.

The emergence of non-local edge states showed us the necessity of reviewing transport properties in condensed matter. The polarization theory, for instance, needed to be well defined for a periodic system (12, 13). One could naively imagine that, since the periodicity is present, the eigenfunctions are delocalized, and the polarization would not be well defined. Nonetheless, the topological properties (supposedly had no immediate relation) solve this problem.

Looking at the framework of topological systems, a class of quasi-particles is the Majorana fermions (14, 15). There is an ongoing debate concerning their experimental observation (for instance, see references (16, 17)) in one-dimensional spin-orbit coupled nanowires or magnetic sites embedded in superconductors. These fermionic quasi-particles exhibit non-abelian statistics, such that the Pauli Exclusion principle is violated. This feature in systems with dimensions above one indicates the realization of anyons (18, 19).

Majorana fermions-like excitations are expected to be of interest in quantum computers (20, 21, 22), since the ground state in the topological phase is protected by symmetries, indicating robustness against perturbations and operations (that do not break the symmetries). Unfortunately, the experimental realization is challenging (involves exotic superconductors), and the observation is even worse, many features of this class of excitations are currently unknown.

The main objectives of this dissertation are to understand and explore quantum phase transitions, topological properties, and phases in one-dimensional condensed systems. The specific goals of the work are to characterize in the Majorana basis, different topological phases (presented in works (23, 24, 25) for the Kitaev chain), explore edge modes in finite chains, and clarify some fermion parity relations, similarly as done by (26, 27), on the wave function with topological properties for long-range (28) and infinite range (29, 30, 31, 32, 33) extensions of the Kitaev chain.

Topological properties of one-dimensional condensed matter systems are reviewed in this work. The second chapter develops the formalism of the topologi-

cal band theory, showing the hallmark quantized quantity, the Berry/Zak phase. In the third chapter one of the simplest one-dimensional topological insulator models, the SSH model, is explored. In the fourth chapter, the Kitaev p-wave superconductor model, supporting Majorana fermions, is studied and extended for long-range interactions, keeping the symmetries intact and looking for information about such Majoranas. In finite chains, the boundary modes are extensively explored, and approximated wave solutions are calculated, following the discussion of parity and average position properties.

Chapter 2

Topological Band Theory

One of the principal aspects of the topological band theory is the Berry phase. The Berry phase was first observed in another context, explicitly unrelated to Bloch electrons, but to the adiabatic transport of particles in quasi-static fields. This geometric phase describes how the wave function can be varied other than a dynamic effect. Zak realised that adiabatic effects could be applied to Bloch systems, in these cases, the crystalline momentum k is varied over closed circuits (in the band or in the Fermi surface), slowly varying some parameter (usually the electric field) to yield the same topological features. We turn back to this important aspect. For clarity, this chapter is based on references (1, 34, 35, 36, 37).

2.1 The Berry Phase

Consider a general time-dependent hamiltonian

$$\mathcal{H} = \mathcal{H}(\mathbf{R}), \tag{2.1}$$

over the parameters $\mathbf{R} = (R_1, R_2, \ldots, R_n)$, where each $R_i = R_i(t)$ is time dependent. It is of interest to know the solutions of the adiabatic system, i.e. knowing how a system that depends on $\mathbf{R}(t)$ evolves when changing the parameters slowly (relative to the energy scale of the system) over a path $\mathcal{C}$ of the parameter space (closed or open curves can be considered). This can be done introducing an instantaneous orthonormal basis of the eigenstates $\{|n(\mathbf{R})\rangle\}$ of the Hamiltonian family $\mathcal{H}(\mathbf{R})$ for each point of the space. Therefore, the Schrödinger equation

$$\mathcal{H}\,|n(\mathbf{R})\rangle = E(\mathbf{R})\,|n(\mathbf{R})\rangle\,, \tag{2.2}$$

determines the eigenstates of the Hamiltonian (up to a constant phase). This constant phase factor is a degree of freedom (in the case of degenerate states can be a matrix). This degree of freedom can depend on the parameters $\mathbf{R}$, which must commute with the Hamiltonian. Choosing a phase (fixing the gauge) removes its arbitrariness. A natural choice consists in requiring that the phase of each eigenstate $|n(\mathbf{R})\rangle$ is smooth and uniquely determined over the path $\mathcal{C}$ in the parameter space.

It is of interest to analyse the phase of a pure state [1] wave function, with initial condition $|n(\mathbf{R}(0))\rangle$, searching to determine the properties of the adiabatic evolving states following $\mathbf{R}(t)$ over the path $\mathcal{C}$. By the adiabatic theorem, a system prepared at $|n(\mathbf{R}(0))\rangle$ will evolve according to the Hamiltonian $\mathcal{H}(\mathbf{R})$ and remains as an instantaneous eigenstate throughout the whole process.

The phase factor presently is, in reality, the only available degree of freedom. Over the adiabatic evolution of the system, the phase θ of the state

$$|\psi(t)\rangle = e^{-i\theta(t)}\,|n(\mathbf{R}(t))\rangle\,, \tag{2.3}$$

is not necessarily null. As a matter of fact, this phase must not be considered null, since it must contain minimally a dynamic phase factor, related to the eigenvalues of the state. Beyond, there must be a geometric term - the Berry phase, introduced in (34). A geometric term may be visualized by the time evolution of the system, given by

$$\mathcal{H}(\mathbf{R}(t))\,|\psi(t)\rangle = i\hbar\frac{\mathrm{d}}{\mathrm{d}t}|\psi(t)\rangle, \tag{2.4}$$

where $\mathbf{R}(t)$ varies slowly, keeping $\mathcal{H}[\mathbf{R}(t)] = E_n(\mathbf{R}(t))$ eigen-energies, implying the equation

$$\begin{aligned} E_n(\mathbf{R}(t))\,|\psi(t)\rangle &= i\hbar e^{-i\theta(t)}\left[\left(-i\frac{\mathrm{d}\theta(t)}{\mathrm{d}t}\,|n(\mathbf{R})\rangle\right) + \frac{\mathrm{d}}{\mathrm{d}t}|n(\mathbf{R}(t))\rangle\right], \\ &= \hbar e^{-i\theta(t)}\left(\frac{\mathrm{d}\theta}{\mathrm{d}t}\,|n(\mathbf{R})\rangle + i\frac{\mathrm{d}}{\mathrm{d}t}|n(\mathbf{R})\rangle\right). \end{aligned} \tag{2.5}$$

[1] The preparation of the state in a pure state is crucial, since the Berry phase is only defined in such states.

Multiplying to the left in both sides by $\langle n(\mathbf{R}(t))|$ and assuming that the state is normalized (namely, $\langle n(\mathbf{R}(t))|n(\mathbf{R}(t))\rangle = 1$) it is obtained

$$\begin{aligned} E_n(\mathbf{R}(t))e^{-i\theta(t)} \langle n(\mathbf{R}(t))|n(\mathbf{R}(t))\rangle &= E_n(\mathbf{R}(t))e^{-i\theta(t)} \\ E_n(\mathbf{R}(t))e^{-i\theta(t)} &= \hbar e^{-i\theta(t)} \left(\frac{\mathrm{d}\theta}{\mathrm{d}t} + i \langle n(\mathbf{R}(t))| \frac{\mathrm{d}}{\mathrm{d}t} |n(\mathbf{R}(t))\rangle \right); \quad (2.6) \\ E_n(\mathbf{R}(t)) - i\hbar \langle n(\mathbf{R}(t))| \frac{\mathrm{d}}{\mathrm{d}t} |n(\mathbf{R}(t))\rangle &= \hbar \frac{\mathrm{d}\theta}{\mathrm{d}t}. \end{aligned}$$

The phase $\theta(t)$ is then given by the solution

$$\theta(t) = \frac{1}{\hbar} \int_0^t E_n(\mathbf{R}(\tau))d\tau - i \int_0^t \langle n(\mathbf{R}(\tau))| \frac{\mathrm{d}}{\mathrm{d}\tau} |n(\mathbf{R}(\tau))\rangle d\tau. \quad (2.7)$$

The first part of $\theta(t)$ is constituted simply by the conventional dynamical part, coming from the Hamiltonian. The second part of $\theta(t)$ is called the Berry Phase. Writing now

$$|\psi(t)\rangle = \exp\left\{ \frac{1}{\hbar} \int_0^t E_n(\mathbf{R}(\tau))d\tau \right\} \exp\{-\gamma_n\} |n(\mathbf{R}(t))\rangle, \quad (2.8)$$

and the Berry phase γ_n is

$$\gamma_n = i \int_0^t \langle n(\mathbf{R}(\tau))| \frac{\mathrm{d}}{\mathrm{d}\tau} |n(\mathbf{R}(\tau))\rangle d\tau, \quad (2.9)$$

the Berry phase arises from the distinction of the eigenkets $|n(\mathbf{R}(t))\rangle$ from $|n(\mathbf{R}(t+dt))\rangle$, which has a slightly different direction in the Hilbert space. Time can be explicitly removed from the Berry phase and the only (explicit) dependence comes from the parameters. Such a procedure can be done applying the chain rule

$$\begin{aligned} \gamma_n &= i \int_0^t \langle n(\mathbf{R}(\tau))| \frac{\mathrm{d}\mathbf{R}}{\mathrm{d}\tau} \frac{\partial}{\partial \mathbf{R}} \left(|n(\mathbf{R}(\tau))\rangle \right) d\tau, \\ &= i \oint_{\mathcal{C}} \langle n(\mathbf{R})| \nabla_{\mathbf{R}} |n(\mathbf{R})\rangle \, d\mathbf{R}. \quad (2.10) \end{aligned}$$

By analogy to the transport of the electromagnetic field, the last equation introduces a new vectorial function, called Berry Connection (or Berry Potential vector)

$$\mathbf{A}_n(\mathbf{R}) = i \langle n(\mathbf{R})| \frac{\partial}{\partial \mathbf{R}} |n(\mathbf{R})\rangle; \quad (2.11)$$

$$\gamma_n = \int_{\mathcal{C}} \mathbf{A}_n(\mathbf{R}) \cdot d\mathbf{R}. \quad (2.12)$$

The Berry phase γ_n is a real quantity, otherwise would it be a "Berry decaying". It happens because the Berry Connection is, by itself a purely imaginary quantity

$$\langle n(\mathbf{R})| \nabla_{\mathbf{R}} |n(\mathbf{R})\rangle = -\langle n(\mathbf{R})| \nabla_{\mathbf{R}} |n(\mathbf{R})\rangle^* , \tag{2.13}$$

therefore, the phase can be written as

$$\gamma_n = -\text{Im} \int_{\mathcal{C}} \langle n(\mathbf{R})| \nabla_{\mathbf{R}} |n(\mathbf{R})\rangle \cdot d\mathbf{R}. \tag{2.14}$$

The Berry potential vector $\mathbf{A}_n(\mathbf{R})$ is obviously dependent of the gauge. A general transformation of the gauge is

$$\mathbf{A}(\mathbf{R}) \rightarrow e^{i\zeta(\mathbf{R})}\mathbf{A}(\mathbf{R}), \tag{2.15}$$

where $\zeta(\mathbf{R})$ is a smooth and singled-valued gauge. The vector transforms according to

$$\mathbf{A}_n(\mathbf{R}) \rightarrow \mathbf{A}_n(\mathbf{R}) - \frac{\partial \zeta}{\partial \mathbf{R}}, \tag{2.16}$$

and γ_n is altered by a factor

$$\int_{\mathcal{C}} \frac{\partial \zeta}{\partial \mathbf{R}} d\mathbf{R} = \zeta(\mathbf{R}(t)) - \zeta(\mathbf{R}(0)), \tag{2.17}$$

being t a large time, and $\mathcal{C}$ concluded slowly. Previously to the work of Berry (34), it was speculated that for a particular interesting choice of gauge ζ, the phase could be nulled, therefore of no interest [2].

Considering closed paths $\mathcal{C}$ in the parameter space, the configurations should be identical $\mathbf{R}(t) = \mathbf{R}(0)$. On those trajectories, the fact of choosing a uniquely defined eigenstates basis, implies that the eigenstates should hold the equation $|n(\mathbf{R}(0))\rangle = |n(\mathbf{R}(t))\rangle$. The gauge transformations must always follow this property, i.e.

$$\exp\{i\zeta(\mathbf{R}(\mathbf{0}))\} |n(\mathbf{R}(0))\rangle = \exp\{i\zeta(\mathbf{R}(\mathbf{t}))\} |n(\mathbf{R}(t))\rangle = \exp\{i\zeta(\mathbf{R}(\mathbf{0}))\} |n(\mathbf{R}(t))\rangle , \tag{2.18}$$

respecting the following condition

[2] This statement is clearly wrong.

$$\zeta(\mathbf{R}(t)) - \zeta(\mathbf{R}(0)) = 2\pi m, \tag{2.19}$$

where m is an integer. Consequently, over a closed path, the Berry Phase is only null if it is an integer.

Closed trajectories are of true interest. Considering that the parameter space is three dimensional $\mathbf{R}$ is $\mathbf{R} = (R_1, R_2, R_3)$, the Berry phase in these paths is gauge invariant, independent of the form that $\mathbf{R}$ behaves in time. In a closed path, the Stokes Theorem implies that

$$\begin{aligned}\gamma_n &= -\text{Im}\int (\nabla \times \langle n(\mathbf{R})| \nabla |n(\mathbf{R})\rangle) \cdot d\mathbf{S} = -\text{Im}\int \epsilon_{ijk}\nabla_j \langle n(\mathbf{R})| \nabla_k |n(\mathbf{R})\rangle \,, \\ &= -\text{Im}\int (\langle \nabla n(\mathbf{R})| \times |\nabla n(\mathbf{R})\rangle) \cdot d\mathbf{S}, \end{aligned} \tag{2.20}$$

and now the quantities $\langle \nabla n(\mathbf{R})| \times |\nabla n(\mathbf{R})\rangle$ defines the Berry Curvature ${F_{jk}}^3$. More precisely

$$F^n_{jk} = \langle \nabla_j n(\mathbf{R}) | \nabla_k n(\mathbf{R})\rangle - \langle \nabla_k n(\mathbf{R}) | \nabla_j n(\mathbf{R})\rangle \,, \tag{2.21}$$

such that

$$\gamma_n = \text{Im}\int \epsilon_{ijk} F_{jk} dS_i, \tag{2.22}$$

the Berry Curvature $\mathbf{F}^n$ is obtained via Berry Potential Vector, through the contraction with the Levi-Civita ϵ_{ijk} (similar to the magnetic field, obtained by the rotational of the Potential Vector).

2.2 Gauge Invariance

Now, wishing to obtain specific relations about the Berry phase, i.e. the interest now is how to calculate it in practical situations. From what is known, the computation of the phase is not trivial, containing derivatives of the eigenstates.

To obtain a formula that shows the gauge invariance, first it is interesting to invoke the closure relation (for each point of the parameter space), in this way,

[3] Known as Berry Field, as well.

$$\epsilon_{ijk} \langle \nabla_j n(\mathbf{R}) | \nabla_k n(\mathbf{R}) \rangle = \epsilon_{ijk} \left(\langle \nabla_j n(\mathbf{R}) | n \rangle \langle n | \nabla_k n(\mathbf{R}) \rangle + \sum_{n \neq m} \langle \nabla_j n | m \rangle \langle m | \nabla_k n \rangle \right), \tag{2.23}$$

the first term of the sum is irrelevant, since $\langle \nabla_j n(\mathbf{R}) | n \rangle$ and $\langle n | n(\nabla_k \mathbf{R}) \rangle$ are purely imaginary (their product is real). Now, the Berry phase is therefore

$$\gamma_n = \mathrm{Im} \iint dS_i \sum_{m \neq n} \langle \nabla_j n(\mathbf{R}) | m \rangle \langle m | \nabla_k n(\mathbf{R}) \rangle , \tag{2.24}$$

the term $\langle m | \nabla n \rangle$ can be decomposed when multiplied by E_n, removing the derivative from the eigenstate

$$E_n \langle \nabla n | = E_n \nabla \langle n | = \nabla E_n \langle n | = \nabla (\mathcal{H} \langle n |) = (\nabla \mathcal{H}) \langle n | + \mathcal{H} \nabla \langle n | ; \tag{2.25}$$

$$\langle m | \nabla n \rangle = \frac{1}{E_n - E_m} \langle m | \nabla \mathcal{H} | n \rangle , \tag{2.26}$$

similarly, $\langle \nabla n | m \rangle = (E_n - E_m)^{-1} \langle n | \nabla \mathcal{H} | m \rangle$ and the Berry phase is computed through a modified version of the Berry Curvature

$$\gamma_n(\mathcal{C}) = - \iint_{\mathcal{C}} \mathrm{Im} \sum_{m \neq n} \frac{\langle n(\mathbf{R}) | (\nabla_{\mathbf{R}} \mathcal{H}) | m(\mathbf{R}) \rangle \times \langle m(\mathbf{R}) | (\nabla_{\mathbf{R}} \mathcal{H}) | n(\mathbf{R}) \rangle}{(E_m(\mathbf{R}) - E_n(\mathbf{R}))^2} \cdot d\mathbf{S}. \tag{2.27}$$

This final expression of γ_n is gauge independent. It has the advantage over other expressions independent of gauge, since it doesn't depend on the phases of $|n\rangle$ and can be calculated over any gauge choice. The derivatives are applied in the Hamiltonian, not in the states, so there is no need to find smooth and single-valued states and gauges. This way, the Berry curvature can be thought of as the result of the interaction of $|n\rangle$ with other levels $|m\rangle$ over an adiabatic interaction. Summing all phases of all occupied states, the result must (for non degenerate energies) be zero.

An important application of the Berry phase is the classification of degeneracy. Consider two states $|\psi\rangle$ of a system, with energies $E_+(\mathbf{R})$ greater than $E_-(\mathbf{R})$, while at $\mathbf{R} = \mathbf{R}^*$, the energies are degenerate. In this context, the Hamiltonian can be linearized near $\mathbf{R}^*$

$$\mathcal{H}_L(\mathbf{R}) \approx \mathcal{H}(\mathbf{R}^*) + (\mathbf{R} - \mathbf{R}^*) \cdot \nabla \mathcal{H}(\mathbf{R}^*), \tag{2.28}$$

and the Berry Curvature, from the definition 2.27 implies

$$\mathbf{F}^{+}(\mathbf{R}) = \mathrm{Im}\frac{1}{(E_{+}(\mathbf{R}) - E_{-}(\mathbf{R}))^{2}} \langle +(\mathbf{R})| \left(\nabla \mathcal{H}(\mathbf{R}^{*})\right) |-(\mathbf{R})\rangle \times \langle -(\mathbf{R})| \left(\nabla \mathcal{H}(\mathbf{R}^{*})\right) |+(\mathbf{R})\rangle , \tag{2.29}$$

by the exchanges of $|+(\mathbf{R})\rangle , |-(\mathbf{R})\rangle \rightarrow |-(\mathbf{R})\rangle , |+(\mathbf{R})\rangle$, the Berry Curvature and phase are known $\mathbf{F}^{+} = -\mathbf{F}^{-}$ and $\gamma_{+} = -\gamma_{-}$ (because the sum of the levels gets null). Looking at the denominator of the equation above, at the degeneracy point $\mathbf{R}^{*}$, since $\mathbf{F}_{\pm}(\mathbf{R})$ only involves two terms, it corresponds to a monopole in parameter space. This way, considering the cases of E_n single degenerate, the Berry phase is abelian and only two levels are relevant for the analysis. We come to this below.

2.3 Two Levels System

The generic form of a two levels Hamiltonian is

$$\mathcal{H} = \epsilon(\mathbf{R})\sigma_0 + \mathbf{d}(\mathbf{R}) \cdot \boldsymbol{\sigma}, \tag{2.30}$$

where σ_i are the Pauli matrices and $\mathbf{d}(\mathbf{R})$ is a vector depending on parameters $\mathbf{R}$. This model describes many interesting systems in condensed matter (like graphene, spin-orbit coupled systems, Bogoliubov quasi-particles, etc). The Hamiltonian is rewritten as

$$\begin{aligned} \mathcal{H} &= \epsilon\sigma_0 + d_1\sigma_1 + d_2\sigma_2 + d_3\sigma_3; \\ &= \begin{pmatrix} \epsilon & 0 \\ 0 & \epsilon \end{pmatrix} + \begin{pmatrix} 0 & d_1 \\ d_1 & 0 \end{pmatrix} + \begin{pmatrix} 0 & -id_2 \\ id_2 & 0 \end{pmatrix} + \begin{pmatrix} d_3 & 0 \\ 0 & -d_3 \end{pmatrix}; \\ &= \begin{pmatrix} \epsilon + d_3 & d_1 - id_2 \\ d_1 + id_2 & \epsilon - d_3 \end{pmatrix} = \begin{pmatrix} a & b \\ c & d \end{pmatrix}. \end{aligned} \tag{2.31}$$

Calculating now the eigenvalues, the characteristic equation is

$$E_{\pm}(\mathbf{R}) = \epsilon(\mathbf{R}) \pm \sqrt{\mathbf{d} \cdot \mathbf{d}}, \tag{2.32}$$

with $\epsilon(\mathbf{R})$ an additive constant. The vector $\mathbf{d}(\mathbf{R})$ can be parameterized in spherical coordinates (d, θ, ϕ), as

$$\mathbf{d} = \begin{pmatrix} d\sin\theta\cos\phi \\ d\sin\theta\sin\phi \\ d\cos\theta \end{pmatrix}. \tag{2.33}$$

Considering a case of $\epsilon = 0$, then $E_\pm = \pm\sqrt{\mathbf{d}\cdot\mathbf{d}} = \pm d$, the eigenvectors are obtained by the eigenvalue equation

$$\begin{pmatrix} d_3 - E_\pm & d_1 - id_2 \\ d_1 + id_2 & -d_3 - E_\pm \end{pmatrix} = \begin{pmatrix} d_3 \mp \sqrt{\mathbf{d}\cdot\mathbf{d}} & d_1 - id_2 \\ d_1 + id_2 & -d_3 \mp \sqrt{\mathbf{d}\cdot\mathbf{d}} \end{pmatrix};$$
$$\begin{pmatrix} \cos\theta \mp 1 & \sin\theta\cos\phi - i\sin\theta\sin\phi \\ \sin\theta\cos\phi + i\sin\theta\sin\phi & -\cos\theta \mp 1 \end{pmatrix} \sim \begin{pmatrix} \cos\theta \mp 1/2 & e^{-i\phi}\sin\theta \\ e^{i\phi}\sin\theta & -\cos\theta \mp 1/2 \end{pmatrix}, \tag{2.34}$$

for the eigenvalue E_+, the eigenvector $|+\rangle = (a_1, a_2)^T$ is

$$\begin{pmatrix} \cos\theta - 1 & e^{-i\phi}\sin\theta \\ e^{i\phi}\sin\theta & -(\cos\theta + 1) \end{pmatrix} \sim \begin{pmatrix} -2\sin^2\theta/2 & e^{-i\phi}\sin\theta \\ e^{i\phi}\sin\theta & -2\cos^2\theta/2 \end{pmatrix}; \tag{2.35}$$

$$a_1 = \frac{e^{-i\phi}}{2}\frac{\sin\theta}{\sin^2\theta/2}a_2; \tag{2.36}$$

$$a_2 = \frac{e^{i\phi}}{2}\frac{\sin\theta}{\cos^2\theta/2}a_1, \tag{2.37}$$

choosing $a_2 = \sin\theta/2$, so $a_1 = (e^{-i\phi}\cos\theta/2)$. The resulting eigenstate is expressed by

$$|+(\mathbf{R})\rangle = \begin{pmatrix} e^{-i\phi}\cos\frac{\theta}{2} \\ \sin\frac{\theta}{2} \end{pmatrix}. \tag{2.38}$$

Analogously, the eigenstate $|-\rangle = (b_1, b_2)^T$ of the eigenenergy E_- is

$$|-(\mathbf{R})\rangle = \begin{pmatrix} e^{-i\phi}\sin\frac{\theta}{2} \\ -\cos\frac{\theta}{2} \end{pmatrix}. \tag{2.39}$$

remembering that this basis is orthonormal, meaning $\langle\pm|\pm\rangle = 1$ and $\langle\pm|\mp\rangle = 0$.

By the gauge invariance, and disregarding the component A_d of the vector potential, remains the necessity of calculating A_ϕ, A_θ represented by

$$A^n_\theta = i\left\langle n(\mathbf{R})\right| \frac{\partial}{\partial\theta}\left(\left|n(\mathbf{R})\right\rangle\right), \qquad A^n_\phi = i\left\langle n(\mathbf{R})\right| \frac{\partial}{\partial\phi}\left(\left|n(\mathbf{R})\right\rangle\right), \tag{2.40}$$

taking the state $|-\rangle$, the Berry potential vector component A^-_θ is

$$
\begin{aligned}
A_\theta^- &= i \begin{pmatrix} e^{i\phi}\sin\frac{\theta}{2} & -\cos\frac{\theta}{2} \end{pmatrix} \partial_\theta \begin{pmatrix} e^{-i\phi}\sin\frac{\theta}{2} \\ -\cos\frac{\theta}{2} \end{pmatrix}; \\
&= i \begin{pmatrix} e^{i\phi}\sin\frac{\theta}{2} & -\cos\frac{\theta}{2} \end{pmatrix} \begin{pmatrix} \frac{e^{-i\phi}}{2}\cos\frac{\theta}{2} \\ \frac{1}{2}\sin\frac{\theta}{2} \end{pmatrix}; \\
A_\theta^- &= \frac{i}{2}\Big[\sin\frac{\theta}{2}\cos\frac{\theta}{2} - \cos\frac{\theta}{2}\sin\frac{\theta}{2}\Big] = 0,
\end{aligned}
\tag{2.41}
$$

and for the component A_ϕ^-

$$
\begin{aligned}
A_\phi^- &= i \begin{pmatrix} e^{i\phi}\sin\frac{\theta}{2} & -\cos\frac{\theta}{2} \end{pmatrix} \partial_\phi \begin{pmatrix} e^{-i\phi}\sin\frac{\theta}{2} \\ -\cos\frac{\theta}{2} \end{pmatrix}; \\
&= i \begin{pmatrix} e^{i\phi}\sin\frac{\theta}{2} & -\cos\frac{\theta}{2} \end{pmatrix} \begin{pmatrix} -ie^{-i\phi}\sin\frac{\theta}{2} \\ 0 \end{pmatrix}; \\
A_\phi^- &= \sin^2\frac{\theta}{2}.
\end{aligned}
\tag{2.42}
$$

The only thing left is the Berry curvature $F_{\theta\phi}$, obtained by

$$
F_{\theta\phi} = \frac{\partial A_\phi^-}{\partial\theta} - \frac{\partial A_\theta^-}{\partial\phi} = \frac{\partial \sin^2\frac{\theta}{2}}{\partial\theta} = \frac{\sin\theta}{2}. \tag{2.43}
$$

Observation 1. *Consider now the ground state of a two level system $\{|\psi\rangle\} = \{|-\rangle, |+\rangle\}$ varying the configurations in parameter space $\mathbf{d} = \mathbf{d}(\theta, \phi)$. Taking the lower energy (the specific properties of the wave functions depend on the dispersion relation $E = \pm\sqrt{\mathbf{d}^2} = \pm d$). Since $\mathbf{d} \neq 0$ (avoid band cross) for all parameter values, it is possible to flatten the bands, i.e. make the energy constant. To analyze the gauge invariance of the curvature, one realizes that the eigenstates defined above are not well defined in the 'south pole' where $\theta = \pi$. One obtains*

$$
|-(\mathbf{R})\rangle = \begin{pmatrix} e^{-i\phi} \\ 0 \end{pmatrix}, \tag{2.44}
$$

which is in fact, not well defined, since

$$
\phi = \arctan\frac{d_y}{d_x}. \tag{2.45}
$$

Recall that in the chosen gauge, $A_\theta^- = 0$. The Berry connection associated with the ground state is known, as $A_\phi^- = \sin^2\theta/2$. Choosing now a new gauge, for instance $|-'(\mathbf{R})\rangle = e^{i\phi}|-\rangle$, the Berry connection in this gauge ($|-'\rangle$) is

$$
A_\phi^{-'} = -\cos^2\frac{\theta}{2}, \tag{2.46}
$$

the difference between both gauges is exactly unitary.

Berry realised that the integrals over the connections in closed loops in the space of parameters are independent of gauge. Considering the circulations of the connections obtained above, integrated over $\theta = cte$ curves, this leads to

$$\gamma_- = \int_{\mathcal{C}_\theta} A_\phi^- d\phi = \sin^2\frac{\theta}{2}\int_0^{2\pi} d\phi = 2\pi\sin^2\frac{\theta}{2}; \tag{2.47}$$

$$\gamma_{-'} = \int_{\mathcal{C}_\theta} A_\phi^{-'} d\phi = -\cos^2\frac{\theta}{2}\int_{\mathcal{C}_\theta} d\phi = -2\pi\cos^2\frac{\theta}{2}. \tag{2.48}$$

The difference between the circulations $\gamma^- - \gamma^{-'} = 2\pi$ and, consequently, describes the same phase. The Berry Curvature is exactly the same

$$F_{\theta\phi} = \frac{\sin\phi}{2}, \tag{2.49}$$

as expected (the Berry vector potential is depended on the gauge choice). Realising that in reality the Berry phase is not a relevant gauge independent quantity, but the Wilson Loop is (integral realised over a closed loop).

In the case of a $\mathbf{d}$ vector dependent on the parameters, then by the product rule

$$F_{R_iR_j} = F_{\theta\phi}\frac{\partial(\theta,\phi)}{\partial(R_i,R_j)} = \frac{\sin\theta}{2}\frac{\partial(\theta,\phi)}{\partial(R_i,R_j)} = -\frac{1}{2}\frac{\partial(\cos\theta,\phi)}{\partial(R_i,R_j)}, \tag{2.50}$$

where $\frac{\partial(\theta,\phi)}{\partial(R_i,R_j)}$ is the Jacobian of the transformation from $\mathbf{R} \to (\theta,\phi)$.

The intensity of the Berry Field $F_i = \epsilon_{ijk}F_{jk}$ provides an expression for the components

$$F_i^- = \epsilon_{ijk}F_{R_jR_k} = \epsilon_{ijk}F_{\theta\phi}^-\frac{\partial(\theta,\phi)}{\partial(R_j,R_k)} \to \qquad F_{R_i}^- = \frac{\sin\theta}{2}\frac{\partial(\theta,\phi)}{\partial(R_j,R_k)}, \tag{2.51}$$

remembering that the Jacobian $\frac{\partial(R_i,R_j)}{\partial(\phi,\theta)} = R^2\sin\theta$ and by the theorem of the inverse function, the Jacobian $\frac{\partial(\theta,\phi)}{\partial(R_i,R_j)} = -\left\langle\frac{\partial(\theta,\phi)}{\partial(R_i,R_j)}\right\rangle^{-1}$, then the ith component of the field is

$$F_i^- = -\frac{1}{2}\frac{1}{R^2}; \qquad \mathbf{F}^- = -\frac{1}{2}\frac{\mathbf{R}}{R^3}. \tag{2.52}$$

expressed in an arbitrary direction. Now this field is proven equivalent to a monopole (in the space of parameters) of intensity $1/2$, localized at the degeneracy point. For the band $|+(\mathbf{R})\rangle$, the monopole has intensity $-1/2$. The degeneracy points act as sources and sinks of the curvature of the Berry phase.

Example 1 (Perturbative Approach)**.** *Considering $\epsilon(\mathbf{R}) = 0$, the energy of a generic system is*

$$\mathcal{H} = \pm\mathbf{d}\cdot\vec{\sigma},$$

(assuming a degeneracy at $\mathbf{R}^* = 0$), a translation over the space of parameters. Given these considerations, for values sufficiently near of $\mathbf{R}^*$ (the origin), then $\mathbf{d}(0) = 0$ or $\mathbf{d}(\mathbf{R}) = \mathbf{R}$. A generic hamiltonian is written by

$$\mathcal{H}(\mathbf{R}) = x\sigma_x + y\sigma_y + z\sigma_z, \tag{2.53}$$

for $\mathbf{R} = (x, y, z)$.

The eigenenergies are given by $E_\pm = \pm R$ and the degeneracy is an isolated point at which the parameters x, y, z are all null. Near the degeneracy point

$$\nabla\mathcal{H} = \vec{\sigma},$$

and it is possible to determine the Berry phases through the Berry Field, expressed as

$$\mathbf{F}^- = Im\frac{1}{4R^2}\left\langle -\right|\left(\nabla_{\mathbf{R}}\mathcal{H}\right)\left|+\right\rangle \times \left\langle +\right|\left(\nabla_{\mathbf{R}}\mathcal{H}\right)\left|-\right\rangle, \tag{2.54}$$

and the matrix elements of the Berry field can be given by the following relations

$$\sigma_x\left|\pm\right\rangle = \left|\mp\right\rangle, \qquad \sigma_y\left|\pm\right\rangle = \pm i\left|\mp\right\rangle \qquad \sigma_z\left|\pm\right\rangle = \mp\left|\pm\right\rangle, \tag{2.55}$$

considering that, as a spin system conserves the angular momentum, then it is always possible to align the z component in the direction of $\mathbf{R}$ in the parameter space, so that it is obtained the components of the Berry field

$$
\begin{aligned}
F_x &= Im\frac{1}{4R^2}\langle -|\,(\sigma_y)\,|+\rangle\langle +|\,\sigma_z\,|-\rangle = Im\frac{1}{4R^2}\langle -|\,i\,|-\rangle\langle +|\,(-\,|-\rangle) = 0;\\
F_y &= Im\frac{1}{4R^2}\langle -|\,\sigma_z\,|+\rangle\langle +|\,\sigma_x\,|-\rangle = 0;\\
F_z &= Im\frac{1}{4R^2}\left(\langle -|\,\sigma_x\,|+\rangle\langle +|\,\sigma_y\,|-\rangle - \langle -|\,\sigma_y\,|+\rangle\langle +|\,\sigma_x\,|-\rangle\right)\\
&= Im\frac{1}{4R^2}\left(\langle -|-\rangle\left(-i\,\langle +|+\rangle\right) - i\,\langle -|-\rangle\langle +|+\rangle\right) = -\frac{1}{2R^2},
\end{aligned}
\tag{2.56}
$$

or, more generally, for any direction of $\mathbf{R}$ *(without align the direction of the* z *component of the spin matrices with* $\mathbf{R}$*), the Berry field is*

$$
\mathbf{F}^{-} = -\frac{\mathbf{R}}{2R^3}. \tag{2.57}
$$

A field of the form of Equation 2.52, gives us a Berry phase

$$
\begin{aligned}
\gamma_{\pm}(\mathcal{C}) &= -\iint_{\partial S=\mathcal{C}} \pm\frac{\mathbf{R}}{2R^3}\cdot d\mathbf{S} = \mp\frac{1}{2}\iint_{\partial S=\mathcal{C}}\frac{1}{R^3}\mathbf{R}\cdot d\mathbf{S};\\
&= \mp\frac{1}{2}\frac{1}{R^2}\iint_{\partial S=\mathcal{C}}\hat{\mathbf{R}}\cdot\hat{\mathbf{n}}d\sigma = \mp\frac{1}{2}\frac{A(\mathcal{C})}{R^2} = \mp\frac{1}{2}\Omega(\mathcal{C}),
\end{aligned}
\tag{2.58}
$$

where $\Omega(\mathcal{C})$ is the solid angle of the closed curve $\mathcal{C}$ subtended by the origin. The exponential of the Berry phase can be written by

$$
\exp\{i\gamma_{\pm}(\mathcal{C})\} = \exp\left\{\mp\frac{i}{2}\Omega(\mathcal{C})\right\}, \tag{2.59}
$$

realising that the phase factor is independent of the surface that generates the curve, since Ω can only change over multiplets of 4π (it occurs by crossing a degeneracy).

Definition 1. *Dirac fermions are fermions that obey a momentum space Hamiltonian given by*

$$
\mathcal{H} = \sum_i k_i\sigma_i, \tag{2.60}
$$

in the Brillouin zone, similar to the developed Hamiltonian in the last sections.

One of the principal consequences of transporting a two dimensional Dirac fermion over a trajectory $\mathcal{C}$ in the parameter space, is the attachment of a Berry phase.

The value of this phase is obtained using the results derived until now. In the case studied of a two level system, the solid angle subtended by the curve is 2π if it surrounds the degeneracy, and zero if not.

This proves that the Berry phase of two dimensional gapless Dirac fermions in the Fermi surface is equal to π.

2.4 Chern Number

From the definitions given above, in the two levels system, the integral of

$$\int_{\mathcal{C}_\theta} \left(A_\phi^{-'}(\theta,\phi) - A_\phi^{-}(\theta,\phi) \right) d\phi = \gamma^{-'} - \gamma^{-} = 2\pi, \tag{2.61}$$

and realising that this equality is the same as the integral of the Berry curvature over a closed sphere containing a monopole, the Stokes Theorem asserts

$$\int_{\mathcal{C}_\theta} \left(A_\phi^{-'}(\theta,\phi) - A_\phi^{-}(\theta,\phi) \right) d\phi = \int_{\mathcal{C}_\theta} \nabla \times \left(A_\phi^{-'}(\theta,\phi) - A_\phi^{-}(\theta,\phi) \right) d\theta d\phi = \int_{S^2} F_{\theta\phi} d\theta d\phi. \tag{2.62}$$

By equation 2.61, the above integral is the same

$$\oint_{S^2} F_{\theta\phi} d\theta d\phi = 2\pi. \tag{2.63}$$

The integral of the Berry curvature over a manifold is, for general fields, equal to $2\pi \times m$, with $m \in \mathbb{Z}$ the number of monopoles inside the manifold. From this integral, one of the principal topological indexes is defined, responsible for a wide gamma of quantized effects in the theory of condensed matter, the Chern Number, defined as

$$Ch = \oint_{S^2} F_{\theta\phi} d\theta d\phi = 2\pi m. \tag{2.64}$$

The quantization rule imposed by the Chern number (quantization of the Berry Flux) is valid for any two dimensional manifold, for example the Torus $\mathbb{T}^2$ or the sphere $\mathbf{S}^2$.

2.5 Zak phase in Condensed Matter Systems

Considering the previously discussed aspects of the previous sections, it is interesting now to focus on condensed matter systems, i.e. proposed systems in periodic potentials (lattice - Bravais- potentials $V(\mathbf{r})$). It is known that the Schrödinger equation

$$\mathcal{H}\left|\psi(\mathbf{r})\right\rangle = \left(-\frac{1}{2m}\nabla^2 + V(\mathbf{r})\right)\left|\psi(\mathbf{r})\right\rangle = \epsilon\left|\psi\right\rangle, \tag{2.65}$$

captures the dynamics of a particle, submitted to a periodic potential $V(\mathbf{r})$

$$V(\mathbf{r}) = V(\mathbf{r} + \mathbf{a}_i), \tag{2.66}$$

for $\mathbf{a}_i$ the lattice vectors. For a system with multiple bands, the Bloch theorem guarantees the existence of eigenfunctions of the form

$$\left|\psi_{n\mathbf{k}}(\mathbf{r})\right\rangle = e^{i\mathbf{k}\cdot\mathbf{r}}\left|n\mathbf{k}\right\rangle, \tag{2.67}$$

called Bloch waves, with quantum numbers n (band index). Writing this expression as

$$e^{i\mathbf{k}\cdot\mathbf{R}}\left|\psi(\mathbf{r})\right\rangle = \left|\psi(\mathbf{r}+\mathbf{R})\right\rangle, \tag{2.68}$$

the translation operator $T_{\mathbf{R}}$ is defined (which commutes with the Hamiltonian).

Global phases of the wave function, of the type $\exp\{i\phi\}$, are harmless. This symmetry is commonly known as a Global Phase Symmetry $U(1)$. The conservation law that corresponds to such an invariance is the conservation of the probability density

$$\frac{\mathrm{d}}{\mathrm{d}t}\left(\int d^3r|\psi|^2\right) = 0. \tag{2.69}$$

2.5.1 Local Phase Symmetry

Now we start looking to local symmetries, invariances and more important, phases that can be measured (like $e^{i\phi(\mathbf{k})}$). Defining a state $\langle\mathbf{r}|\psi_{n\mathbf{k}}\rangle = \exp\{i\mathbf{k}\cdot\mathbf{r}\}u(\mathbf{r})$

as the Bloch wave, then is interesting to obtain information about any state of the kind $\langle \mathbf{r}|\psi'_{n\mathbf{k}}\rangle = \exp\{i\mathbf{k}\cdot\mathbf{r}\}\,\langle \mathbf{r}|\psi_{n\mathbf{k}}\rangle$. For that, substituting these in the Schrödinger equation

$$\begin{aligned}\mathcal{H}\,|\psi'_{n\mathbf{k}}\rangle &= \left(-\frac{1}{2m}\nabla^2 + V(\mathbf{r})\right)\exp\{i\phi(\mathbf{k})\}\,|\psi_{n\mathbf{k}}\rangle\,;\\ &= \exp\{i\phi(\mathbf{k})\}\left(-\frac{1}{2m}\nabla^2 + V(\mathbf{r})\right)|\psi_{n\mathbf{k}}\rangle\,;\\ &= \exp\{i\phi(\mathbf{k})\}\epsilon_{n\mathbf{k}}\,|\psi_{n\mathbf{k}}\rangle = \epsilon_{n\mathbf{k}}\,|\psi'_{n\mathbf{k}}\rangle\,,\end{aligned} \tag{2.70}$$

the addition of a local phase factor preserves the Hamiltonian invariant in the reciprocal space. For the independent electron, this invariance requires momentum conservation.

The remaining task is to describe the degrees of freedom of the local phase. One way to do this is analogous to gauge transformations in quantum mechanics. It means to take local phases in the position space, considering transformations of the wave functions by local phases. The Schrödinger equation applied to these functions results in

$$\begin{aligned}\left(-\frac{1}{2m}\nabla^2 + V(r)\right)\exp\{i\phi\}\,|\psi\rangle &= i\frac{\partial}{\partial t}\left(\exp\{i\phi\}\,|\psi\rangle\right);\\ -\frac{1}{2m}\nabla\cdot\left[\left(\nabla e^{i\phi}\right)|\psi\rangle + e^{i\phi}\left(\nabla\,|\psi\rangle\right)\right] + e^{i\phi}V\,|\psi\rangle &= -\frac{\partial\phi}{\partial t}e^{i\phi}\,|\psi\rangle + ie^{i\phi}\frac{\partial\,|\psi\rangle}{\partial t};\\ -\frac{1}{2m}\left[i\nabla\cdot(\nabla\phi)\,e^{i\phi}\,|\psi\rangle + \nabla\cdot\left(e^{i\phi}\nabla\,|\psi\rangle\right)\right] + V\,|\psi'\rangle &= -\frac{\partial\phi}{\partial t}e^{i\phi}\,|\psi\rangle + ie^{i\phi}\frac{\partial\,|\psi\rangle}{\partial t},\end{aligned} \tag{2.71}$$

the first term in the left hand side of the equation is

$$\begin{aligned}i\nabla\cdot(\nabla\phi)\exp\{i\phi\}\,|\psi\rangle &= i\left(\nabla^2\phi\right)\exp\{i\phi\}\,|\psi\rangle + i(\nabla\phi)\cdot\left[i\left(\nabla\phi\right)\exp\{i\phi\}\,|\psi\rangle + e^{i\phi}\nabla\,|\psi\rangle\right];\\ &= \left\{\left[i\nabla^2\phi - \left(\nabla\phi\right)^2\right]|\psi\rangle + i\left(\nabla\phi\right)\cdot\left(\nabla\,|\psi\rangle\right)\right\}\exp\{i\phi\},\end{aligned} \tag{2.72}$$

and the second term in the left hand side of the equation is

$$\begin{aligned}\nabla\cdot\left(\exp\{i\phi\}\nabla\,|\psi\rangle\right) &= i(\nabla\phi)\cdot\left(\nabla\,|\psi\rangle\right)\exp\{i\phi\} + \exp\{i\phi\}\nabla^2\,|\psi\rangle\,;\\ &= \left[i\left(\nabla\phi\right)\cdot\left(\nabla\,|\psi\rangle\right) + \nabla^2\,|\psi\rangle\right]\exp\{i\phi\},\end{aligned} \tag{2.73}$$

the Schrödinger equation is, substituting the left hand side terms

$$-\frac{1}{2m}\left\{\left[i\nabla^2\phi-(\nabla\phi)^2\right]|\psi\rangle+i\left(\nabla\phi\right)\cdot\left(\nabla|\psi\rangle\right)+i\left(\nabla\phi\right)\cdot\left(\nabla|\psi\rangle\right)+\nabla^2|\psi\rangle\right\}+V|\psi\rangle= -\frac{1}{2m}\left\{\left[i\nabla^2\phi-(\nabla\phi)^2\right]|\psi\rangle+2i\left(\nabla\phi\right)\cdot\left(\nabla|\psi\rangle\right)+\nabla^2|\psi\rangle\right\}+V|\psi\rangle, \tag{2.74}$$

or yet

$$-\frac{1}{2m}\left\{\left[i\nabla^2\phi-(\nabla\phi)^2\right]|\psi\rangle+2i\left(\nabla\phi\right)\cdot\left(\nabla|\psi\rangle\right)+\nabla^2|\psi\rangle\right\}+V|\psi\rangle=-\frac{\partial\phi}{\partial t}|\psi\rangle+i\frac{\partial|\psi\rangle}{\partial t};$$
$$\left\{\frac{1}{2m}\left[(\nabla\phi)^2-i\nabla^2\phi\right]|\psi\rangle-\frac{i}{m}\left(\nabla\phi\right)\cdot\left(\nabla|\psi\rangle\right)+\frac{\partial\phi}{\partial t}|\psi\rangle\right\}-\frac{1}{2m}\nabla^2|\psi\rangle+V|\psi\rangle=i\frac{\partial|\psi\rangle}{\partial t}, \tag{2.75}$$

i.e. the local phase does not maintain the Schrödinger equation invariant (in the coordinate space). Realising that

$$\begin{aligned}(-i\nabla+\nabla\phi)^2|\psi\rangle&=(-i\nabla+\nabla\phi)\cdot(-i\nabla|\psi\rangle+|\psi\rangle\nabla\phi);\\&=-\nabla^2|\psi\rangle-i(\nabla|\psi\rangle)\cdot(\nabla\phi)-i|\psi\rangle\nabla^2\phi-i(\nabla|\psi\rangle)\cdot(\nabla\phi)+(\nabla\phi)^2|\psi\rangle;\\&=(\nabla\phi)^2|\psi\rangle-i(\nabla^2\phi)|\psi\rangle-2i(\nabla|\psi\rangle)\cdot(\nabla\phi)-\nabla^2|\psi\rangle,\end{aligned} \tag{2.76}$$

the Hamiltonian can be described by

$$\frac{1}{2m}(-i\nabla+\nabla\phi)^2|\psi\rangle+\frac{\partial\phi}{\partial t}|\psi\rangle+V|\psi\rangle=i\frac{\partial|\psi\rangle}{\partial t}. \tag{2.77}$$

From the classical electromagnetism, the momentum operator is substituted through a gauge transformation $\mathbf{p}\rightarrow\mathbf{p}+(q/c)\mathbf{A}$, for the vector potential $\mathbf{A}$ and the time derivatives are substituted by $\frac{\partial}{\partial t}(\cdot)\rightarrow\frac{\partial}{\partial t}(\cdot)+q\Phi$, where Φ is the electric field potential (scalar field). Making the substitution, an effective Hamiltonian is obtained

$$\begin{aligned}\frac{1}{2m}\left(-i\nabla-\frac{e}{c}\mathbf{A}\right)^2\psi(x,t)+V(x)\psi(x,t)+e\Phi\psi(x,t)&=i\frac{\partial\psi}{\partial t};\\\frac{1}{2m}\left[-\nabla^2\psi+\frac{ie}{c}\left(\nabla\cdot(\mathbf{A}\psi)+\mathbf{A}\cdot(\nabla\psi)\right)+\frac{e^2}{c^2}\mathbf{A}^2\psi\right]+(V+e\Phi)\psi&=i\frac{\partial\psi}{\partial t};\\\left\{\frac{i}{2m}\left[\frac{e}{c}\left(\nabla\cdot\mathbf{A}\right)+\frac{e^2}{c^2}\mathbf{A}^2\right]\psi+\frac{ie}{mc}\mathbf{A}\cdot(\nabla\psi)+e\Phi\psi\right\}-\frac{1}{2m}\nabla^2\psi+V\psi&=i\frac{\partial\psi}{\partial t}.\end{aligned} \tag{2.78}$$

Making a gauge transformation of the kind

$$\Phi' \to \Phi - \frac{1}{e}\frac{\partial \phi}{\partial t}; \tag{2.79}$$

$$\mathbf{A}' \to \mathbf{A} + \frac{c}{e}\nabla\phi, \tag{2.80}$$

the wave function must be altered to

$$\psi'(x,t) \to \exp\Big\{i\frac{e}{c}\phi\Big\}\psi(x,t), \tag{2.81}$$

local symmetries are then a manifestation of the gauge field. For a Bloch wave, having the same local symmetry in the reciprocal space, is interesting to take the gauge fields in the k-space.

2.5.2 Berry Connection and Curvature

Remembering the Equation 2.11 previously defined, the Berry connection in the parameter space, can be now extended to the reciprocal space

$$\mathbf{A}_n \equiv i \left\langle n\mathbf{k}\right| \nabla_k \left|n\mathbf{k}\right\rangle, \tag{2.82}$$

and taking a local phase $\phi(\mathbf{k})$, the Berry connection is

$$\begin{aligned}\mathbf{A}'_n &= i \left\langle n\mathbf{k}\right| e^{-i\phi(\mathbf{k})}\nabla_k e^{i\phi(\mathbf{k})} \left|n\mathbf{k}\right\rangle = i \left\langle n\mathbf{k}\right| \nabla_k \left|n\mathbf{k}\right\rangle + i \left\langle n\mathbf{k}\right| \left(i\nabla_k\phi(\mathbf{k})\right) \left|n\mathbf{k}\right\rangle; \\ &= \mathbf{A}_n - \nabla_k\phi(\mathbf{k}) \left\langle n\mathbf{k}|n\mathbf{k}\right\rangle = \mathbf{A}_n - \nabla_k\phi(\mathbf{k}),\end{aligned} \tag{2.83}$$

that behaves identically to the electromagnetic vector potential. However this field lives in the reciprocal space.

The Berry Curvature is defined in the same way, by $\mathbf{F}_n$

$$\mathbf{F}_n \equiv \nabla \times \mathbf{A}_n = i\epsilon_{ijk}\frac{\partial}{\partial k_i}\left(\left\langle n\mathbf{k}\right|\right)\frac{\partial}{\partial k_j}\left(\left|n\mathbf{k}\right\rangle\right) = i\epsilon_{ijk}\left\langle \partial_{k_i}u_{n\mathbf{k}}\middle|\partial_{k_j}u_{n\mathbf{k}}\right\rangle. \tag{2.84}$$

In the absence of a lattice, the position and momentum operators can be viewed as gradients in their reciprocal spaces, i.e. $\mathbf{r} = i\nabla_k$ and $\mathbf{k} = -i\nabla_r$. In the presence of a Bravais lattice, the position operator (and the momentum operator too) is defined similarly

Definition 2. *A Bloch wave, has the position operator given by*

$$\mathbf{r} = i\nabla_k \delta_{mn} - \mathbf{A}_{mn} = i\nabla_k \delta_{mn} - \langle m\mathbf{k}| \nabla_k |n\mathbf{k}\rangle , \tag{2.85}$$

and $\mathbf{A}_{mn}$ is exactly the Berry connection when $m = n$, or $\mathbf{A}_{nn} = \mathbf{A}_n$.

Observation 2. *Initially, the aim is to show that the real expression to the position operator in the absence of a lattice is correct. To see this, expanding the wave function in the real and reciprocal spaces, in terms of plane waves*

$$\langle \mathbf{r}|\psi\rangle = \int \langle \mathbf{r}|\mathbf{k}\rangle \langle \mathbf{k}|\psi\rangle \, d^3k = \int d^3k \psi(\mathbf{k}) e^{i\mathbf{k}\cdot\mathbf{r}}; \tag{2.86}$$

$$\langle \mathbf{k}|\psi\rangle = \int \langle \mathbf{k}|\mathbf{r}\rangle \langle \mathbf{r}|\psi\rangle \, d^3k = \int d^3r \psi(\mathbf{r}) e^{-i\mathbf{k}\cdot\mathbf{r}}, \tag{2.87}$$

now simply making $\mathbf{r}|\psi\rangle$, it is aimed to know the action of this operator. Again, using the identity property

$$\begin{aligned} \langle \mathbf{k}| \mathbf{r} |\psi\rangle &= \int \langle \mathbf{k}|\mathbf{r}\rangle \langle \mathbf{r}| \mathbf{r} |\psi\rangle \, d^3r = \int e^{-i\mathbf{k}\cdot\mathbf{r}} \mathbf{r}\psi(\mathbf{r}) d^3r; \\ &= i \int \nabla_{\mathbf{k}} e^{-i\mathbf{k}\cdot\mathbf{r}} \psi(\mathbf{r}) d^3r = i\nabla\psi(\mathbf{k}), \end{aligned} \tag{2.88}$$

and this result makes use of the quantization condition $\mathbf{p} \to -i\nabla_r$.

Now turning back to the lattice case, writing a superposition of Bloch waves (denoted by $|\psi_{n\mathbf{k}}\rangle = e^{i\mathbf{k}\cdot\mathbf{r}} |n\mathbf{k}\rangle$), therefore

$$\begin{aligned} \langle \mathbf{r}|\psi\rangle &= \sum_n \int d^3k \langle \psi_{n\mathbf{k}}|\psi\rangle \langle \mathbf{r}|\psi_{n\mathbf{k}}\rangle = \sum_n \int d^3k \psi_n(\mathbf{k}) \psi_{n,\mathbf{k}}(\mathbf{r}); \\ &= \sum_n \int d^3k \psi_n(\mathbf{k}) u_{n\mathbf{k}}(\mathbf{r}) e^{i\mathbf{k}\cdot\mathbf{r}}, \end{aligned} \tag{2.89}$$

by this transformation similar to a Fourier transform, associated to a weight function $u_{n\mathbf{k}}$ (not only plane waves). Unfortunately, the inverse of this transformation is not so simple as the Fourier inverse. The action of the position operator is known applying over $\psi(\mathbf{r})$

$$\begin{aligned}\mathbf{r}\psi(\mathbf{r}) &= \mathbf{r}\sum_n \int d^3k \psi_n(\mathbf{k}) u_{n\mathbf{k}}(\mathbf{r}) e^{i\mathbf{k}\cdot\mathbf{r}} = \sum_n \int d^3k \psi_n(\mathbf{k}) u_{n\mathbf{k}}(\mathbf{r}) \mathbf{r} e^{i\mathbf{k}\cdot\mathbf{r}};\\ &= -i\nabla_k \left(\sum_n \int d^3k \psi_n(\mathbf{k}) \psi_{n\mathbf{k}}(\mathbf{r}) \right) + i\sum_n \int \nabla_k \big(\psi_n(\mathbf{k}) u_{n\mathbf{k}}(\mathbf{r})\big) e^{i\mathbf{k}\cdot\mathbf{r}} d^3k; \qquad (2.90)\\ &= i\sum_n \int e^{i\mathbf{k}\cdot\mathbf{r}} \Big\{ \nabla_k \big[\psi_n(\mathbf{k})\big] u_{n\mathbf{k}}(\mathbf{r}) + \psi_n(\mathbf{k}) \nabla_k \big[u_{n\mathbf{k}}(\mathbf{r})\big] \Big\} d^3k,\end{aligned}$$

the second derivative inside the integral can be rewritten as

$$\nabla_k \langle \mathbf{r}|n\mathbf{k}\rangle = \nabla_k \int d^3r' \langle \mathbf{r}|\mathbf{r}'\rangle \langle \mathbf{r}'|n\mathbf{k}\rangle = \int \delta(\mathbf{r}-\mathbf{r}') \nabla_k u_{n\mathbf{k}}(\mathbf{r}') d^3r', \qquad (2.91)$$

and the action of $\mathbf{r}$ *is*

$$\begin{aligned}\mathbf{r}\psi(\mathbf{r}) &= i\sum_n \int \left[\nabla_k \left(\psi_n(\mathbf{k})\right) \psi_{n\mathbf{k}}(\mathbf{r}) + \psi_n(\mathbf{k}) e^{i\mathbf{k}\cdot\mathbf{r}} \int \delta(\mathbf{r}-\mathbf{r}') \nabla_k u_{n\mathbf{k}}(\mathbf{r}') \right] d^3k;\\ &= i\sum_n \int d^3k \psi_{n\mathbf{k}}(\mathbf{r}) \nabla_k \left(\psi_n(\mathbf{k})\right) +\\ &\quad -\sum_n \int \psi_n(\mathbf{k}) \left[\sum_m e^{i\mathbf{k}\cdot\mathbf{r}} u_{m\mathbf{k}}(\mathbf{r}) \left(-i \int \delta(\mathbf{r}-\mathbf{r}') u^*_{m\mathbf{k}}(\mathbf{r}) \nabla_k u_{n\mathbf{k}}(\mathbf{r}') d^3r' \right) \right] d^3k;\\ &= \sum_n \int d^3k \left(\psi_{n\mathbf{k}} i\nabla_k - \sum_m \psi_{m\mathbf{k}}(\mathbf{r}) \mathbf{A}_{mn} \right) \psi_n(\mathbf{k}), \qquad (2.92)\end{aligned}$$

and the proposed form of the operator is valid.

In a single band problem, the m index (and the respective summation) can be dropped and the Berry Curvature is reobtained

$$\mathbf{r}\psi(\mathbf{r}) = \int d^3k \left(\psi_{n\mathbf{k}} i\nabla_k - \psi_{n\mathbf{k}}(\mathbf{r}) \mathbf{A}_n \right) \psi_n(\mathbf{r}). \qquad (2.93)$$

If the energy gap between any two bands is large, then there is no overlap between them, and $\mathbf{A}_{mn}$ can be neglected for $m \neq n$. In this case, the position operator is only

$$\mathbf{r} = i\nabla_k - \mathbf{A}_n. \qquad (2.94)$$

Such conclusion is analogous to the case of the momentum operator in a system submitted to a electromagnetic field, such that $\mathbf{p} = -i\nabla_r - (e/c)\mathbf{A}$. [4]

Spatially separated electric charges give rise to an electric dipole moment (polarization). The polarization is directly connected to the position average $p \propto \langle \hat{x} \rangle$. However, in the crystalline solid, there is a infinite repetition of the lattice structure, and in this way, the polarization cannot be defined as in the classical way. Specially in the case of delocalized electrons, the classical polarization depends on the choice of the unit cell (which cannot be true). Such a problem can be reinterpreted in terms of the topological invariant, giving a physical interpretation to those quantities, as presented in the works of (13) and reviewed in (38).

Definition 3 (Polarization)**.** *The polarization is classically expressed by the position, usually defined as $p_n = q\mathbf{r}$, for the electric charge q. For delocalized electrons, the polarization cannot depend on the choice of the unit cell, such that $i\nabla_k$ must vanish and the polarization must be*

$$\begin{aligned} p_n &= -\frac{q}{\#\textit{occupied states}} \sum_{o.s.} \mathbf{r}; \\ p_n &= -\frac{q}{2\pi} \int_{ZB} \mathbf{A}_n dk = -\frac{q}{2\pi} \Phi_n, , \end{aligned} \tag{2.95}$$

for a single band effect, where Φ_n is the Zak phase of the n-th band. Since the Zak phase is defined up to 2π, the polarization must stay defined in

$$p_n = -\frac{q}{2\pi} \Phi_n \; mod(e) = -\frac{q}{2} \nu \; mod(e). \tag{2.96}$$

(See further details about polarization in refs. (13, 38)).

Now that the topological band formalism has been developed, the Berry and Zak phase were introduced, generic two band models were firstly investigated and one topological invariant was defined - the Chern number. From the above definitions, it is possible to proceed and analyse specific problems of two band models, which is the idea of the next two chapters 3,4, one insulating and one superconductor model.

[4] In the case of Hall effect, terms like $\mathbf{A}_{mn}$ do not contribute. Just like is proven in the previous section, $\mathbf{r}$ is a local phase symmetry in the reciprocal space, such that $|n\mathbf{k}\rangle \rightarrow e^{i\phi_n(\mathbf{k})} |n\mathbf{k}\rangle$ is invariant.

Chapter 3

One dimensional Insulator: SSH Model

The simplest model of an insulator holding topological properties is the two band model for Polyacetylene, known as SSH model: Su-Schrieffer-Heeger, (39, 40, 41). Considering the Hamiltonian in second quantization of a dimerized one-dimensional chain

$$\mathcal{H} = \sum_{i=1}^{N} (t+\delta t)\, c_{Ai}^{\dagger} c_{Bi} + \sum_{i=1}^{N-1} (t-\delta t)\, c_{Ai+1}^{\dagger} c_{Bi} + \text{h.c.} = \sum_{i=1}^{N} v c_{Ai}^{\dagger} c_{Bi} + \sum_{i=1}^{N-1} w c_{Ai+1}^{\dagger} c_{Bi} + \text{h.c.} \tag{3.1}$$

where $c_{A(B)i}^{\dagger}/c_{A(B)i}$ are creation and annihilation operators of the sub-lattice A/B, respectively. In this model, each cell consists of two different atoms A, B and an average hopping term t connecting nearest neighbour sites. In addition, there is a difference between the hopping amplitudes in-site/off-site, characterized by δ.

Considering the unit cell with $a = 1$, the Fourier transform of the creation and annihilation operators are

$$c_{Ai}^{\dagger} = \frac{1}{\sqrt{N}} \sum_{k} e^{-ikx_i} a_k^{\dagger}; \qquad c_{Bi}^{\dagger} = \frac{1}{\sqrt{N}} \sum_{k} e^{-ikx_i} b_k^{\dagger}, \tag{3.2}$$

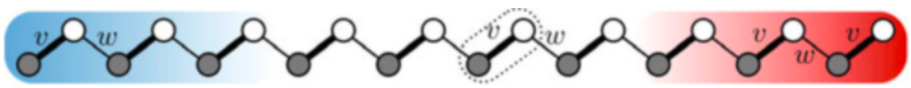

FIGURE 3.1. Schematic view of a Polyacetilene chain, taken from (1), with $v/t = 1 + \delta$ the intra-cell hopping and $w/t = 1 - \delta$ the inter-cell hopping amplitudes.

and the Hamiltonian is expressed by a matrix (through the spinor $\psi_k = (a_k\,,\, b_k)^T$)

$$\mathcal{H} = t\sum_k \left[(1+\delta)\left(a_k^\dagger b_k + b_k^\dagger a_k\right) + (1-\delta)\left(e^{-ika}a_k^\dagger b_k + e^{ika}b_k^\dagger a_k\right)\right] = t\sum_k \psi_k^\dagger h_k \psi_k, \quad (3.3)$$

for h_k, the hopping matrix. This matrix can be expressed as a linear combination of the Pauli matrices (as already done in the previous chapter, see section 2.3)

$$\begin{aligned} h_k &= t\begin{pmatrix} 0 & (1+\delta)+(1-\delta)e^{-ika} \\ (1+\delta)+(1-\delta)e^{ika} & 0 \end{pmatrix}, \\ &= t\begin{pmatrix} 0 & (1+\delta)+(1-\delta)\left(\cos ka - i\sin ka\right) \\ (1+\delta)+(1-\delta)\left(\cos ka + i\sin ka\right) & 0 \end{pmatrix}, \\ &= t\left[(1+\delta)+(1-\delta)\cos\left(ka\right)\right]\sigma_x + (1-\delta)\sin\left(ka\right)\sigma_y = \mathbf{d}(k)\cdot\boldsymbol{\sigma}. \end{aligned} \quad (3.4)$$

The vector $\mathbf{d}$ is confined in the xy plane of the Pauli matrices $\boldsymbol{\sigma}$

$$\mathbf{d}(k) = t\begin{pmatrix} (1+\delta)+(1-\delta)\cos k \\ (1-\delta)\sin k \\ 0 \end{pmatrix}. \quad (3.5)$$

Diagonalization for this two level system is given as

$$\epsilon_\pm(k) = \pm t\sqrt{\mathbf{d}^2} = \pm t\sqrt{2+2\delta^2+2(1-\delta^2)\cos k} = \pm t\sqrt{2\left[1+\delta^2+\cos k\,(1-\delta^2)\right]}, \quad (3.6)$$

the way the expression is derived, the Hamiltonian $\mathcal{H}$ is referred to as a *periodic Hamiltonian*.

Observation 3 (Canonical Bloch Hamiltonian)**.** *Considering relative positions of the sublattices, creation and annihilation operators are expressed as*

$$x_i^A = X_i + x_A; \qquad x_i^B = X_i + x_B, \quad (3.7)$$

the Hamiltonian is written as

$$\mathcal{H} = t\sum_k \left[(1+\delta)\left(e^{ika/2}a_k^\dagger b_k + e^{-ika/2}b_k^\dagger a_k\right) + (1-\delta)\left(e^{-ika/2}a_k^\dagger b_k + e^{ika/2}b_k^\dagger a_k\right)\right], \quad (3.8)$$

realising that

$$\left[(1+\delta)\,e^{ik/2}+(1-\delta)\,e^{-ik/2}\right]a_k^\dagger b_k=\left(2\cos\frac{k}{2}+2\delta i\sin\frac{k}{2}\right)b_k^\dagger a_k; \tag{3.9}$$

$$\left[(1+\delta)\,e^{-ik/2}+(1-\delta)\,e^{ik/2}\right]a_k^\dagger b_k=\left(2\cos\frac{k}{2}-2\delta i\sin\frac{k}{2}\right)b_k^\dagger a_k, \tag{3.10}$$

the Hamiltonian is written as

$$\mathcal{H}_c=t\sum_k\psi_k^\dagger\left(2\cos\frac{k}{2}\sigma_x+2\delta\sin\frac{k}{2}\sigma_y\right)\psi_k, \tag{3.11}$$

in this approach, the Hamiltonian is known as the Canonical Bloch Hamiltonian. In this form, the periodicity is doubled.

The dispersion of the system is

$$\epsilon_\pm(k)=t\sqrt{2\left(1+\delta^2+(1-\delta^2)\cos k\right)}=2t\sqrt{\cos^2\frac{k}{2}+\delta^2\sin^2\frac{k}{2}}, \tag{3.12}$$

and the same relations as before are obtained, since for $\delta=0$ there is no gap.

The vector $\mathbf{d}$ is required to find the eigenstates of the bands. Luckily, these eigenstates are known from section 2.3 and it defines the angle $\phi(k)$ as

$$\phi(k)\equiv\tan^{-1}\left(\frac{d_y}{d_x}\right)=\tan^{-1}\frac{(1-\delta)\sin k}{(1+\delta)+(1-\delta)\cos k}, \tag{3.13}$$

therefore, the eigenstates are

$$|\pm\rangle=\frac{1}{\sqrt{2}}\begin{pmatrix}\pm e^{-i\phi}\\1\end{pmatrix}, \tag{3.14}$$

still realising that the eigenstates are well defined over all possible values of the BZ.

3.1 Edge States

One of the main features of topological band theory is the appearance of non-local states for systems that break translational invariance (open boundary conditions or impurities). This feature is a general correspondence of the boundary to the bulk properties as calculated above, usually called *Bulk-Boundary Correspondence*.

In the case of the SSH insulator, taking first the case of $\delta = \pm 1$, the chain will be exactly dimerized, leading to flattened energy bands given by $\epsilon_{\pm}(k) = \pm 2t$. When $\delta = 1$, the resulting states are bonded "in" the i-th site. On the other hand, for $\delta = -1$, the dimerization happens between sites, with the sub-lattice B site connecting with the A sub-lattice of the next site. The Hamiltonian operates individually in the bonding sites by the relation

$$\mathcal{H}\left(c^{\dagger}_{Ai+1} \pm c^{\dagger}_{Bi}\right)|0\rangle = \pm\left(c^{\dagger}_{Ai+1} \pm c^{\dagger}_{Bi}\right)|0\rangle\,, \tag{3.15}$$

since the group velocity is null, the addition of an electron to the system do not spread to the entire chain. Opening the boundary conditions, there will exist two site operators that does not appear in the Hamiltonian (for $\delta = -1$), namely c_{A1} and c_{BN}. Since the Hamiltonian must commute with them, their eigenenergies must be zero, and

$$\mathcal{H}c^{\dagger}_{A1}|0\rangle = \mathcal{H}c^{\dagger}_{BN}|0\rangle = 0, \tag{3.16}$$

remembering that in-site potentials are not considered in the model. For a finite system of $N = 30$ unit cells, is it possible to determine the exact energies in terms of the parameter δ, as shown in the Figure 3.2, showing that the persistence of the zero modes persists if $\delta < 0$, in the limit of delocalization.

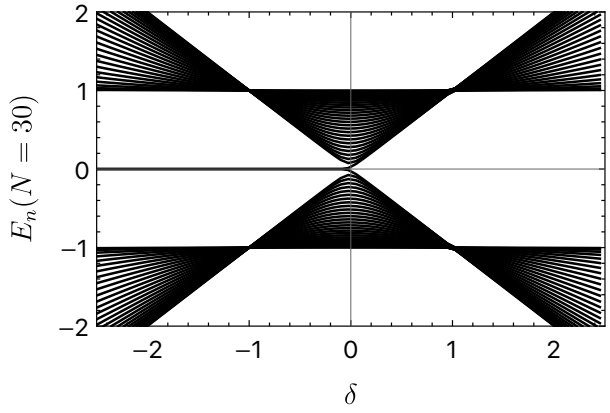

FIGURE 3.2. Diagram shows the relation between the energies relative to the parameter δ, in a system with $N = 30$ unit cells.

3.2 Topological Invariant: Winding Number

From the Hamiltonian, the vector $\mathbf{d}(k)$ is given by Equation 3.5 and the dispersion relation (periodic Hamiltonian) from the Equation 3.6. Considering $\mathbf{d}(k) \neq 0$, for all values of momentum k, the system is gapped (disregarding $\delta = 0$, the only value that turns the system gapless, at $k = \pi$). It is possible to make a schematic diagram of the trajectories of the vector $\mathbf{d}(k)$ in the plane, as $k \in [-\pi, \pi)$ varies along the BZ, the resulting trajectories can be seen in the Figure 3.3. The paths that $\mathbf{d}(k)$ traces are circles centered at the point $\mathbf{d}^0 = (d_x^0, d_y^0) = (1 + \delta, 0)$ with radius $1 - \delta$.

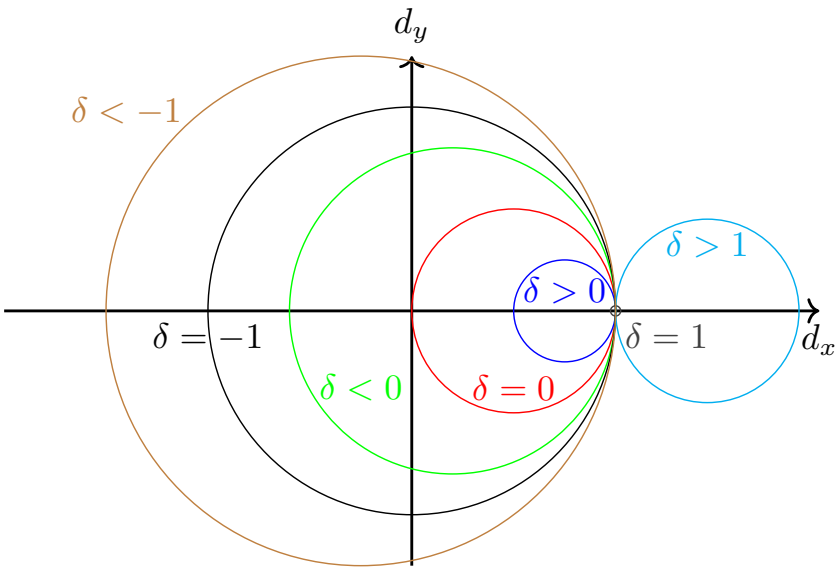

FIGURE 3.3. Trajectories of the curve $\mathbf{d}(k)$ in the (d_x, d_y)-plane, varying k over all Brillouin Zone. Different colors correspond to different values of the parameter δ.

From the schematic figure above, when $\delta < 0$, the circle encloses the origin, while for $\delta > 0$ the circle stay with $d_x > 0$ for all values of k. Taking only the direction of $\mathbf{d}$,

$$\hat{\mathbf{d}}(k) \equiv \frac{\mathbf{d}}{|\mathbf{d}|} = \frac{\mathbf{d}}{E_+}, \tag{3.17}$$

the internal structure of the eigenstates is determined in the Bloch Sphere, where $d_z = 0$ indicates the equator of the Bloch sphere [1] S^1.

[1] For generic d_z, its necessary to include all the sphere S^2

Given the condition for the gap closure, it is interesting to know the bulk properties of each insulating phase. In particular, show that the mapping of the vector $\mathbf{d}$ over the BZ into the Bloch sphere provides a topological invariant, the Winding Number ν, defined via the Zak/Berry phase. This topological invariant is defined as

$$\nu \equiv \frac{1}{\pi}\Phi_{-}. \tag{3.18}$$

From the previous sections, integrating the Berry Connection over the BZ is

$$\Phi_{\pm} = i\int_{ZB} A(k)\cdot d\mathbf{k}, \tag{3.19}$$

and this integral is dependent of the states of each band. From the eigenstates 3.14 and local phase $\phi(k)$ 3.13, the Berry Connection can be computed as

$$\begin{aligned}
\partial_k |\pm\rangle &= \frac{1}{\sqrt{2}}\partial_k \begin{pmatrix} \pm e^{-i\phi} \\ 1 \end{pmatrix} = \frac{1}{\sqrt{2}} \begin{pmatrix} \mp i(\partial_k\phi)e^{-i\phi} \\ 0 \end{pmatrix}; \\
\langle\pm|\,\partial_k\,|\pm\rangle &= \frac{1}{2}\begin{pmatrix} \pm e^{-i\phi} & 1 \end{pmatrix}\begin{pmatrix} \mp i(\partial_k\phi)e^{-i\phi} \\ 0 \end{pmatrix} = -i\frac{1}{2}\partial_k\left[\tan^{-1}\left(\frac{d_y}{d_x}\right)\right]; \\
&= -i\frac{1}{2}\frac{d_x\frac{\mathrm{d}d_y}{\mathrm{d}k} - d_y\frac{\mathrm{d}d_x}{\mathrm{d}k}}{d_x^2+d_y^2} = -i\frac{1}{2E_+^2}\mathbf{d}\times\frac{\mathrm{d}\mathbf{d}}{\mathrm{d}k},
\end{aligned} \tag{3.20}$$

and rescaling the solution $\tan^{-1}\left(\frac{d_y}{d_x}\right) = \tan^{-1}\left(\frac{\hat{d}_y}{\hat{d}_x}\right)$, such that $\hat{d}_x^2 + \hat{d}_y^2 = 1$. The Berry Connection is

$$\mathbf{A}_{\pm} = i\,\langle\pm|\,\partial_k\,|\pm\rangle = \frac{1}{2}\hat{\mathbf{d}}\times\frac{\mathrm{d}\hat{\mathbf{d}}}{\mathrm{d}k}, \tag{3.21}$$

which has only one component (z component). Finally the Zak phase can be expressed only in terms of the direction of the vector $\mathbf{d}$

$$\Phi_{\pm} = \frac{1}{2}\int_{-\pi}^{\pi}\hat{\mathbf{d}}\times\frac{\mathrm{d}\hat{\mathbf{d}}}{\mathrm{d}k}dk = \int_{-\pi}^{\pi}\frac{1}{2E_{\pm}^2}\mathbf{d}\times\frac{\mathrm{d}\mathbf{d}}{\mathrm{d}k}dk. \tag{3.22}$$

Computation of the Zak phase, depends on the above integral, which cannot always fulfill the requirements of the Fundamental Theorem of Calculus. The derivative of $\hat{\mathbf{d}}$ is

$$\frac{\mathrm{d}\hat{\mathbf{d}}}{\mathrm{d}k} = \frac{1}{E_+}\frac{\mathrm{d}\mathbf{d}}{\mathrm{d}k} + \frac{\mathrm{d}}{\mathrm{d}k}\left(\frac{1}{E_+}\right)\mathbf{d}, \tag{3.23}$$

and since the cross product is insensitive to parallel vectors, and the second term vanishes (and the reason that the rescaled Berry Connection is right). In the specific case of the SSH model, the vector $\mathbf{d}$ is known and

$$\begin{aligned}\frac{\mathrm{d}\mathbf{d}}{\mathrm{d}k} &= \begin{pmatrix} -(1-\delta)\sin k \\ (1-\delta)\cos k \\ 0 \end{pmatrix}; \\ \mathbf{d}\times\left(\frac{\mathrm{d}\mathbf{d}}{\mathrm{d}k}\right)_z &= \left[1+\delta+(1-\delta)\cos k\right](1-\delta)\cos k + (1-\delta)^2\cos^2 k; \\ &= (1-\delta^2)\cos k + (1-\delta)^2,\end{aligned} \tag{3.24}$$

the z component of the Berry Connection is simply

$$A_z = \frac{(1-\delta^2)\cos k + (1-\delta)^2}{2\left(1+\delta^2+(1-\delta^2)\cos k\right)} = \frac{1}{2} - \frac{\delta}{1+\delta^2+(1-\delta^2)\cos k}. \tag{3.25}$$

The integral of the Berry Connection over the BZ is

$$\nu = \frac{1}{2\pi}\int_{-\pi}^{\pi}\left(\frac{1}{2} - \frac{2\delta}{1+\delta^2+(1-\delta^2)\cos k}\right)dk. \tag{3.26}$$

Defining the parameter $a = (1+\delta^2)/(1-\delta^2)$ (with $|a| > 1$) such that $|\delta| = \sqrt{(a-1)/(a+1)}$, the second integral is

$$\frac{\delta}{1-\delta^2}\int_{-\pi}^{\pi}\frac{1}{\cos k + \frac{1+\delta^2}{1-\delta^2}}dk = \frac{\delta}{1-\delta^2}\int_{-\pi}^{\pi}\frac{1}{\cos k + a}dk, \tag{3.27}$$

the indefinite integral is obtaind via

$$\int\frac{1}{\cos k + a}dk = \frac{2}{\sqrt{a^2-1}}\tan^{-1}\left(\sqrt{\frac{a-1}{a+1}}\tan\frac{k}{2}\right) + cte, \tag{3.28}$$

and now putting upper and lower bounds, the integral becomes definite, as

$$\begin{aligned}\int_{-\pi}^{\pi}\frac{1}{\cos k + a}dk &= \frac{2}{\frac{2|\delta|}{1-\delta^2}}\left\{\tan^{-1}\left[|\delta|\tan\left(\frac{\pi}{2}\right)\right] - \tan^{-1}\left[|\delta|\tan\left(-\frac{\pi}{2}\right)\right]\right\}; \\ &= \frac{1-\delta^2}{|\delta|}\mathrm{sgn}(\delta)\pi,\end{aligned} \tag{3.29}$$

and the topological invariant is

$$\nu = \frac{1}{2}\left[1 - \text{sgn}\left(\delta\right)\right], \Longrightarrow \qquad \nu = \begin{cases} \nu = 1 & \text{if} \quad \delta < 0, \\ \nu = 0 & \text{if} \quad \delta > 0. \end{cases} \tag{3.30}$$

The winding number is seen in the schematic Figure 3.3, as the two different geometry of the circles, one circulates the origin ($\delta < 0$) and the other doesn't. Since the generated curve of the vector $\mathbf{d}(k)$ over the Brillouin Zone provides information about the winding number, it is called the Winding Vector.

One could say that there exists ambiguity in the topological phase, since it is possible to choose the unit cell in the sequence AB or BA. But, the way it is derived, since the amplitude of the in-site hopping is defined as $t + \delta t$ and the off-site hopping $t - \delta t$, the ambiguity disappears.

The non-vanishing topological invariant admits non-local states at the edges of the system. Such edge states have zero energy, as shown in the previous subsection, in Figure 3.2.

Since the integral is not so trivial to obtain for generic values of the parameter[2], and very often it is much harder to obtain the integral of more complex curves, it is interesting to avoid the complex integral, and focus on the geometrical aspect of the topological invariant. The winding number can be identified in a closed loop by the following procedure:

a) Since the curve $\mathbf{d}$ is oriented, it is possible to trace a similar curve always in the left side $\mathcal{C}_L$ and another similar curve always in the right side $\mathcal{C}_R$;

b) Taking an arbitrary curve $\mathcal{L}$ leaving from the origin to infinity in any direction (one possible choice is the ray $d_y = 0$ and $d_x \geq 0$);

c) Identify the intersections of $\mathcal{L}$ with $\mathbf{d}$;

d) To each intersection it is imposed a signature: $+1$ if the ray $\mathcal{L}$ intersects first $\mathcal{C}_R$ and -1 if the ray $\mathcal{L}$ intersects first $\mathcal{C}_L$.

[2]Remembering that the curve is just a circumference.

e) The winding number is the summation of the signatures.

To modify the winding number, it is necessary to close the gap or add a term breaking the symmetries of the system, allowing states (in the Bloch sphere) out of the equator.

From the winding number, it is possible to produce a topological phase diagram, shown in Figure 3.4, for different values of $v \equiv 1 + \delta$ and $w \equiv 1 - \delta$ (δ is not a relevant quantity), such that $v + w \neq 2$.

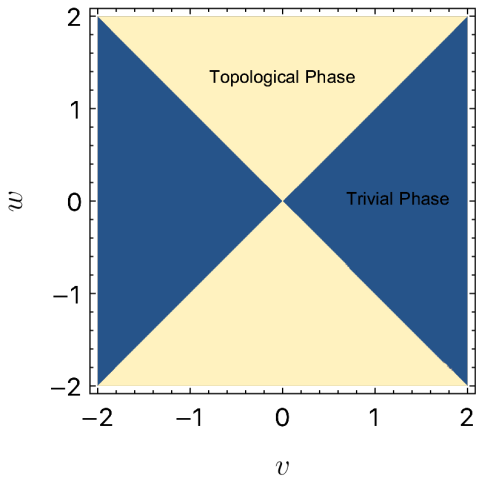

FIGURE 3.4. Topological phase diagram for the SSH model shows topological and trivial phases exhibited by ν considering the parameters v, w.

3.2.1 Polarization

For the SSH model, the polarization is known by the relation obtained previously in 2.96. The way to put the polarization is

$$p_{\pm} = -\frac{q}{2}\nu \bmod(e) = \frac{q}{4}(1 - \mathrm{sgn}(\delta)), \Longrightarrow \qquad \nu = \begin{cases} p_{\pm} = \frac{e}{2} & \text{if} \quad \delta < 0, \\ \nu = 0 & \text{if} \quad \delta > 0, \end{cases} \tag{3.31}$$

and the distinction between polarization eigenvalues are related to the topological phases. In the trivial phase, $\delta > 0$, there is no polarization since all states are combined in the interior of the chain unit cell.

Considering now the topological phase ($\delta < 0$), the hopping between sites of different cells is greater than the hopping inside one cell, has a special meaning. For

open chains, the edges become unpaired, generating an excess of charge in one edge and a lack at the other.

3.3 Symmetries and Ten-Fold Way

Beyond the usual symmetries (like the global/local phase symmetry and the symmetries of the point group), there is another class of non-spatial symmetries: time reversal, particle-hole and chiral, as shown by (42, 43).

Definition 4 (Non-Unitary Symmetries)**.** *The non-unitary symmetries obey the following properties*

(i) *Time reversal: Operators act on the (first quantized) Hamiltonian $h(k)$ of the reciprocal space according to the relations as $T \equiv U_T K$, is a anti-unitary and commuting symmetry*

$$Th(k)T^{-1} = U_T h^*(-k)U_T^{-1} = h(-k). \tag{3.32}$$

(ii) *Particle-hole: Operators act on the reciprocal space Hamiltonian following the relations as $C \equiv U_C K$, is anti-unitary and anti-commuting symmetry*

$$Ch(k)C^{-1} = U_C h^*(-k)U_C^{-1} = -h(-k). \tag{3.33}$$

(iii) *Chiral: Operators act on the reciprocal space Hamiltonian according to the relations as $S \equiv U_S$, is unitary and anti-commuting*

$$Sh(k)S^{-1} = -h(k), \tag{3.34}$$

the chiral symmetry can be interpreted as the product of the time reversal and the particle hole symmetry, which can be expressed as $S = TC = U_T U_C$. This result, guarantees to each positive/negative energy, another state with negative/positive energy.

The presence/absence of different possible choices of such non-unitary symmetries are summarized in the usually called ten-fold way, as follows in the Table 3.1.

Symmetry Class	Time Reversal T	Particle-Hole C	Chiral S
BDI	$+1$	$+1$	1
CII	-1	-1	1
CI	$+1$	-1	1
DIII	-1	$+1$	1
AI	$+1$	0	0
AII	-1	0	0
D	0	$+1$	0
C	0	-1	0
AIII	0	0	1
A	0	0	0

TABLE 3.1. Classification of non-unitary symmetries. The presented signs indicate the the sign of the square operator $\mathcal{O}^2$, for the operators $\mathcal{O} = \mathcal{T}, \mathcal{C}, \mathcal{S}$.

Unitary spatial symmetries are of interest too. Specially, it is important to remember the action of the inversion operator (inversion symmetry when commutes with the Hamiltonian)

$$Ih(k)I^{-1} = h(-k) \tag{3.35}$$

in the above table, the SSH model has the time reversal symmetry, the particle hole symmetry (both squared to plus one, $T^2 = C^2 = +1$) and consequently the chiral symmetry. Those are known the BDI systems.

3.3.1 Chiral Symmetry

Since the BDI class has all symmetries and the chiral symmetry is identified as the product of both time reversal and particle hole, then is sufficient to study this symmetry. From the above definition, it must be true that $S^\dagger = S$ and $S^2 = \mathbb{1}$. Equivalently, is it possible to define projector operators of the sublattices P_A, P_B

$$P_A\mathcal{H}P_A = P_B\mathcal{H}P_B = 0; \qquad P_A\mathcal{H}P_B + P_B\mathcal{H}P_A = \mathcal{H}, \tag{3.36}$$

a different approach to define the sub-lattice symmetry[3] meaning that being in one of the sub-lattices, cannot transition to the same species.

[3]Synonym of chiral symmetry.

The SSH model is bipartite, the projectors can be constructed as

$$P_A = \sum_{m=1}^{N} c_{Am} c_{Am}^{\dagger} = \sum_{m=1}^{N} \left(1 - c_{Am}^{\dagger} c_{Am}\right), \quad P_B = \sum_{m=1}^{N} c_{Bm} c_{Bm}^{\dagger} \sum_{m=1}^{N} \left(1 - c_{Bm}^{\dagger} c_{Bm}\right), \quad (3.37)$$

and the chiral operator S is

$$S = P_A - P_B = -\sum_{m=1}^{N} \left(c_{Am}^{\dagger} c_{Am} - c_{Bm}^{\dagger} c_{Bm}\right) = -\sum_{m=1}^{N} \sigma_z. \quad (3.38)$$

The operator S obviously commutes with the Hamiltonian, since (in the coordinate space, for the spinor $\psi_n = (c_{An}, c_{Bn})^T$) writing

$$\begin{aligned} S\mathcal{H}S &= \sum_m \sigma_z \sum_{j=1}^{N-1} \left((t+\delta t) c_{Aj}^{\dagger} c_{Bj} + (t-\delta t) c_{Bj}^{\dagger} c_{Aj+1} + \text{h.c.}\right) \sum_n \sigma_z; \\ &= \sum_m \sigma_z \left((t+\delta t) \sum_{j=1}^{N} \psi_n^{\dagger} \sigma_x \psi_n + (t-\delta t) \sum_{j=1}^{N-1} \psi_n^{\dagger} \sigma_x \psi_{n+1}\right) \sum_n \sigma_z = -\mathcal{H}, \end{aligned} \quad (3.39)$$

the second sum, in the parentheses of the second line indicates "off"-site hopping (making the Fourier transform, there will appear the e^{ik} term), in other words, as $\mathcal{H}$ does not depend on the z component of the Pauli matrices, the chiral operator is a symmetry. Beyond that, since hopping amplitudes can depend on the position and there will be no symmetry breaking, the symmetry is robust.

Example 2 (Chiral SSH Model)**.** *Considering now the SSH model with complex hopping parameters $v, w = |w|e^{i\delta} \in \mathbb{C}$, as in (44, 45), the Hamiltonian*

$$h(k) = \left[\frac{v}{w} + \cos(k-\delta)\right] \sigma_x + \sin(k-\delta)\, \sigma_y, \quad (3.40)$$

breaks the time reversal and the particle-hole symmetries, since $h^*(-k) \neq \pm h(k)$. As long as there is no σ_z in $h(k)$, the chiral symmetry remains, and from Table 3.1, the symmetry class is now AIII.

A subtle point is that, making a Gauge transformation of $c_n \to e^{i\delta n} c_n$, the non-unitary symmetries are recovered, and the model again is of the BDI class. Considering at least two interacting chains of AIII class, the gauge transformation above does not recover the non-unitary symmetries.

Example 3 (Chiral Symmetry Breaking: Rice-Mele Model)**.** *Introduced by Rice and Mele (46), a staggered local potential Δ in the SSH model (more information on the literature such as (1, 36, 47)), the Hamiltonian is now expressed as*

$$\mathcal{H} = \sum_{i=1}^{N} \left[\Delta \left(c_{iA}^{\dagger} c_{iA} - c_{iB}^{\dagger} c_{iB} \right) + (t + \delta t)\, c_{Ai}^{\dagger} c_{Bi} \right] + \sum_{i=1}^{N-1} (t - \delta t)\, c_{Ai+1}^{\dagger} c_{Bi} + h.c.$$
$$h(k) = \left(\frac{v}{w} + \cos k \right) \sigma_x + \sin k \sigma_y + \Delta \sigma_z, \tag{3.41}$$

as now it is introduced a σ_z term in the Hamiltonian the chiral symmetry is broken and there are no topological phases.

Example 4 (Chiral Symmetry Breaking: Pump Model)**.** *Adding a cyclic adiabatic evolution to the parameters $v = v(t), w = w(t)$ and $\Delta = \Delta(t)$ and requiring that $h(k,t) = h(k, t+T)$ for a time $T \ll \hbar / min\,(2v(t), 2w(t), 2\Delta(t))$, such that the evolution of the Hamiltonian is quasi-static, then a new topological feature can be explored. This model is 'two dimensional, and has no time reversal symmetry, so there is a Chern number associated (associated to a polarization, or the number of transported electrons from one edge to the other). This cyclic evolution is also called Adiabatic Pump, and for the case of the Rice-Mele pump model, is called Thouless Charge Pump.*

Example 5 (Chiral Symmetry Breaking: Spin Pump Model)**.** *Introducing spin to the above adiabatic problem, the pump is called Fu-Kane spin Pump. Time reversal symmetry is recovered and the Chern number is not an invariant (since time reversal implies a vanishing Chern number), and the invariant is a $\mathbb{Z}_2$ invariant (corresponding to a spin flip in the edges of the chain).*

3.3.2 Inversion Symmetry

The SSH model has an additional (unitary) symmetry, the inversion symmetry. In the reciprocal space, the Hamiltonian obeys the property

$$\sigma_x h_k \sigma_x = h_{-k}. \tag{3.42}$$

It is observed that for $k = 0$ and $k = \pi$, the Hamiltonian maps to itself (for the reciprocal lattice vector $K = 2\pi$). In these points, the Hamiltonian commutes with inversion

and consequently the eigenvalue is also eigenvalue of the inversion operator. For the mentioned points, the hamiltonian is simply

$$\mathcal{H}(0) = 2\sigma_x; \qquad \mathcal{H}(\pi) = 2\delta\sigma_x, \tag{3.43}$$

and the eigenvalues are $\epsilon_\pm(0) = \pm 2$ and $\epsilon_\pm(\pi) = \pm 2\delta$. By that, at half filling, just the band with smaller eigenvalue is filled.

Since at $k = 0$, the dispersion is independent, then $|\sigma_x = -1\rangle$ is the eigenstate of the occupied band. And, this state is also the eigenstate of the inversion operator, with eigenvalue $\hat{\pi}_{k=0} = -1$.

Now, for $k = \pi$, the eigenvalue depends on δ, and for $\delta > 0$ the same eigenstate is filled ($|\sigma_x = -1\rangle$) and again the eigenvalue of the inversion operator is $\hat{\pi}_{k=\pi} = -1$. Now, for $\delta < 0$, the filled eigenstate has another energy, and the parity operator has different eigenvalue $\hat{\pi}_{k=\pi} = +1$. Now the product of the inversion symmetric points gives rise to another version of the topological invariant, which can be expressed as

$$\nu_{\mathbb{Z}_2} \equiv \hat{\pi}_0\hat{\pi}_\pi = \pm 1. \tag{3.44}$$

The different phases cannot be connected without closing the gap. In the case of BDI class systems (with inversion symmetry), the winding number and the inversion symmetric invariant represents the same topological phase.

Insulating systems like the Rice Mele model, beyond breaking the chiral symmetry, breaks the inversion symmetry for generic values of the parameters (36, 48). For instance, choosing a specific path for the parameters, the inversion symmetry is recovered, alternating the system from the SSH model limit ($\Delta = 0$ from 3.41) to the *charge density wave* limit, for $v = w$, and the system is called *topological crystalline insulator*. In superconductor physics, the spatial symmetries also play an important role (49, 50).

The principal results obtained in the chapter are the new topological invariant defined (winding number) and the derived phase diagram. From the theory of polarization 2.96, the physical interpretation of the topological phase is given by the net polarization in a finite chain (for example Polyacetilene). Finally, the determination of

non-unitary symmetry conditions for the topological properties, give us information about deformations that supposedly maintain robust the behavior of such emergent phenomena.

Chapter 4

One dimensional p-wave Superconductor

4.1 Majorana Basis

This chapter deals with a different kind of constituent. New particles arise from the symmetry properties of the ground state. Changing the perspective of the degrees of freedom in the particle-hole space, as done in the last chapter, it is now interesting to make a change in the constituents of a Dirac fermion from the Majorana point of view (essentially, a basis change). In the Majorana basis, the (Dirac) fermionic operators are written in terms of new real fields η_j^A, η_j^B, the Majorana fermionic operators

$$c_j = \frac{1}{\sqrt{2}}\left(\eta_j^A + i\eta_j^B\right); \qquad c_j^\dagger = \frac{1}{\sqrt{2}}\left(\eta_j^A - i\eta_j^B\right), \tag{4.1}$$

$$\eta_j^A = \frac{1}{\sqrt{2}}\left(c_j + c_j^\dagger\right); \qquad \eta_j^B = \frac{i}{\sqrt{2}}\left(c_j^\dagger - c_j\right), \tag{4.2}$$

the matrix of basis change between spinors is

$$\eta_j = \begin{pmatrix} \eta_j^A \\ \eta_j^B \end{pmatrix} = \frac{1}{\sqrt{2}} \begin{pmatrix} 1 & 1 \\ -i & i \end{pmatrix} \begin{pmatrix} c_j^\dagger \\ c_j \end{pmatrix} = B\psi_j, \tag{4.3}$$

as shown schematically in the Figure 4.1.

The anti-commutation relations are given by

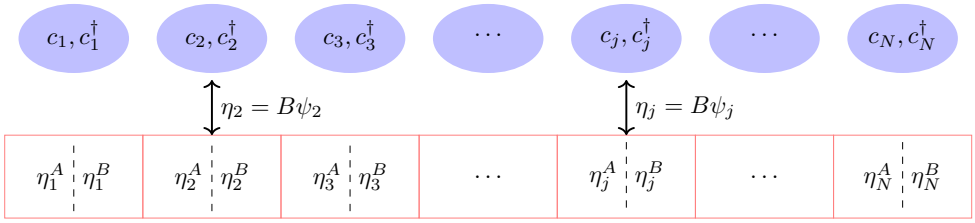

FIGURE 4.1. Majorana basis change, following the transformation B defined at equation 4.3, the upper chain, represent the sites, ad the bottom the corresponding real Majorana operators. The hopping operators are not presented in this scheme.

$$\begin{aligned}\{\eta_j^A, \eta_{j'}^A\} &= \frac{1}{2}\{c_j + c_j^\dagger, c_{j'} + c_{j'}^\dagger\} = \frac{1}{2}\left(\{c_j, c_{j'}\} + \{c_j, c_{j'}^\dagger\} + \{c_j^\dagger, c_{j'}\} + \{c_j^\dagger, c_{j'}^\dagger\}\right); \\ &= \frac{1}{2}\left(\{c_j, c_{j'}^\dagger\} + \{c_j^\dagger, c_{j'}\}\right) = \delta_{jj'}; \qquad (4.4)\\ \{\eta_j^B, \eta_{j'}^B\} &= -\frac{1}{2}\left(\{c_j - c_j^\dagger, c_{j'} - c_{j'}^\dagger\}\right) = -\frac{1}{2}\left(\{c_j, c_{j'}\} - \{c_j, c_{j'}^\dagger\} - \{c_j^\dagger, c_{j'}\} + \{c_j^\dagger, c_{j'}^\dagger\}\right); \\ &= \frac{1}{2}\{c_j, c_j^\dagger\} + \{c_j^\dagger, c_{j'}\} = \delta_{jj'}, \qquad (4.5)\end{aligned}$$

and between the two species η_j^A, η_j^B, the relations are

$$\begin{aligned}\{\eta_j^A, \eta_{j'}^B\} &= \frac{i}{2}\{c_j + c_j^\dagger, c_{j'}^\dagger - c_{j'}\} = \frac{i}{2}\left(\{c_j, c_{j'}^\dagger\} - \{c_j, c_{j'}\} + \{c_j^\dagger, c_{j'}^\dagger\} - \{c_j^\dagger, c_{j'}\}\right); \\ &= i\left(\{c_j, c_{j'}^\dagger\} - \{c_j^\dagger, c_j\}\right) = 0. \qquad (4.6)\end{aligned}$$

So, for Majorana fermions, there is a new relation $\eta^\dagger = \eta$. Essentially, Majoranas are their own antiparticles. Since the anti-commuting relations are still valid, the Majorana operators are generators of a Clifford Algebra.

Taking a generic quadratic Hamiltonian (such as a superconductor or an insulator), given in terms of a spinor $\Psi = (\psi_1, \ldots, \psi_N, \psi_1^\dagger, \ldots, \psi_N^\dagger)^T$, it is possible to write

$$\mathcal{H} = \Psi^\dagger H \Psi. \qquad (4.7)$$

However, it is interesting to analyze the problem on a Majorana basis. This change of the internal degrees of freedom (in site degrees of freedom) is expressed as the matrix B 4.3. The Hamiltonian in the Majorana basis is expressed in terms of the species η_j^A, η_k^B, such that the Hamiltonian is

$$\mathcal{H} = i\sum_{i,j} \eta_i^A A_{ij} \eta_j^B = \frac{i}{2}\sum_{i,j,n} \eta_i^n A_{ij} \eta_j^{\bar{n}}, \qquad (4.8)$$

in the case of non-interacting chains, there are no interactions like $\eta_i^A \eta_j^A$, just $\eta_i^A \eta_j^B, \eta_i^B \eta_j^A$. Therefore, the matrix A_{ij} is a real anti-symmetric matrix of dimension $2N \times 2N$. Writing a new spinor of the form $\eta = (\eta_1^A, \ldots, \eta_N^A, \eta_1^B, \ldots, \eta_N^B)^T$, the Hamiltonian in the Majorana basis can be expressed as

$$\mathcal{H} = \frac{i}{2} \sum_{i,j,n} \eta_i^n A_{ij} \eta_j^{\bar{n}} = \frac{i}{2} \eta^T \begin{pmatrix} 0 & -A^T \\ A & 0 \end{pmatrix} \eta. \tag{4.9}$$

Given a similarity transformation W, real and orthogonal ($W^T = W^{-1}$), it acts in the Majorana basis as

$$\vec{b} = \begin{pmatrix} b_1^A \\ \vdots \\ b_N^A \\ b_1^B \\ \vdots \\ b_N^B \end{pmatrix} = W \begin{pmatrix} \eta_1^A \\ \vdots \\ \eta_N^A \\ \eta_1^B \\ \vdots \\ \eta_N^B \end{pmatrix} = W\eta \Longleftrightarrow \qquad \eta = W^T \vec{b}, \tag{4.10}$$

and the operators $b_j^{A(B)}$ are states of the Hamiltonian that obey the relation $\mathcal{H}_D b_i^B b_i^A = \epsilon_i b_i^B b_i^A$ with eigenenergy ϵ_j. The diagonalization of the Hamiltonian provides a 2×2 block diagonal matrix in the following form

$$\mathcal{H} = \frac{i}{2} \eta^T A \eta \Longrightarrow \mathcal{H}_D = \mathbf{b}^T W A W^T \mathbf{b} = \mathbf{b}^T \begin{pmatrix} 0 & \oplus_{\lambda_i}(-\epsilon_{\lambda_i}) \\ \oplus_{\lambda_i} \epsilon_{\lambda_i} & 0 \end{pmatrix} \mathbf{b}. \tag{4.11}$$

4.2 Ground State

Superconducting Hamiltonians, as exemplified in the works of (51, 52), can be written in terms of Bogoliubov excitations

$$\mathcal{H} = \sum_{k \in ZB} E_k \gamma_k^\dagger \gamma_k = \sum_{k>0} E_k \left(\gamma_k^\dagger \gamma_k - \gamma_{-k} \gamma_{-k}^\dagger \right), \tag{4.12}$$

and, from this expression, the ground state can be determined, as the state without Bogoliubov excitations, such that

$$\gamma_k \left| GS \right\rangle = 0, \tag{4.13}$$

for every value of k. The ground state is, therefore, determined in terms of $|0\rangle$ as

$$\begin{aligned}
|GS\rangle &= \prod_{k>0} \gamma_{-k}\gamma_k |0\rangle = \prod_{k>0} \left(u_{-k}c_{-k} + v_{-k}c_k^\dagger\right)\left(u_k c_k + v_k c_{-k}^\dagger\right)|0\rangle\,; \\
&= \prod_{k>0} \left[\left(u_k c_{-k} - v_k c_k^\dagger\right)\left(u_k c_k + v_k c_{-k}^\dagger\right)\right]|0\rangle\,; \\
&= \prod_{k>0} \left(u_k^2 c_{-k}c_k + u_k v_k c_{-k}c_{-k}^\dagger - v_k u_k c_k^\dagger c_k - v_k^2 c_k^\dagger c_{-k}^\dagger\right)|0\rangle\,; \\
&= \prod_{k>0} \left(v_k u_k - v_k^2 c_k^\dagger c_{-k}^\dagger\right)|0\rangle\,,
\end{aligned} \tag{4.14}$$

being that $u_{-k} = u_k, v_{-k} = -v_k$ and $c_k|0\rangle = 0$. The normalized state is

$$|GS\rangle = \prod_{k>0} \left(u_k - v_k c_k^\dagger c_{-k}^\dagger\right)|0\rangle\,. \tag{4.15}$$

From the superconducting terms, the fermionic number $\hat{n}$ is not a conserved quantity, but since all operators appear in pairs, the fermion parity is a conserved quantity, therefore the parity operator is well-defined:

Definition 5 (Parity Operator)**.** *The parity operator is the operator that shows us the parity (even/odd) of the system*

$$\mathcal{P} \equiv e^{i\pi \sum_{j=1}^{N} c_j^\dagger c_j}. \tag{4.16}$$

Lemma 1. *For any quadratic system, the parity is conserved. Only systems with odd products of fermionic operators do not conserve the parity (e.g. $(c_j + c_j^\dagger)$).*

Proof. The aim is to prove that the parity operator $\mathcal{P}$ is a conserved quantity, i.e. that the commutator $[\mathcal{P}, \mathcal{H}] = 0$, for a Hamiltonian that has an even product of creation or annihilation. The commutator is

$$[\mathcal{P}, \mathcal{H}] = \left[e^{i\pi \sum_j c_j^\dagger c_j}, \mathcal{H}\right] = \left[e^{i\pi \hat{N}}, \mathcal{H}\right], \tag{4.17}$$

the Hamiltonian does not necessarily commute to the number operator $\hat{N}$. Instead, since there is an even number of creation/annihilation operators in the Hamiltonian, the parity sector (even/odd) must stay the same before/after the product of Hamiltonian, and the commutator is

$$[\mathcal{P}, \mathcal{H}] = e^{\pm i\pi}\mathcal{H} - \mathcal{H}e^{\pm i\pi} = 0, \tag{4.18}$$

hence the Hamiltonian commutes with the parity operator. □

One way of measuring parity switches was introduced in the paper of Kitaev and is currently used in other works, like (9, 26, 53, 27). The fermionic parity, defined previously, can be written in the Majorana basis as the product

$$\mathcal{P} \equiv \prod_{i=1}^{N} \eta_i^A \eta_i^B, \tag{4.19}$$

so the contribution of all operators is relevant.

Since there is a basis for which the Hamiltonian gets diagonalized, see the orthogonal transformation W (equations 4.10,4.11), and realizing that the determinant of the Hamiltonian will always be non-negative (skew-symmetric matrix), it is interesting to analyze the Pfaffian. The Pfaffian for a finite matrix can be written as

$$\mathrm{Pf}(-i\mathcal{H}) = \mathrm{Pf}\left(\frac{1}{2}\begin{pmatrix} 0 & -A^T \\ A & 0 \end{pmatrix}\right) = \det\{A\} = \det\{A^T\}. \tag{4.20}$$

Since the interest comes for the parity, the interest lies in the sign of the Pfaffian, so the fermionic parity of the ground state is

$$\mathcal{P} = \mathrm{sgn}\left[\mathrm{Pf}\left(-i\mathcal{H}\right)\right] = \mathrm{sgn}\left(\det\{A\}\right). \tag{4.21}$$

4.3 The Kitaev Chain

One of the simplest models of a one-dimensional p-wave superconductor is the spinless chain called Kitaev Chain, initially developed in (9). This model is described by the following Hamiltonian

$$\mathcal{H} = -\mu \sum_{j=1}^{N} c_j^\dagger c_j - \sum_{j=1}^{N-1} \left[t\left(c_j^\dagger c_{j+1} + c_{j+1}^\dagger c_j\right) - \Delta\left(c_{j+1}^\dagger c_j^\dagger + c_j c_{j+1}\right)\right], \tag{4.22}$$

for hopping amplitude t, superconducting gap Δ, and chemical potential μ (parameters are supposed real-valued). The operators $c_j/c_j^\dagger$ are the spinless fermionic annihilation/creation operators, obeying the standard anti-commuting relations

$$\{c_i, c_j\} = \{c_i^\dagger, c_j^\dagger\} = 0; \qquad \{c_i, c_j^\dagger\} = \delta_{ij}. \tag{4.23}$$

Via the Fourier transformation over the first Brillouin Zone of the operators, then

$$c_j = \frac{1}{\sqrt{N}} \sum_k e^{ikj} c_k, \tag{4.24}$$

and the Hamiltonian is rewritten as

$$\begin{aligned}
\mathcal{H} =& -\mu \sum_{j=1}^{N} \frac{1}{N} \sum_{k,k'} e^{ikj} c_k^\dagger e^{-ik'j} c_{k'} - \sum_{j=1}^{N-1} \frac{1}{N} \left[t \sum_{k,k'} \left(e^{ikj} c_k^\dagger e^{-ik(j+1)} c_{k'} + e^{ik'(j+1)} c_k^\dagger c_{k'} e^{-ik'j} \right) \right. \\
&\left. + \Delta \sum_{k,k'} \left(e^{ik(j+1)} c_k^\dagger e^{ik'j} c_{k'}^\dagger + e^{-ikj} c_k e^{-ik'(j+1)} c_{k'} \right) \right]; \\
\mathcal{H} =& -\mu \sum_k c_k^\dagger c_k - t \sum_k \left(e^{-ik} + e^{ik} \right) c_k^\dagger c_k + \\
&+ \frac{\Delta}{N} \sum_{j=1}^{N-1} \sum_{k,k'} \left(e^{ikj + ik'j + ik} c_k^\dagger c_{k'}^\dagger + e^{-ikj - ik'j - ik'} c_k c_{k'} \right).
\end{aligned} \tag{4.25}$$

The last term on the right-hand side is

$$\begin{aligned}
&\frac{\Delta}{N} \sum_{j=1}^{N-1} \sum_{k,k'} \left(e^{ikj + ik'j + ik'} c_k^\dagger c_{k'}^\dagger + e^{-ikj - ik - ik'j} c_k c_{k'} \right); \\
&= \Delta \sum_{k,k'} \left(\sum_j \frac{1}{N} e^{i(k+k')j} e^{ik'} c_k^\dagger c_{k'}^\dagger + \sum_j \frac{1}{N} e^{-i(k+k')j} e^{-ik'} c_k c_{k'} \right); \\
&= \Delta \sum_{k,k'} \delta_{-k,k'} e^{ik} \left(c_k^\dagger c_{-k}^\dagger + c_k c_{-k} \right),
\end{aligned} \tag{4.26}$$

and the Hamiltonian in k-space turns into

$$\mathcal{H} = \sum_k \left[-\mu c_k^\dagger c_k - 2t \cos k \, c_k^\dagger c_k + \Delta e^{ik} \left(c_k^\dagger c_{-k}^\dagger + c_k c_{-k} \right) \right], \tag{4.27}$$

From the fermionic creation/annihilation operators and remembering from the particle-hole symmetry, $h(k) = h(-k) \longrightarrow c_k c_k^\dagger = c_{-k} c_{-k}^\dagger$ provides exactly the number of holes in the system (leaving aside constant terms), we obtain

$$\mathcal{H} = \sum_k \left[-\left(\frac{\mu}{2} + t\cos k\right)\left(c_k^\dagger c_k - c_k c_k^\dagger\right) + \Delta e^{ik}\left(c_k^\dagger c_{-k}^\dagger + c_k c_{-k}\right)\right], \tag{4.28}$$

The Hamiltonian can be written in the Bogoliubov-de Gennes form in the Nambu basis, remembering that p-wave potentials must be antisymmetric so that

$$\begin{aligned}\mathcal{H} &= \frac{1}{2}\sum_k \begin{pmatrix} c_k^\dagger & c_{-k} \end{pmatrix}\begin{pmatrix} -\mu - 2t\cos k & 2i\Delta\sin k \\ -2i\Delta\sin k & \mu + 2t\cos k \end{pmatrix}\begin{pmatrix} c_k \\ c_{-k}^\dagger \end{pmatrix}; \\ \mathcal{H} &= \sum_k \psi^\dagger h_k \psi = \sum_k \psi^\dagger\big(-(\mu + 2t\cos k)\,\tau_z - 2\Delta\sin k\tau_y\big)\psi, \end{aligned} \tag{4.29}$$

for τ_i the Pauli matrices that operate in the Nambu space (particle-hole space). Introducing again the vector $\mathbf{d}(k)$

$$\mathbf{d}(k) = \sqrt{(-\mu - 2t\cos k)^2 + 4\Delta^2\sin^2 k}\begin{pmatrix} 0 \\ \sin\theta \\ \cos\theta \end{pmatrix}; \qquad \tan\theta \equiv \frac{2\Delta\sin k}{\mu + 2t\cos k}. \tag{4.30}$$

The Hamiltonian and the basis change of $\psi_k \to \gamma_k$ is expressed by the following

$$h(\phi) = E(k)\begin{pmatrix} \cos\theta & -i\sin\theta \\ i\sin\theta & -\cos\theta \end{pmatrix}, \tag{4.31}$$

$$\begin{pmatrix} \gamma_k \\ \gamma_{-k}^\dagger \end{pmatrix} = \begin{pmatrix} \cos\frac{\theta}{2} & i\sin\frac{\theta}{2} \\ -i\sin\frac{\theta}{2} & \cos\frac{\theta}{2} \end{pmatrix}\begin{pmatrix} c_k \\ c_{-k}^\dagger \end{pmatrix}. \tag{4.32}$$

The bands of the system are again given by the norm of the vector $\mathbf{d}(k)$, so that

$$E_\pm(k) = \pm\sqrt{(\mu + 2t\cos k)^2 + 4\Delta^2\sin^2 k}, \tag{4.33}$$

for $\Delta \neq 0$, at $\mu_c = -2t$, there is a quantum phase transition. This critical point separates two distinct superconducting phases (i) when $|\mu| < |\mu_c|$ and (ii) when $|\mu| > |\mu_c|$.

Observation 4 (Basis Change)**.** *Given the Majorana basis, it is interesting to represent the Kitaev Chain Hamiltonian. From the on-site coupling*

$$\begin{aligned} c_j^\dagger c_j &= \frac{\eta_j^A - i\eta_j^B}{\sqrt{2}}\frac{\eta_j^A + i\eta_j^B}{\sqrt{2}} = \frac{1}{2}\left(\eta_j^A\eta_j^A + i\eta_j^A\eta_j^B - i\eta_j^B\eta_j^A + \eta_j^B\eta_j^B\right); \\ &= i\eta_j^A\eta_j^B + \frac{\eta_j^A\eta_j^A + \eta_j^B\eta_j^B}{2} = \frac{1}{2} + i\eta_j^A\eta_j^B. \end{aligned} \tag{4.34}$$

The operators that appear in the hopping t part imply

$$\begin{aligned} c_j^\dagger c_{j+1} + c_{j+1}^\dagger c_j &= \frac{1}{2}\big[\left(\eta_j^A - i\eta_j^B\right)\left(\eta_{j+1}^A + i\eta_{j+1}^B\right) + \left(\eta_{j+1}^A - i\eta_{j+1}^B\right)\left(\eta_j^A + i\eta_j^B\right)\big]; \\ &= i\left(\eta_j^A\eta_{j+1}^B - \eta_j^B\eta_{j+1}^A\right) = -i\left(\eta_{j+1}^B\eta_j^A - \eta_{j+1}^A\eta_j^B\right), \end{aligned} \tag{4.35}$$

and finally, for the superconducting terms

$$\begin{aligned} c_j c_{j+1} - c_j^\dagger c_{j+1}^\dagger &= \frac{1}{2}\big[\left(\eta_j^A + i\eta_j^B\right)\left(\eta_{j+1}^A + i\eta_{j+1}^B\right) - \left(\eta_j^A - i\eta_j^B\right)\left(\eta_{j+1}^A - i\eta_{j+1}^B\right)\big]; \\ &= i\left(\eta_j^A\eta_{j+1}^B + \eta_j^B\eta_{j+1}^A\right), \end{aligned} \tag{4.36}$$

the Hamiltonian obtained from the change of basis is given by

$$\begin{aligned} \mathcal{H}_{KC} &= \frac{i}{2}\sum_j \left[-\mu\left(\eta_j^A\eta_j^B\right) - t\left(\eta_{j+1}^A\eta_j^B - \eta_{j+1}^B\eta_j^A\right) - \Delta\left(\eta_{j+1}^A\eta_j^B + \eta_{j+1}^B\eta_j^A\right)\right]; \\ \mathcal{H}_{KC} &= -\frac{i}{2}\sum_j \Big[\mu\eta_j^A\eta_j^B + (\Delta - t)\,\eta_{j+1}^B\eta_j^A + (\Delta + t)\,\eta_{j+1}^A\eta_j^B\Big]. \end{aligned} \tag{4.37}$$

The imaginary factor is present to guarantee the hermiticity of the Hamiltonian. One example that shows the need for the imaginary factor is the product

$$\left(\eta_j^A\eta_j^B\right)^\dagger = \left(\eta_j^B\right)^\dagger\left(\eta_j^A\right)^\dagger = \eta_j^B\eta_j^A = -\eta_j^A\eta_j^B, \tag{4.38}$$

the real product would be anti-hermitian. From the imaginary quantities, the operators and the Hamiltonian become hermitian.

Taking now a limiting case, it is already possible to give some insight into the behavior of a topological superconductor.

First, in the limit of $|\mu| \to \infty$, other parameters (t, Δ) can be neglected, so that the Hamiltonian is only

$$\mathcal{H}_{\mu\to\infty} = -\mu\sum_j \left(i\eta_j^A\eta_j^B + 1/2\right) = -\mu\sum_j c_j^\dagger c_j. \tag{4.39}$$

In this case, the ground state is composed of the corresponding harmonic oscillator (vacuum in the case of all sites unoccupied). Adding electrons to the system, by the

Majorana representation, the electron modes are coupled in the sites $\eta_j^A \eta_j^B$ and is possible to fill N electrons in the chain.

The second case happens to the limit case of $\mu = 0$ and $t = -\Delta > 0$. In this case, the Hamiltonian is reduced to

$$\mathcal{H} = it \sum_j \eta_{j+1}^B \eta_j^A , \tag{4.40}$$

now the fermions added to the system are coupled between nearest neighbour sites. The description made above (in finite open chains) results in zero energy modes at the edges of the system, shown in Figure 4.2. The same result is valid for $t = \Delta$, but the roles of each species of the Majoranas are switched.

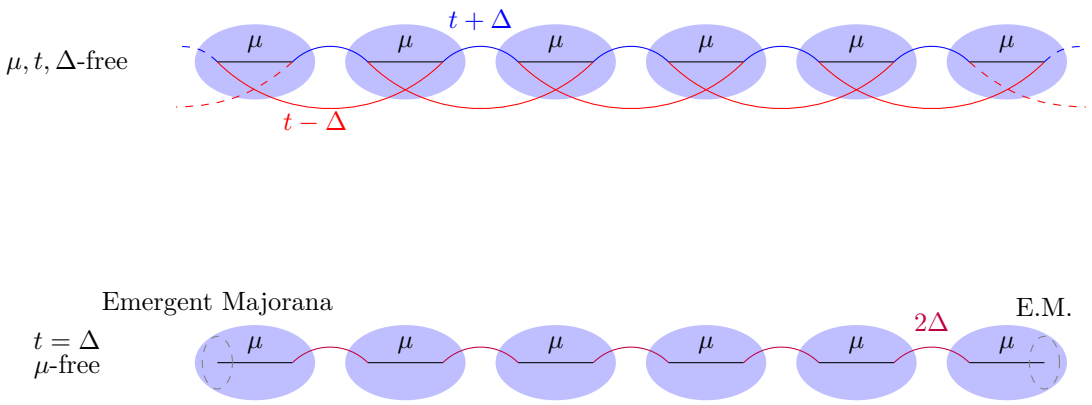

FIGURE 4.2. Schematic diagrams show the hopping interactions between Majorana operators η_i^A, η_j^B in a finite chain. (Upper panel) shows hopping for generic parameters μ, t, Δ, as in the Hamiltonian 4.37. (Bottom panel) hopping interaction for a specific selection of parameters $t = \Delta$; in this case, an Emergent Majorana (E.M.) at the edge of the system becomes relevant when $\mu \ll 2\Delta$.

Taking now a different basis for the fermionic operators,

$$d_j = \frac{1}{\sqrt{2}} \left(\eta_{j+1}^B + i \eta_j^A \right) , \qquad \rightarrow \begin{cases} \eta_{j+1}^B = \frac{1}{\sqrt{2}} \left(c_j + c_j^\dagger \right) , \\ \eta_j^A = \frac{i}{\sqrt{2}} \left(c_j^\dagger - c_j \right) , \end{cases} \tag{4.41}$$

in the proposed limit, substituting the Majorana Operators in the transformation $(\eta_j^A, \eta_j^B) \rightarrow (d_j, d_j^\dagger)$, the Hamiltonian is written as

$$\mathcal{H} = it\sum_{j=1}^{N}\eta_{j+1}^{B}\eta_{j}^{A} = t\sum_{j}\left(d_{j}^{\dagger}d_{j} - \frac{1}{2}\right), \tag{4.42}$$

which is essentially the same Hamiltonian of a local tight-binding model. For open chains, some operators do not appear in the Hamiltonian, namely η_1^B, η_N^A which can be united in a (very) non-local fermion d_0, defined as

$$d_0 = \frac{1}{\sqrt{2}}\left(\eta_1^B + i\eta_N^A\right). \tag{4.43}$$

This mode has zero energy since it does not appear in the Hamiltonian, and for the Majoranas to be uncoupled, this fermion must be unoccupied. In the thermodynamic limit, this non-local fermion is always unoccupied, since the overlap between Majoranas is inexistent.

For a chain model with N sites, both even and odd ground states may exist. In a contrary manner to what could be thought, as in the XY-model (via Jordan-Wigner Transformation) presented in (54, 51), where boundary conditions give rise to different parity sectors, the Kitaev chain is expected to change parity only if the number of sites in the chain changes by unity, since all electron/holes are created in pairs.

A different reason for parity changes in the Kitaev chain is the overlap between Majorana operators η_1^B, η_N^A, allowing a possible non-local fermionic state appear, as defined in 4.43. In the topological phase, the occupancy $n_d = d_0^{\dagger}d_0 = 0$ means that the Majorana fermions are unpaired, while if $n_d = 1$, the fermion is occupied and the chain exhibits a non-local fermion.

4.3.1 Topological Phase Diagrams

The Kitaev chain Hamiltonian is, apart from being written in the particle-hole space, analogous to the Hamiltonian of an insulator. This way, taking a similar path to that obtaining the topological invariant of the superconducting system, from the representation of the Hamiltonian in the reciprocal space, in terms of the angle θ (Equation 4.30) the B-dG excitations are written as

$$\gamma_k = \cos\frac{\theta}{2}c_k - i\sin\frac{\theta}{2}c_{-k}^{\dagger}; \qquad \gamma_{-k}^{\dagger} = i\sin\frac{\theta}{2}c_k + \cos\frac{\theta}{2}c_{-k}^{\dagger}, \tag{4.44}$$

for the single particle eigenstates. Now, making a similarity transformation U over the matrix representation of the Hamiltonian (a rotation of the $\mathbf{d}(k)$ vector such that the Pauli Matrices are transformed as $(\tau_z, \tau_y) \mapsto (\tau_x, \tau_y)$), we get

$$\begin{aligned}\tilde{h}_{BdG} &= U h_{BdG} U^\dagger = e^{-i\pi\tau_y/4} h_{BdG} e^{i\pi\tau_y/4}; \\ &= \left(\cos\frac{\pi}{4}\mathbb{1} - i\sin\frac{\pi}{4}\tau_y\right)\left[-\left(\mu + 2t\cos k\right)\tau_z - \left(2\Delta\sin k\right)\tau_y\right]\left(\cos\frac{\pi}{4}\mathbb{1} + i\sin\frac{\pi}{4}\tau_y\right); \\ \tilde{h}_{BdG} &= \frac{1}{2}\sum_k \left[-\left(\mu + 2t\cos k\right)\tau_x + \left(2\Delta\sin k\right)\tau_y\right] = \sum_k \mathbf{d}(k)\cdot\vec{\tau}.\end{aligned} \tag{4.45}$$

Observation 5. *It is still possible to define a complex number*

$$\rho \equiv -\left(\mu + 2t\cos k\right) + 2i\Delta\sin k, \tag{4.46}$$

equivalent to the vector $\mathbf{d}(k)$.

Now, it is possible to define another angle ϕ, similar to θ

$$\phi = \arctan\frac{2\Delta\sin k}{-\mu - 2t\cos k}. \tag{4.47}$$

The eigenvectors are now identical to the SSH insulator described previously 3.14. The topological properties of the chain are obtained through the Zak phase

$$\Phi_\pm = i\int_{ZB}\langle u_\pm|\partial_k u_\pm\rangle\, dk = \pm\int_{-\pi}^{\pi}\frac{\mathrm{d}\phi}{\mathrm{d}k}dk, \tag{4.48}$$

and the winding number can be determined exactly as in the previous chapter. It is still possible to remove one of the parameters making $\mu \to \mu/t = \mu$ and $\Delta \to \Delta/t = \Delta$. It is already known that $\phi(k)$ is an odd function.

Considering that the function ϕ is continuous, the fundamental theorem of calculus (FTC) would be applied, and the integral of the derivative of ϕ over all the BZ would be zero. But instead, when there are discontinuities, the FTC does not apply anymore.

Realizing that, for $|\mu| < 2$, the function is discontinuous (as shown in Figure 4.3, discontinuous and odd). For the BZ defined over $(-\pi, \pi)$, it is simpler to consider half of the domain (interval $(0, \pi)$). The integral of interest is now confined to the region

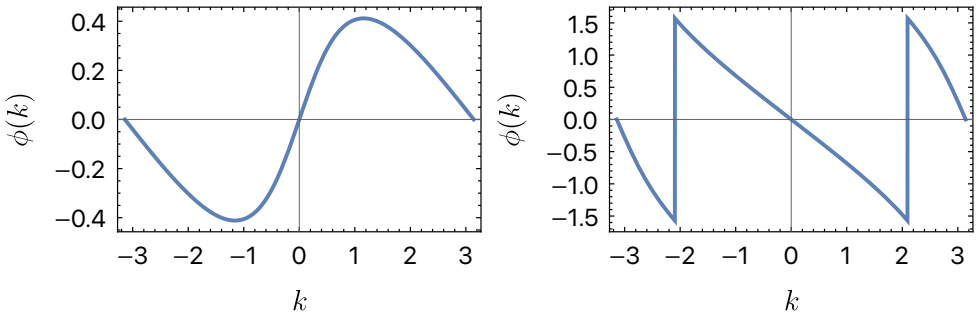

FIGURE 4.3. Both plots show two different limits of the function $\phi(k)$, for $\Delta = 1$, in the left panel: $\mu = -5$ and in the right panel: $\mu = 1$.

$$I = \int_0^{\pi} \frac{\mathrm{d}\phi}{\mathrm{d}k} dk, \tag{4.49}$$

over the continuous parts, the positive and negative integral parts must cancel, but, since there are discontinuities at $\pm k_0 = \arccos(-\mu/2)$, and realizing that at $k_0 - dk$ the sign of $\phi(\pm k_0 - dk)$ over all Brillouin zone are the same, the work of computing the Zak phase (and the topological invariant) reduces to sum the signs of discontinuities. The integral I is decomposed in

$$\Phi = \int_0^{k_0} \frac{\mathrm{d}\phi}{\mathrm{d}k} dk + \int_{k_0}^{\pi} \frac{\mathrm{d}\phi}{\mathrm{d}k} dk, \tag{4.50}$$

In the case of $|\mu| < 2$, the discontinuities go to $\tan^{-1}\left[2\Delta \sin k / \left(-\mu - 2t\cos k_0\right)\right] \to \pm\pi/2$ for $\cos k_0 \to -\mu/2t$. The sign of $\pm\pi/2$ depends on the sign of Δ. Summing over all discontinuities of the Brillouin zone

$$\begin{aligned}\nu = \frac{1}{2\pi}\int_{-\pi}^{\pi} \frac{\mathrm{d}\phi}{\mathrm{d}k} dk = \frac{1}{2\pi}\Bigg\{ &-\phi\left[\cos^{-1}\left(\frac{|\mu|}{2t}\right)^{+}\right] + \phi\left[\cos^{-1}\left(\frac{|\mu|}{2t}\right)^{-}\right] \\ &-\phi\left[\cos^{-1}\left(-\frac{|\mu|}{2t}\right)^{+}\right] + \phi\left[\cos^{-1}\left(-\frac{|\mu|}{2t}\right)^{-}\right]\Bigg\} = \frac{1}{\pi}\int_0^{\pi} \frac{\mathrm{d}\phi}{\mathrm{d}k} dk,\end{aligned} \tag{4.51}$$

the topological invariant must be an integer, such that the topological invariant is $\nu = 0, \pm 1$. The topological invariant ν has a geometrical view, as the number of winds over the origin of the vector $\mathbf{d}$ in the $d_x - d_y$ plane. Considering the results above, it is possible to vary the parameters (μ, Δ) to produce the following phase diagram, in Figure 4.4.

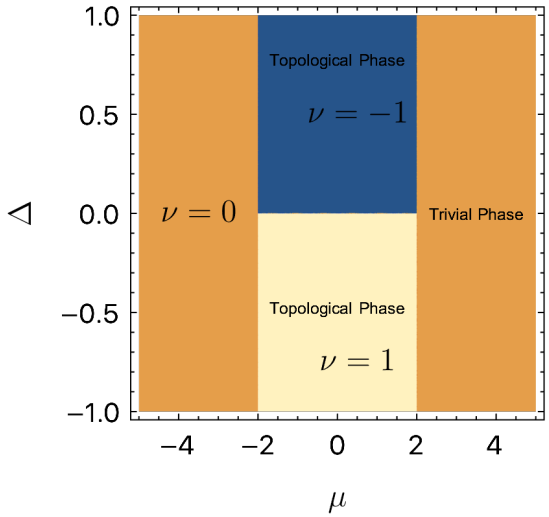

FIGURE 4.4. Phase Diagram shows the topological regions and the trivial phases, with topological invariant $\nu = 0, \pm 1$.

The topological region can be called the *Ising region*, being delimited by *Ising lines*[1] at the transition of the invariant $\nu \neq 0 \rightarrow \nu = 0$. Since the topological invariant changes its sign only because of the pairing parameter sign, and at $\Delta = 0$ the system is a trivial semiconductor, one could consider both of them as the same topological phase.

4.3.2 Parity Conservation and Switches

Considering a finite chain, with N sites, the parity of a chain, expressed in the previous section on equation 4.21, expresses a conserved quantity, the presence/absence of fermionic (abelian) quasi-particles at the edges of the chain. Since it was shown before, the ground state of superconductors is represented (in periodic boundary conditions) as filled by

$$|GS\rangle = \prod_{k \in BZ} \gamma_k \gamma_{-k} |0\rangle , \tag{4.52}$$

in this way, for an even number of sites, there must be an even number of fermionic particles (electrons).

Now, looking at the most simple open Kitaev chain ($N = 2$), the A matrix is

[1] This nomenclature comes from the XY model since this spin model has in the Kitaev chain its fermion analog.

$$A = \frac{1}{2}\begin{pmatrix} \mu & 1-\Delta \\ 1+\Delta & \mu \end{pmatrix} \Longrightarrow \qquad \det\{A\} = \mu^2 + (\Delta^2 - 1), \tag{4.53}$$

for $|\Delta| < 1$ and $|\mu| < 1$ the parity of the system changes following the circle equation

$$\mu^2 + \Delta^2 = 1. \tag{4.54}$$

For a generic system with N sites, there are N changes in the parity, as shown in Figure 4.5.

In the Kitaev original paper (9), he introduced a two-level effective Hamiltonian for the finite open Kitaev chain, only considering the zero energy edge modes ${\mathbf{b_0}}^A, {\mathbf{b_0}}^B$ (in the limit of $|\mu| < 2$). Kitaev claimed that the effective Hamiltonian, expressed by

$$\mathcal{H}_{eff} = t\mathbf{b_0^A b_0^B}, \tag{4.55}$$

where $t > 0$ is the tunneling amplitude over the chain and the presence of unpaired Majorana fermions (non-abelian fermions, without occupancy number) happens in the case of

$$\mathcal{P}_{eff} \equiv \text{sgn}(\mathbf{b_0^A b_0^B}) < 0, \tag{4.56}$$

the bulk Hamiltonian supposedly remains unchanged in both phases.

4.3.3 Transfer Matrix Method

Realizing that the A matrix, presented in the definition of the open chain has $N-2$ identical equations, of the form

$$\left((1-\Delta)\eta_{n-1}^A + \mu\,\eta_n^A + (1+\Delta)\eta_{n+1}^A\right)\eta_n^B = \epsilon_j \eta_n^A \eta_n^B, \tag{4.57}$$

and supposing that there are zero energy modes, $\epsilon_0 = 0$, the basic equations of the system become

$$(1-\Delta)\eta_{n-1}^A + \mu\eta_n^A + (1+\Delta)\eta_{n+1}^A = 0, \quad (1+\Delta)\eta_{n-1}^B + \mu\eta_n^B + (1-\Delta)\eta_{n+1}^B = 0, \tag{4.58}$$

these equations write a transfer matrix system, through the matrices $T_n, T_n^\dagger$

$$\begin{pmatrix} \eta_{n+1}^A \\ \eta_n^A \end{pmatrix} = \begin{pmatrix} \frac{\mu}{1-\Delta} & \frac{\Delta+1}{\Delta-1} \\ 1 & 0 \end{pmatrix} \begin{pmatrix} \eta_n^A \\ \eta_{n-1}^A \end{pmatrix}, \Longrightarrow \qquad a_{n+1} = T_n a_n, \tag{4.59}$$

$$\begin{pmatrix} \eta_{n+1}^B \\ \eta_n^B \end{pmatrix} = \begin{pmatrix} \frac{\mu}{1+\Delta} & \frac{\Delta-1}{\Delta+1} \\ 1 & 0 \end{pmatrix} \begin{pmatrix} \eta_n^B \\ \eta_{n-1}^B \end{pmatrix}, \Longrightarrow \qquad b_{n+1} = T_n^\dagger b_n. \tag{4.60}$$

The eigenvalues of the matrices are easily obtained

$$\lambda_\pm = \frac{-\mu \pm \sqrt{\mu^2 + 4\left(\Delta^2 - 1\right)}}{2(\Delta - 1)}; \qquad \lambda_\pm^\dagger = \frac{\mu \pm \sqrt{\mu^2 + 4\left(\Delta^2 - 1\right)}}{2(\Delta + 1)},$$

and the eigenvectors of the transfer matrix are

$$|a_\pm\rangle = \begin{pmatrix} \lambda_\pm \\ 1 \end{pmatrix}, \qquad |b_\pm\rangle = \begin{pmatrix} \lambda_\pm^\dagger \\ 1 \end{pmatrix}. \tag{4.61}$$

The edge states are localized Majorana states, which means that the Majorana wave function $\mathbf{b_0^A} = (p_1^A\ p_2^A\ \dots\ p_N^A)^T$ must be localized at one end of the chain, while $\mathbf{b_0^B} = (p_1^B\ p_2^B\ \dots\ p_N^B)^T$ is in on the other edge. In other words, the edge states exist when both the eigenvalues $\{\lambda_+, \lambda_-\}$ and $\{\lambda_+^\dagger, \lambda_-^\dagger\}$ have an absolute value greater or smaller than unity. The Majorana wave solution is written as

$$p_n^A = a_+ \lambda_+^{n-N-1} + a_- \lambda_-^{n-N-1}; \qquad p_n^B = b_+ \left(\lambda_+^\dagger\right)^n + b_- \left(\lambda_0^\dagger\right)^n. \tag{4.62}$$

In this way, when both eigenvalues have absolute values smaller than one, the wave function is localized at the beginning of the chain, on the other hand, when both wave functions are greater than the unity, they are localized at the end of the chain.

Until now, the solution is based only on the 'bulk' equations defined above. In other words, there are no boundary conditions expressed in the solution (which is needed). Boundary conditions are introduced in the case of localization, when the Majorana wave function is localized at the beginning of the chain, with the "zeroth" site b_0, where there is no probability of finding a particle, such that

$$p_0^B = b_+ \left(\lambda_+^\dagger\right)^0 + b_- \left(\lambda_-^\dagger\right)^0 = b_+ + b_- = 0, \Rightarrow \qquad b_+ = -b_-. \tag{4.63}$$

In another case, where both eigenvalues are greater than one, it is introduced the $N+1$-th site, where the probability of finding a particle is zero, This way

$$p^A_{N+1} = a_+ + a_- = 0, \Rightarrow \qquad a_+ = -a_-. \tag{4.64}$$

There is still a possibility that the system has complex eigenvalues. These eigenvalues are conjugate, and then the subtraction of the real parts will be zero. This way, taking a phase shift on the eigenvalues, the subtraction gets only the imaginary part $\mathrm{Im}(\lambda_\pm)$.

From the transfer matrix method discussed above, the edge parity of such topological Majorana fermions can be explored from Equation 4.56 by the wave solutions 4.62. It is seen that the fermionic parities $\mathcal{P}$ changes N times for a chosen value of Δ. On the other hand, taking the edge parity $\mathcal{P}_{eff}$, the switching number is doubled, and the ground state changes occur at the same points as the edge parity instabilities.

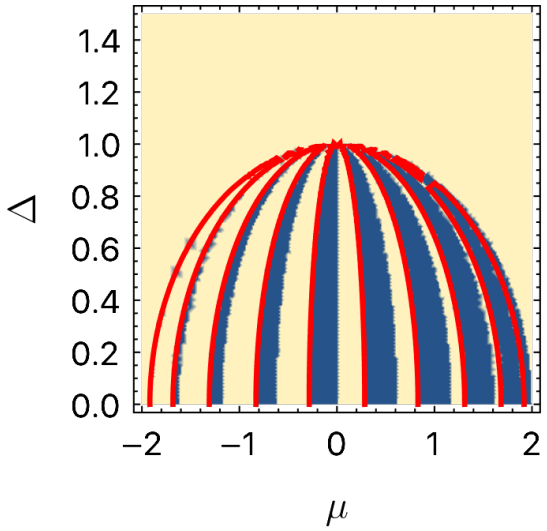

FIGURE 4.5. Filled regions exhibit changes of the edge parity $\mathcal{P}_{eff}$, obtained by the transfer matrix solution for a chain with $N = 10$. The light red curves indicate the ground state fermionic parity $\mathcal{P} = \mathrm{sgn}(\det\{A_{KC}\})$ previously defined in Equation 4.21.

4.4 Extensions of the Kitaev Chain

Now that some of the main topological properties of the Kitaev Chain have been calculated, it is interesting to ask what the properties of other models owing the same

non-unitary symmetries (BDI system). A natural way to extend the superconductor model is to consider the hopping t_{ij} and pairing Δ_{ij} interactions not restricted to first neighbors.

A natural extended system, consisting of a chain with q neighbor interactions on the pairing, and q' neighbor hopping, such that $t_{ij} = 0$ for all $l = |i-j| > q'$. The Hamiltonian is

$$\mathcal{H} = -\mu \sum_j c_j^\dagger c_j - t \sum_j \left(\sum_{l=1}^{q'} \frac{1}{l^\beta} c_j^\dagger c_{j+l} + \Delta \sum_{l=1}^{q} \frac{1}{l^\alpha} c_j c_{j+l} + \text{h.c.} \right), \tag{4.65}$$

for the hopping[2] $t_{ij} = t/|i-j|^\beta$ and pairing $\Delta_{ij} = \Delta/|i-j|^\alpha$. Translating the system by the Fourier representation (for momentum $k \in (-\pi, \pi)$ and unitary displacement between sites $a \equiv 1$), in the reciprocal space, the Hamiltonian is

$$\mathcal{H}(k) = -\mu \sum_k c_k^\dagger c_k - 2 \sum_{l=1}^{q'} \frac{1}{l^\beta} \sum_k \cos(kl) c_k^\dagger c_k + \Delta \sum_{l=1}^{q} \frac{1}{l^\alpha} \sum_k \left(e^{-ikl} c_k c_{-k} + e^{ikl} c_{-k}^\dagger c_k^\dagger \right),$$

considering the anti-commutation relations $c_k^\dagger c_k = 1 - c_k c_k^\dagger \doteq 1 - c_{-k} c_{-k}^\dagger$ and $c_k c_{-k} = -c_{-k} c_k$, the Hamiltonian becomes decoupled in N 2×2-matrices

$$\begin{aligned} \mathcal{H}_k &= \begin{pmatrix} c_k^\dagger & c_{-k} \end{pmatrix} \begin{pmatrix} -\mu - 2\sum_{l=1}^{q'} \frac{1}{l^\beta} \cos(lk) & 2i\Delta \sum_{l=1}^{q} \frac{1}{l^\alpha} \sin(lk) \\ -2i\Delta \sum_{l=1}^{q} \frac{1}{l^\alpha} \sin(lk) & \mu + 2\sum_{l=1}^{q'} \frac{1}{l^\beta} \cos(lk) \end{pmatrix} \begin{pmatrix} c_k \\ c_{-k}^\dagger \end{pmatrix}; \\ \mathcal{H}_k &= \Psi^\dagger \mathbf{d} \cdot \vec{\tau} \Psi, \end{aligned} \tag{4.66}$$

for $\vec{\tau} = \{\tau_1, \tau_2, \tau_3\}$ Pauli matrices in the particle-hole space.

The band energies are given by

$$E_k^\pm = \pm\sqrt{\mathbf{d}^2} = \pm \sqrt{ \left[\mu + 2 \sum_{l=1}^{q'} \frac{1}{l^\beta} \cos(lk) \right]^2 + \left[2\Delta \sum_{l=1}^{q} \frac{1}{l^\alpha} \sin(lk) \right]^2 }, \tag{4.67}$$

and the eigenstates are the two-band solution with angle parameter θ, now given by

$$\eta_\pm = \frac{1}{\sqrt{2}} \begin{pmatrix} \pm e^{-i\theta_k} \\ 1 \end{pmatrix}; \qquad \tan\theta_k = \frac{2\Delta \sum_{l=1}^{q} l^{-\alpha} \sin lk}{\mu + 2\sum_{l=1}^{q'} l^{-\beta} \cos lk}. \tag{4.68}$$

[2] Again, the hopping parameter t is absorbed by the chemical potential $\mu/t \to \mu$ and the pairing parameter $\Delta/t \to \Delta$.

The method used to calculate the winding number of the Kitaev Chain (Equation 4.51), can be used in other systems with an arbitrary range of neighbor interactions (q, q') in the hopping and the pairing. The topological invariant is again computed by $\phi_k = -\theta_k$ (same rotation of the Pauli matrices). The difference now comes from the number of gap closures $E_k = 0$ and the trajectory of the vector $\mathbf{n}(k)$ over the Brillouin zone.

Similarly as made for the Kitaev chain (4.50), and considering that there is a gap closure at an arbitrary point q_0, then ϕ_{q_0} is not well defined, and there is a topological phase transition. In the case of $\cos\phi_{q_1} = 0$ and $E_{q_1} \neq 0$ (gap), ϕ_{q_1} is discontinuous and 'quantized' (in the sense of $\phi_{q_1+dk} - \phi_{q_1-dk} = 2|\phi_{q_1^{\pm}}| = \pi$ having different signs), piling up (at most q) different phases to any phase diagram, that has topological invariant computed by

$$\nu = \frac{1}{2\pi}\int_{-\pi}^{\pi}\frac{\mathrm{d}\phi}{\mathrm{d}k}dk = \frac{1}{\pi}\sum_{j=1}^{q}\left(\phi_{q_j^-} - \phi_{q_{j-1}^+}\right), \tag{4.69}$$

remembering that $\phi_{k_0} = \phi_0 = 0$ and $\phi_{k_q} = \phi_\pi = 0$ (odd function).

Knowing that E_k and $\cos\phi_k$ determines the number of phases of the model, still left unknown $\sin\phi_k$. This quantity tells us the highest number of changes of the topological invariant[3], given by the range of the hopping interaction q'. The topological invariant ν is, from a geometrical point of view, the number of winds of the curve $\mathbf{d}(k)$ around the origin.

From the definition of the winding number for an arbitrarily closed trajectory 4.69 and considering arbitrary values of the range q, q', it is possible to achieve topological phase diagrams, as shown in Figure 4.6 (imposing extra conditions on the remaining parameters, for instance $\Delta = 1$ for all cases, the parameters α, β are explicitly imposed on the plots and captions).

In the diagrams 4.6, the absence of the $\mu \to -\mu$ symmetry (present in the Kitaev chain) becomes evident. This symmetry in the Kitaev chain is present because the gauge transformation $c_j \to (-1)^j c_j$ preserves the Hamiltonian only converting $\mu \mapsto -\mu$. In extended models, interaction terms are separated into even and odd sectors.

[3]Consequently telling too the maximum value of the topological invariant.

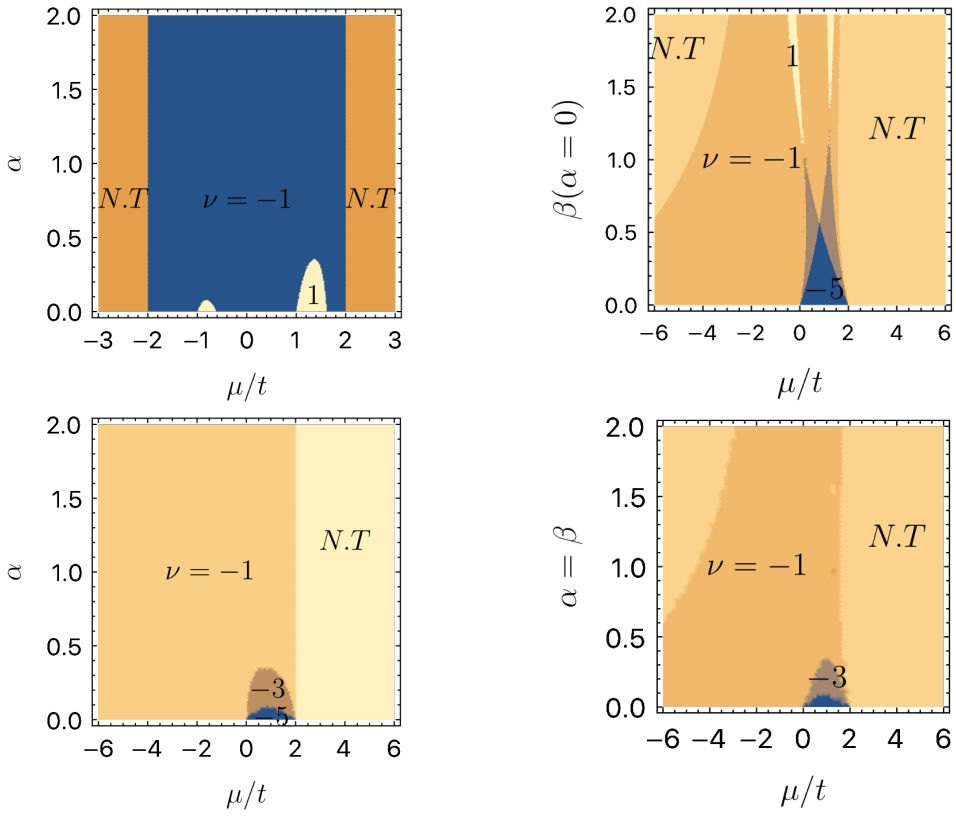

FIGURE 4.6. Phase Diagrams considering distinct imposed parameters for chains with $q = q' = 5$. (Left upper) phase diagram in the limit of $\beta \to \infty$, only have chiral topological phases and $\nu = \pm 1$. (Right upper) phase diagram (μ, β) for $q = q' = 5$, imposing $\alpha = 0$. (Left bottom) phase diagram (μ, α) in the case of $\beta = 0$. (Right bottom) phase diagram of the commonly known homogeneous chain, $(\mu, \alpha = \beta)$.

The above assertions about the winding number integral can be proven. The discontinuities of the function ϕ_k occur at $\cos\phi_k = 0$, such that

$$\begin{aligned}\cos\phi_k &= -\mu - 2\sum_{j=1}^{q'} \frac{1}{j^\beta}\cos jk = \mu + 2\sum_j j^{-\beta}\left(-1 + 2\cos^2\frac{jk}{2}\right); \\ &= \mu - 2\left(\sum_{j=1}^{q'} j^{-\beta}\right) + 4\sum_{j=1}^{q'} j^{-\beta}\cos^2\frac{jk}{2}. \end{aligned} \tag{4.70}$$

It is already noticed that the Ising lines are no longer constant. Returning to the first line, the $\cos jk$ terms, can be decomposed as

$$\cos jk = T_j(\cos k) = \sum_{n=1}^{j} a_n \cos^n k, \tag{4.71}$$

for a_n coefficients and $T_j(x)$ Chebyshev Polynomials of the First kind. Thus

$$\cos\phi_k = -\mu - 2\sum_j \frac{1}{j^\beta} T_j(\cos k) = 0, \tag{4.72}$$

is a polynomial equation (considering $\cos k = x$) and has at most q' real roots for $\cos\phi_k = 0$ (this number determines how many times the integral has phase transitions).

Now, is it possible to know the maximum value of one topological phase (again, $\sin jk$ is expressed as)

$$\sin\phi_k \equiv 2\Delta \sum_{j=1}^{q} \frac{1}{j^\alpha} \sin jk = 0, \qquad \sin jk = U_{j-1}(\cos\theta)\sin\theta, \tag{4.73}$$

and $U_n(x)$ is the Chebyshev Polynomial of the Second kind. This way, $\sin\phi_k$ is

$$\sin\phi_k = 2\Delta \sum_j \frac{1}{j^\alpha} U_{j-1}(\cos k)\sin k = 2\Delta \sin k \sum_j \frac{1}{j^\alpha} U_{j-1}(\cos k), \tag{4.74}$$

and, as $\sin\phi_k = 0$, the remaining term is a polynomial equation of $(j-1)$ degree

$$\sum_j \frac{1}{j^\alpha} U_{j-1}(\cos k) = 0. \tag{4.75}$$

The assertions proven above can be summarized in Table 4.1, where the maximum number of phase transitions and an upper bound of the topological index is obtained, for fixed α, β (horizontal cuts in the diagrams similar to the Figure 4.6).

Limit	Max Number of Phase Transitions	Upper Bound (index ν)
$(\alpha = \beta \to \infty)$	2	-1
$(\alpha, \beta \to \infty)$	$q+1$	± 1
$(\alpha \to \infty, \beta)$	2	-1
$(\alpha = \beta)$	$q+1$	$-q, \ldots, -1$

TABLE 4.1. Relation of phase transitions and topological upper bound and limit cases, considering $(\alpha, \beta = constant)$.

Now that the basic information about the phases of the system is known, it is interesting to analyze specific models of the above general BDI chain.

Observation 6 (Relations to Interacting Chains)**.** *Kitaev chains with long-range interactions can be seen as a collection of max(q, q') chains that interact. This way, for a chain with N sites and n interactions (maximum range between the hopping and pairing interactions) as n different chains composed of N/n sites. The interactions of the coupled chains can be viewed as an extended unit cell where the η_j^χ (j unit cell at χ chain) interact with all n subsequent sites. A schematic view of a chain with $N = 9$ sites and range $n = 3$ is done in Figure 4.7.*

The resultant combination of the chains is similar to a 'tube' of coupled chains, where the j-th site of the n-th chain interacts with all subsequent elements of the unit cell and with the first j elements of the next unit cell. One concrete example is shown in Figure 4.7, in the case of three chains with three sites each.

Considering an extreme case where it is considered only first neighbors and q neighbors interactions, the chain has only in-chain interactions and on neighbors chains (in the case of the Figure 4.7, the thick black lines and thin black lines).

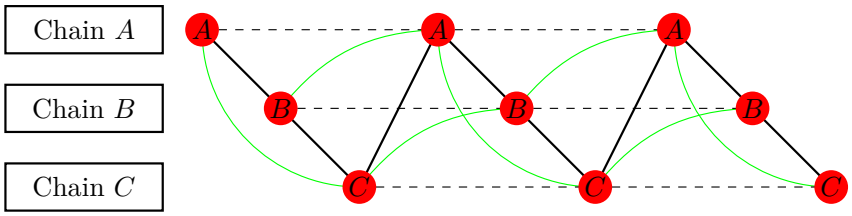

FIGURE 4.7. Schematic example of three interacting Kitaev chains. The thick black lines correspond to the first neighbor's interactions (interaction between chains, for a ladder), the green curves represent second neighbor interactions (interaction between second neighbor chains) and the black dashed lines are the third neighbor interactions (in the ladder context, the usual first neighbor interaction). The local interaction $\mu\eta_i^A\eta_i^B$ is squeezed inside the local sites A, B, C.

4.4.1 Infinite-Range Limit

From the works of (28, 29, 31, 32, 33, 55), considering the range of the interactions as the limit case where all sites interact with each other, e.g. limit $q, q' \to \infty$. The chain has the following Hamiltonian in momentum space

$$\mathcal{H}_k = \begin{pmatrix} c_k^\dagger & c_{-k} \end{pmatrix} \begin{pmatrix} -\mu - 2\,\mathrm{Re}\left[\mathrm{Li}_\alpha\left(e^{ik}\right)\right] & 2i\Delta\,\mathrm{Im}\left[\mathrm{Li}_\alpha\left(e^{ik}\right)\right] \\ -2i\Delta\,\mathrm{Im}\left[\mathrm{Li}_\alpha\left(e^{ik}\right)\right] & \mu + 2\,\mathrm{Re}\left[\mathrm{Li}_\alpha\left(e^{ik}\right)\right] \end{pmatrix} \begin{pmatrix} c_k \\ c_{-k}^\dagger \end{pmatrix};$$
$$\mathcal{H}_k = \Psi^\dagger \mathbf{d}_\infty \cdot \vec{\tau} \Psi, \tag{4.76}$$

for the Pauli matrices $\vec{\tau} = \{\tau_1, \tau_2, \tau_3\}$ in the particle-hole space.

The band energies are given by

$$E_k^\pm = \pm\sqrt{\mathbf{d}_\infty^2} = \pm\sqrt{\left\{\mu + 2\mathrm{Re}\left[\mathrm{Li}_\beta\left(e^{ik}\right)\right]\right\}^2 + \left\{2\Delta\mathrm{Im}\left[\mathrm{Li}_\alpha\left(e^{ik}\right)\right]\right\}^2}, \tag{4.77}$$

as the parameter θ_k is now defined as

$$\tan\phi_k = \frac{2\Delta\mathrm{Im}\left[\mathrm{Li}_\alpha\left(e^{ik}\right)\right]}{-\mu - 2\mathrm{Re}\left[\mathrm{Li}_\beta\left(e^{ik}\right)\right]}, \tag{4.78}$$

and the function $\mathrm{Li}(x)$, called PolyLogarithm, is a generalization of the Riemann Zeta Function $\zeta(s)$ and $\Gamma(x)$ is the Gamma function, for $k \in (-\pi, \pi)$

$$\mathrm{Li}_\alpha(e^{ik}) \equiv \sum_{j=1}^{\infty} \frac{\left(e^{ik}\right)^j}{j^\alpha} = \Gamma(1-\alpha)\left(-k\right)^{1-\alpha} + \sum_{j=0}^{\infty} \frac{k^j}{j!}\zeta(\alpha - j), \tag{4.79}$$

In the long-range limit, the Winding Vector $\mathbf{d}_\infty$ is always different than zero except at one point, if any of the decay rates (α or β) are smaller than one. There is an immediate consequence, there is only one trivial phase, and one topological phase, in contrast with other BDI systems studied above (topological phase restricted to the Ising lines). On the other hand, if both parameters are greater than one, then the system has two gapless points ($\mathbf{d}_\infty(k) = 0$).

Considering the specific cases of $(i)\,\alpha \to \infty, (ii)\,\beta \to \infty, (iii)\,\alpha = \beta$, the parameters are reduced, such that for $\Delta = 1$ it is possible to evaluate topological phase diagram to these cases. The Winding vector and the corresponding phase diagrams are shown in Figure 4.8. As expected from the assertions made in the previous section, when $\alpha \to \infty$, the Winding vector is stretched from a circle to a loop that closes in infinity $d_x \to -\infty$, the model exhibits the same topological phases as the normal Kitaev Chain, but the Ising lines are no longer constant.

Considering now the cases of $\alpha < \infty$, there exists a transition line of one to two gapless points, because the PolyLogarithmic function has discontinuities when $\alpha < 1$.

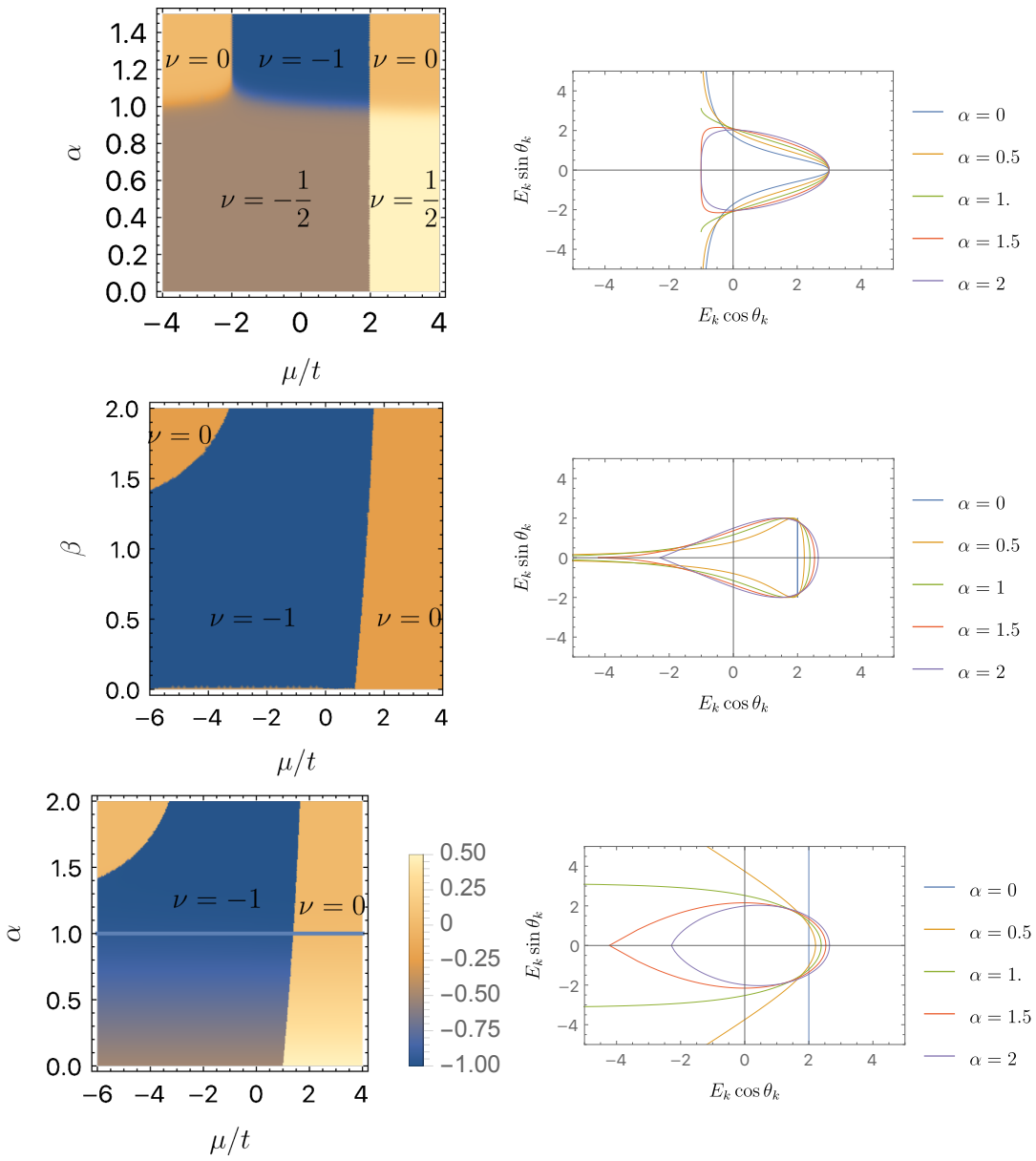

FIGURE 4.8. Deformations of the Winding vector $\mathbf{d}(k)$ (for $\mu - 1$, and $\Delta = 1$) and the subsequent phase diagrams in the long-range limit of the extended Kitaev Chain. (Left Panel) Topological phases of the chain with long-range only in the pairing interaction. (Center Panel) Topological phases of the chain with long-range only in the hopping interaction. (Right Panel) Topological phases of a homogeneous long-range chain ($\alpha = \beta$).

This can be seen firstly from the vector $\mathbf{d}_\infty(k)$, that do not form a closed path, as seen in the upper panels of the cases $\alpha = \beta$ and $\beta \to \infty$. Analyzing the real and imaginary parts of the PolyLogarithm function

$$\mathrm{Li}_\alpha(e^{ik}) = \sum_l \frac{\left(e^{ik}\right)^l}{l^\alpha} = \sum_l \frac{e^{ilk}}{l^\alpha} \rightarrow \qquad \mathrm{Re}\left(\mathrm{Li}_\alpha(e^{ik})\right) = \sum_l \frac{\cos lk}{l^\alpha} \tag{4.80}$$

$$\mathrm{Im}\left(\mathrm{Li}_\alpha(e^{ik})\right) = \sum_l \frac{\sin lk}{l^\alpha}. \tag{4.81}$$

Supposing that $\beta = \infty$, it is expected that the gap closes at the Ising lines $\mu = \pm 2$, at the points $k = \pm\pi$ or $k = 0$ (In the Kitaev Chain). The presence of the series changes the behavior of the band energies. Looking at the energies in the vicinity of $k \approx \pi$ and performing an expansion of the sine function

$$\sin(kl)_{k\to\pi} \approx (-1)^l l(k-\pi) - \frac{(-1)^l}{6} l^3 (k-\pi)^3 + \mathcal{O}(k^5), \tag{4.82}$$

$$\mathrm{Li}_\alpha(e^{ik}) \approx \sum_l \left(\frac{(-1)^l l}{l^\alpha}(k-\pi) - \frac{(-1)^l l^3}{l^\alpha}(k-\pi)^3 \right), \tag{4.83}$$

and the energies near $k = \pm\pi$ are

$$E^{\mu=2}(k\to\pi) \approx \frac{1}{2}\sqrt{(k-\pi)^4 + 4\Delta^2\left[\left(\sum_l \frac{(-1)^l}{l^{\alpha-1}}\right)(k-\pi) - \left(\sum_l \frac{(-1)^l}{l^{\alpha-3}}\right)(k-\pi)^3\right]^2};$$

$$E^{\mu=2} \approx \frac{1}{2}\sqrt{4\Delta^2\left[\sum_l \frac{(-1)^\alpha}{l^{\alpha-1}}\right]^2 (k-\pi)^2 + \left[1 - \frac{1}{3}\sum_{m,n}\frac{(-1)^{m+n}}{m^{\alpha-1}n^{\alpha-3}}\right](k-\pi)^4}; \tag{4.84}$$

$$E^{\mu=2}(k\to\pi) \approx |\Delta| \left|\sum_l \frac{(-1)^l}{l^{\alpha-1}}\right| |k-\pi|. \tag{4.85}$$

The above series is convergent when $\alpha > 1$. On the other hand, for $\alpha < 1$, it is possible to regularize the summation (since this is an alternate series). A consequence of the regularization procedure is the absence of a parity in the chain. On the thermodynamic limit, this is not a problem.

For the case of $\mu = -2$, the gap closes at $k = 0$, and now the same series obtained above is not alternating. Linearizing the Polylogarithm

$$\mathrm{Im}\left(\mathrm{Li}_\alpha(e^{ik})\right) = \sum_l \frac{lk - \frac{1}{6}l^3k^3}{l^\alpha} + \mathcal{O}(k^4), \tag{4.86}$$

and the lowest energies are obtained

$$E^{\mu=-2}(k\to 0) = \frac{1}{2}\sqrt{x^4 + 4\Delta^2\left(\sum_l \frac{l}{l^\alpha}k - \frac{1}{6}\frac{l^3}{l^\alpha}k^3\right)^2}; \\ = \frac{1}{2}\sqrt{4\Delta^2\left(\sum_l l^{1-\alpha}\right)k^2 + \mathcal{O}(k^4)} \approx |\Delta|k\sum_l l^{1-\alpha}. \tag{4.87}$$

Since there is no regularization, the series only converges when $\alpha > 2$ and the gap closes linearly. For $\alpha < 2$ there are two possibilities, (i) $\alpha < 1$ the gap does not close, since $\mathrm{Im}(\mathrm{Li}_\alpha(1))$ is not defined; (ii) $1 < \alpha < 2$, the gap closes at $k = 0$, since exactly $\mathrm{Im}(\mathrm{Li}_\alpha(1)) = 0$, but not linearly and the function is not analytic.

The same argument exposed above is valid for a chain with $\beta < \infty$, but the gap closing does not happen at the Brillouin zone points $k \to \{0, \pm\pi\}$, but at the μ-dependent points, roots of the transcendental equation

$$\mathrm{Re}\left[\mathrm{Li}_\beta\left(e^{ik}\right)\right] + \frac{\mu}{2} = 0. \tag{4.88}$$

The topological phase diagrams were obtained by solving this transcendental equation numerically.

4.4.2 Next-Nearest Neighbours

Taking now the specific limit of $q = q' = 2$. This model has been already studied in other situations, as (28, 56). The model couples the first and second neighbors of the chain. The reciprocal space Hamiltonian is

$$\mathcal{H}(k) = \sum_k \Psi_k^\dagger \begin{pmatrix} -\mu - 2\left(\cos k + 2^{-\beta}\cos 2k\right) & 2\Delta i\left(\sin k + 2^{-\alpha}\sin 2k\right) \\ -2\Delta i\left(\sin k + 2^{-\alpha}\sin 2k\right) & \mu + 2\left(\cos k + 2^{-\beta}\cos 2k\right) \end{pmatrix}\Psi_k, \tag{4.89}$$

and from the $\theta(k)$ angle, the pairing term Δ is not relevant to topological properties in the thermodynamic limit (as long as it is not null).

For this model, four distinct cases were considered ($\beta \to \infty, \alpha \to \infty, \beta = 0$ and $\alpha = \beta$), phase diagrams were calculated, shown in the lower panels of Figure 4.9. Above the diagrams, the winding vector $\mathbf{d}(k)$ is drawn for some specific values of α.

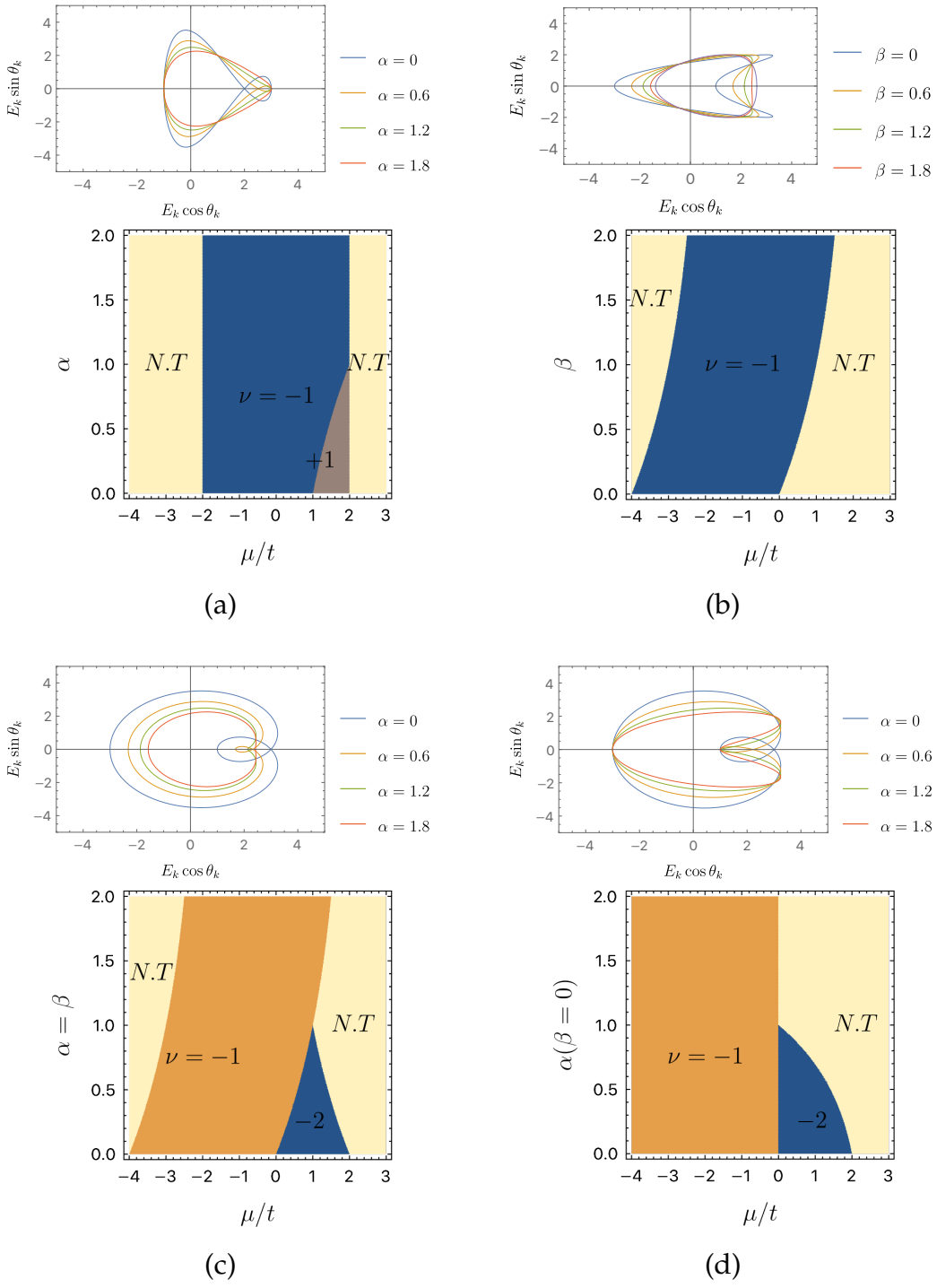

FIGURE 4.9. Plots shows (in superior panels) the deformations of the Winding Vector $\mathbf{d}(k)$ (for $\mu = -1$ and $\Delta = 1$) and (in inferior panels) topological phase diagrams of the extended Kitaev chain with next nearest neighbors ($q = q' = 2$). (a) Limit case of $\beta \to \infty$. (b) Limit case of $\alpha \to \infty$. (c) Case of intermediate interaction, of the homogeneous chain ($\alpha = \beta$). (d) Case of $\beta = 0$, and topological phase diagram for (μ, β).

In this approximation, the model exhibits new phases and transition lines compared to the Kitaev chain and the long-range limit.

A general analysis, made from the previous results of Section 4.4 associated with Figure 4.9, shows that models with $\alpha \to \infty$ (one neighbor interaction in the pairing) have only one topological phase ($\nu = -1$) and non-constant Ising lines (dependence on the chemical potential).

When $\beta \to \infty$, the models can exhibit q chirality exchanges, as shown in (a) panel of Figure 4.9. For $\alpha < 1$, the topological phase diagram shows the phases $\nu = \pm 1$ inside the Ising lines.

For the last case, where $\alpha, \beta < \infty$ (in particular, the limit of the homogeneous chain), the topological phases can (cannot) exhibit chirality changes. The winding number ν increases/decreases from zero to at most $q = q'$, and there is more than one edge mode solution in the chain.

4.4.2.1 Chiral Majorana Modes

Now that the phase diagrams in the next nearest neighbor limit are established, the interest returns to know the solutions and properties of zero energy modes[4]. The analysis is made again by the transfer matrix method. For finite chains, the C matrix gives again $T_n, T_n^\dagger$ matrices, but now the dimensionality of the matrix is augmented by the range of the interactions. For the next nearest model ($\beta \to \infty$), the transfer matrix is given by

$$T_n = \begin{pmatrix} -2^\alpha \frac{1+\Delta}{\Delta} & -2^\alpha \frac{\mu}{\Delta} & -2^\alpha \frac{1-\Delta}{\Delta} & 1 \\ 1 & 0 & 0 & 0 \\ 0 & 1 & 0 & 0 \\ 0 & 0 & 1 & 0 \end{pmatrix}, \tag{4.90}$$

and the solutions are equivalent to the obtained in the previous section 4.3.3, for an appropriate selection of eigenvalues. The main difference is that there are now more possible choices (a priori) to take into account. Looking at the conditions of the formation of a Majorana edge mode ($\lambda_i, \lambda_j < 1$ or $\lambda_i, \lambda_j > 1$) the possible solutions are

[4]Nearly zero energy solutions in finite chains.

reduced to two (one in the beginning and the other at the end of the chain). The computation of the properties was made considering the same boundary conditions as in the previous section (the dimension of the system increases, but still depends on a combination of two eigenvalues).

From the edge modes $\mathbf{b_0^A} = (p_1^A, p_2^A, \ldots, p_N^A)^T, \mathbf{b_0^B} = (p_1^B, p_2^B, \ldots, p_N^B)^T$ obtained by the transfer matrices $T_n, T_n^\dagger$, it is possible to analyze the average position of the wave solutions. The components $p_i^{A/B}$ of the modes give the probability amplitude to find an A/B Majorana fermion species at the i-th site of the chain. This way, the average position of 'occupation'[5] is for a chain with N sites

$$\bar{n}^{A/B} = \sum_{j=1}^{N} j \left(p_j^{A/B}\right)^2 .$$

From the transfer matrix solution discussed above, firstly it indicates that the topological phase transition changes the Majorana species of each end of the chain, thus the 'Chiral' behavior. The calculated properties of the chain are (i) average position $\bar{n}^{A/B(i)}$ of the solutions at the end of the chain, (ii) the fermionic edge parity $\mathcal{P}_{eff}$ of the effective model $\mathcal{H}_{eff} = -J\mathbf{b^A b^B}$ (iii) fermionic parity $\mathcal{P}$ switches of chains ground state. Figures 4.10 and 4.11 show diagrams of these quantities for different parameter values of μ, α, considering $\Delta = 1$ and $\beta \to \infty$.

Near the phase transitions, the average position of the edge mode $\mathbf{b^A}, \mathbf{b^B}$ at the ends of the chain, seems to be related to parity and effective parity changes. Comparing Figures 4.10 and 4.11 the parity changes occur near the maximum value of the average.

Mainly, the effective parity changes do not follow the same pattern of the Kitaev chain (in the Kitaev chain $\mathcal{P}_{eff}$ changes in the same points as $\mathcal{P}$ and also in between such transitions, shown in 4.5). In the next-nearest neighbor limit for the wave solutions calculated from the transfer matrix, with $\beta \to \infty$, the ground state fermionic parity appears to be determined only by the bulk part of the chain, contrary to what might be thought.

[5]Majorana fermions do not occupy any site, since $\{\eta_i^A \eta_j^A\} = \delta_{ij}$.

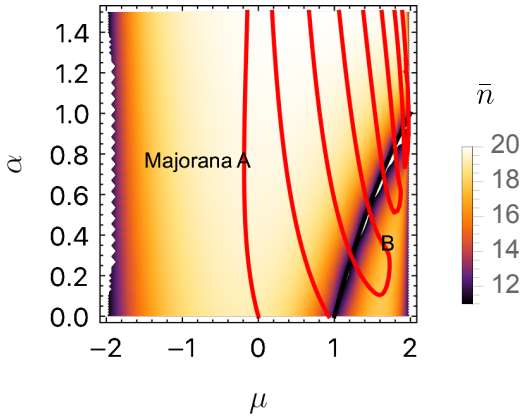

FIGURE 4.10. Plot shows the dependence of the average position of the edge modes at the end of a chain (with $N = 20$ sites) on the parameters (μ, α). (Left of phase transition) part of the plot the Majorana mode solution is of A-species. (Right of the phase transition) part, the Majorana solution is of B-species. The red curves represent fermionic parity switches of the ground state $\mathcal{P}$. These switches exhibit a pattern that, near the phase transition corresponds to the minima of the average position $\bar{n}$.

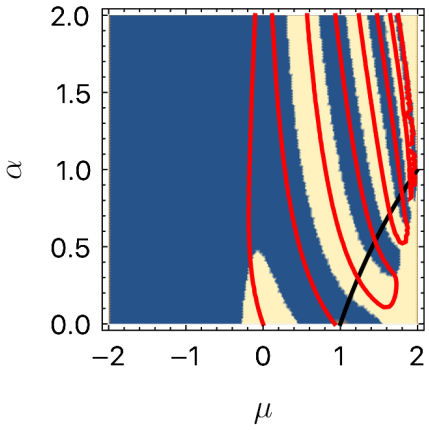

FIGURE 4.11. Filled blue and beige regions show the effective parity $\mathcal{P}_{eff}$ for a chain with $N = 20$ sites in the case of nearest neighbor interaction only in the pairing. The red curves indicate fermionic parity switches of the chain. Comparing the filled regions to the curve, it is seen that the effective parity changes ($\mathcal{P}_{eff}$) always follows near the parity switches ($\mathcal{P}$) in the $\nu = -1$ phase. On the $\nu = +1$ phase, parity changes have a different pattern. In between the red curves, the effective parity switches. In the blue region near $\mu/t \approx -0{,}4$, the parity switch seems to be a finite-size defect.

4.4.2.2 Two Majorana Modes

Looking now at the $\alpha, \beta < \infty$ limit, both phase diagrams (bottom panels of 4.9) show topological phases with $\nu = -2$. The transfer matrix $T_n^{\alpha\beta}$ has now a region where all eigenvalues $|\lambda_i|$ are smaller than the unity, therefore from the formation conditions, two distinct modes exist, thus the topological invariant ν tells the number of edge modes available in the system. In the limit of $\beta \to \infty$ (chiral modes), there is no trivial way to see a completely localized Majorana mode. Now for a finite chain, with $\alpha = \beta$ and $t = \Delta$ a clear limit of four Majorana operators 'decoupled' η_1^B, η_2^B and η_N^A, η_{N-1}^A, as shown in the schematic Figure 4.12.

The figure (4.12) can make us naively believe that adding Majorana edge modes

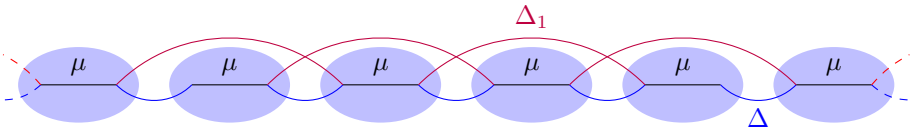

FIGURE 4.12. Diagrammatic scheme of a finite chain in the $\alpha, \beta < \infty$ limit, considering $t = \Delta, t_1 = \Delta_1$ and $\alpha = \beta$. Supposing that $\mu = 0$, the η_1^A and η_N^B site becomes completely decoupled, and the η_2^A,η_{N-1}^B have only the Δ interaction, while every other operator has two interactions (dashed lines represent the missing interactions).

to the chain turns these modes more internal (the first Majorana operator in the second site has two interactions, and for $\mu = 0$ only one). Considering now a different imposition to the eigenvalues from the boundary condition, now taken as

$$p_n^A = \mathrm{Re}\left[\lambda_+^n - \frac{\mathrm{Re}\left(\lambda_+^{L+1}\right)}{\mathrm{Re}\left(\lambda_-^{L+1}\right)}\lambda_-^n\right]. \tag{4.91}$$

The expectation value of these modes (same way as made in the chiral limit), is shown in Figures 4.13 that the different modes remain in the same average position. This average would usually be forbidden since these modes are fermions, but once the Majorana modes are real, the Pauli exclusion principle plays no role. Even more, both plots present the same two superposed patterns.

In the region where two Majoranas exist (from the phase diagram figure 4.9), one could again expect different solutions, since there are ground state parity fluctuations (by the parity formula $\mathcal{P} = \mathrm{sgn}\left(\det\{A\}\right)$). From Figures 4.13 both modes have similar behavior and one should not expect parity fluctuations, thus keeping the system parity (always changing in pairs). The left bottom panel of Figure 4.12 shows parity fluctuations in the two-mode region. In this region ($\mu \in (0, 1/2)$ and $\alpha \approx 0$), the edge modes are distinct, but both exhibit the same vertical pattern (expected from the parity switches of the ground state). From the chiral limit, the average position of the edge modes and the parity are related, this, is necessary to look properly at the edge parity.

To explore the parity changes is interesting to compute the parity of the effective model (containing now four edge modes $\{\mathbf{b}_{(1)}^{\mathbf{A}}, \mathbf{b}_{(2)}^{\mathbf{A}}, \mathbf{b}_{(1)}^{\mathbf{B}}, \mathbf{b}_{(2)}^{\mathbf{B}}\}$). Generalizing Equation 4.56 in the presence of N_m distinct edge states (with effective Hamiltonian $\mathcal{H}_{eff}^{N_m} = t\sum_i \mathbf{b}_{(i)}^{\mathbf{A}}\mathbf{b}_{(i)}^{\mathbf{B}}$), is obtained

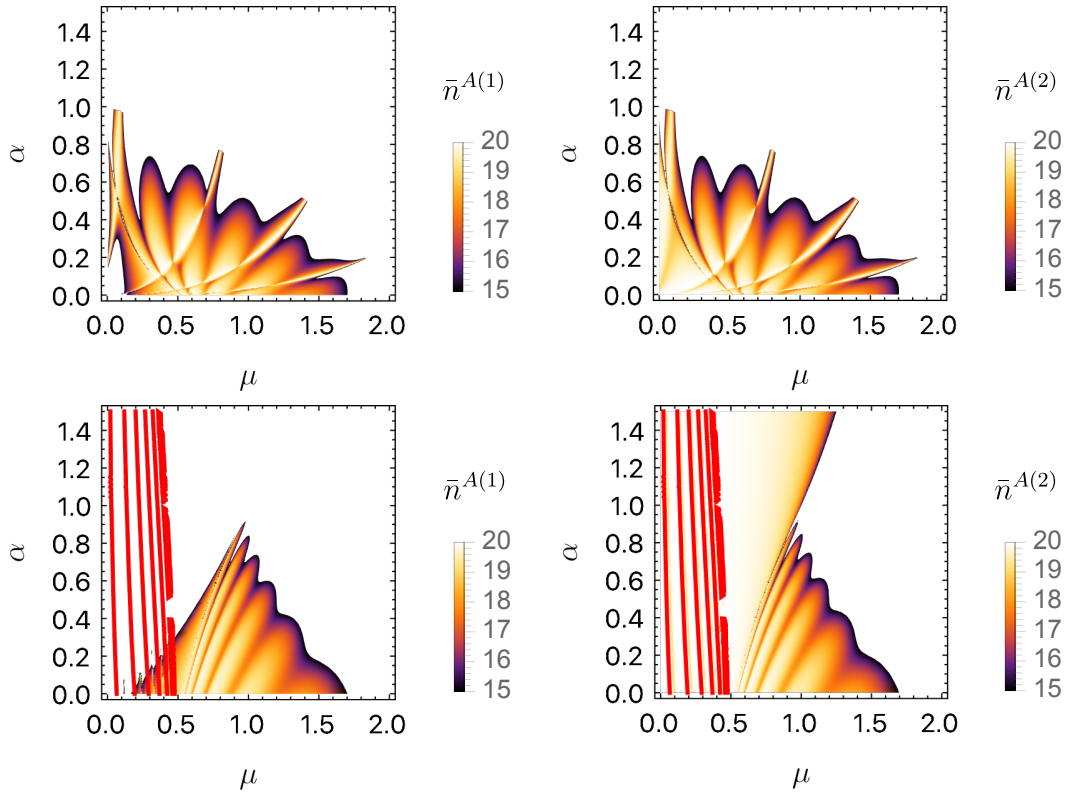

FIGURE 4.13. The figures of the upper panels show the average position of both Majorana modes obtained by the transfer matrix method imposing $\beta = 0$. In the bottom panels, the average position is calculated for $\alpha \approx \beta$. Red lines show the switches of the parity $\mathcal{P} = \det\{A\}$. Computed average positions for chains with $N = 20$ sites.

$$\mathcal{P}_{eff}^{N_m} = \text{sgn} \prod_{i=1}^{N_m} \left(\mathbf{b}_{(\mathbf{i})}^{\mathbf{A}} \mathbf{b}_{(\mathbf{i})}^{\mathbf{B}} \right). \tag{4.92}$$

Comparing the chain parity $\mathcal{P}$ calculated in the limits of the Figure 4.13 ($\beta = 0$ and $\alpha \approx \beta$[6]) with the effective parity defined above, two cases are possible. (i) one mode does not change its 'own parity' and the other does; (ii) both modes do/don't change their 'own' parity and the parity change happens only from bulk rearrangement.

From the hypothesis made above, Figure 4.14 shows the parities of the chain. In the two-mode region, there are (doubled) parity changes of $\mathcal{P}_{eff}$ (considering the calculated edge modes). These changes occur in between the parity changes of $\mathcal{P}$ (the entire chain). Thus, parity shifts of $\mathcal{P}$ may not caused by the edge modes, such that the variation comes from the bulk.

In summary, in this chapter a topological superconductor was studied, the Ki-

[6]The parameters α, β cannot be equal, since the transfer matrix would be undefined.

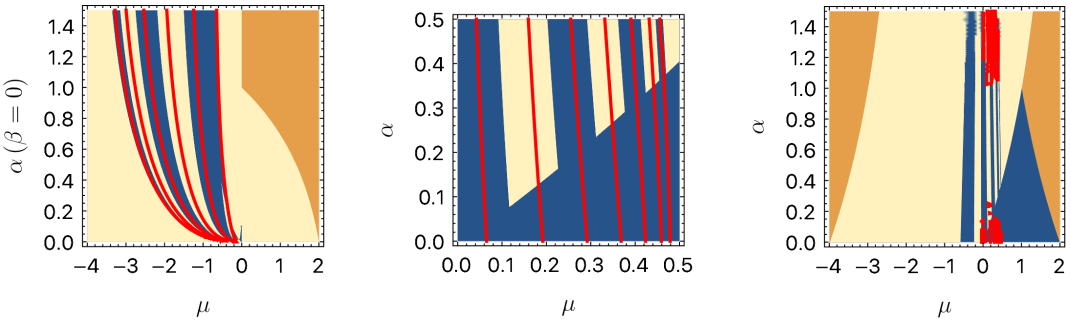

FIGURE 4.14. Diagrams exhibit the parities $\mathcal{P}, \mathcal{P}_{eff}$ of the chain in the two limits discussed above in Figure 4.13. The red curves represent the points at which the ground state parity $\mathcal{P}$ changes. The orange filling in both the right and left diagrams represents the trivial phase, and the beige and blue regions represent the parity $\mathcal{P}_{eff}$ of the effective model. (Central Panel) Zoom of the two Majorana regions for the case of $\alpha \approx \beta$. Stripes centered in the red curves can indicate parity transitions (for $\mu < 1/2$) of the effective parity in the two Majorana regions.

taev Chain. The Kitaev Chain has the same BDI symmetries as the topological insulator (SSH model) studied in the previous chapter. A topological phase diagram is set up and finite chain properties are analyzed, like the fermion parity of the ground state solution, comparing it with an effective model for calculating the parity via eigenfunctions obtained exactly from a transfer matrix.

After taking the Kitaev chain model, we introduced an extended range generalization of the chain (with algebraic decaying parameters α, β). First, considering a truncated range (first q, q'-nearest neighbors interacting) version of the model is analytically studied, where some specific cases were discussed.

A long-range version of the model is introduced too. In the thermodynamic limit, the Winding vector does not form a closed path, such that the winding number is not an integer and there is no topological phase (of the BDI class) in the case of low algebraic parameters since the infinite range breaks the convergence of the Fourier series in the reciprocal space.

Finally, in the limit of the next nearest neighbors ($q = q' = 2$), topological phase diagrams were obtained for specific combinations of the parameters. For finite chains, ground state parity changes are studied, analyzing the parity of the Majorana edge modes. Comparing both parities, unlike what can be thought, it is seen that parity changes are intimately related to the bulk, not only to the edges of the system.

Chapter 5

Conclusions

In this dissertation, we reviewed in the second chapter some of the main features of topological band theory, like the Berry phase, Berry connection, and curvature. As a topological invariant, it exemplified the Chern number in generic two-band models in two dimensions.

In the third chapter, some central concepts reviewed were used in a specific model, the SSH model. The studied model of a simple topological insulator was analyzed, describing why such topological behavior is intriguing: namely, the appearance of edge modes. In one dimension, a topological invariant is introduced, the *winding number*. It is shown how this invariant is directly related to a measurable quantity, the polarization. A topological phase diagram is then computed. Still, in this third chapter, a central aspect of non-interacting systems is explored, the imposed non-unitary symmetries. Those important symmetries are divided into symmetry classes. Some other symmetry-related one-dimensional models are discussed.

In the fourth chapter, which is the main chapter, a one-dimensional topological model (the Kitaev p-wave superconductor chain), belonging to the same symmetry class of the SSH model, namely the BDI class, is studied. Again, a topological phase diagram is constructed. Instead of the interpretation of a topological insulator, in the superconductor one, the edge modes present are unpaired Majoranas, so their main properties are introduced and analyzed.

Taking small finite chains, a new property is explored: the fermion parity of the ground state. An effective model to analyze the edge modes properties was introduced

and related to the Kitaev fermion parity fluctuation, and a transfer matrix approach was set up to calculate the wave function. From the analysis of the emergent Majorana modes, their effective parity fluctuations are determinants for the fluctuations of the chain. Different from what is currently expressed in the literature, the bulk properties play a significant role in the determination of the chain parity.

Subsequently, a generalization of the Kitaev chain is introduced and studied. Two different specific models with extended range are studied, (i) the long-range limit, where all sites interact and the interactions decrease algebraically; (ii) the next-nearest limit. Such cases are shown to have specific configurations of many interacting chains.

In the first case with long-range limit and for non-converging algebraically decrease (α, and $\beta < 1$), the topological edge modes are lost, since the path taken over the Brillouin Zone is open, as explained in the text.

For the second neighbor approximation, the topological invariant presents more phases, exhibiting a chirality transition $\nu = \pm 1 \rightarrow \mp 1$ considering the second neighbor interaction in the pairing only. For hopping and pairing interactions, the obtained phase diagrams show new transitions to higher winding numbers $\nu = \pm 1 \rightarrow \pm 2$, for which we have some explanations.

Lastly, taking finite chains in the limit of the next nearest neighbors, the edge modes can again be calculated by a modified transfer matrix approach and the fermion parity is again explored. In contrast to the Kitaev chain, extended-range models do not present the same rules for parity fluctuations. In those models, the parity does not always change from effective parity fluctuations.

Both Majorana modes have the same parity, and thus there is no 'effective' parity fluctuation. Instead, analyzing the full chain, the parity has fluctuations, such that its occurrence happens because of the behavior of the bulk.

Bibliography

1 ASBÓTH, J. K.; OROSZLÁNY, L.; PÁLYI, A. *A Short Course on Topological Insulators*. Springer International Publishing, 2016. Disponível em: <https://doi.org/10.1007\%2F978-3-319-25607-8>.

2 KLITZING, K. von. The quantized Hall effect. *Rev. Mod. Phys.*, American Physical Society, v. 58, p. 519–531, Jul 1986. Disponível em: <https://link.aps.org/doi/10.1103/RevModPhys.58.519>.

3 VOLOVIK, G. Analog of the quantum Hall effect in a superfluid ^{3}He film. *Soviet Physics-JETP (English Translation)*, v. 67, n. 9, p. 1804–1811, 1988.

4 HORAVA, P. Stability of Fermi Surfaces and K Theory. *Phys. Rev. Lett.*, American Physical Society, v. 95, p. 016405, Jun 2005. Disponível em: <https://link.aps.org/doi/10.1103/PhysRevLett.95.016405>.

5 ZHAO, Y. X.; WANG, Z. D. Topological Classification and Stability of Fermi Surfaces. *Physical Review Letters*, American Physical Society (APS), v. 110, n. 24, jun 2013. Disponível em: <https://doi.org/10.1103%2Fphysrevlett.110.240404>.

6 HALDANE, F. D. M. Model for a Quantum Hall Effect without Landau Levels: Condensed-Matter Realization of the "Parity Anomaly". *Phys. Rev. Lett.*, American Physical Society, v. 61, p. 2015–2018, Oct 1988. Disponível em: <https://link.aps.org/doi/10.1103/PhysRevLett.61.2015>.

7 STORMER, H. L.; TSUI, D. C.; GOSSARD, A. C. The fractional quantum Hall effect. *Reviews of Modern Physics*, APS, v. 71, n. 2, p. S298, 1999.

8 BERNEVIG, B. A.; HUGHES, T. L.; ZHANG, S.-C. Quantum spin Hall effect and topological phase transition in HgTe quantum wells. *Science*, American Association for the Advancement of Science, v. 314, n. 5806, p. 1757–1761, 2006.

9 KITAEV, A. Y. Unpaired majorana fermions in quantum wires. *Physics-Uspekhi*, Uspekhi Fizicheskikh Nauk (UFN) Journal, v. 44, n. 10S, p. 131–136, oct 2001. Disponível em: <https://doi.org/10.1070%2F1063-7869%2F44%2F10s%2Fs29>.

10 RUDNER, M. S. et al. Anomalous edge states and the bulk-edge correspondence for periodically driven two-dimensional systems. *Physical Review X*, APS, v. 3, n. 3, p. 031005, 2013.

11 SHAPIRO, J. The bulk-edge correspondence in three simple cases. *Reviews in Mathematical Physics*, World Scientific, v. 32, n. 03, p. 2030003, 2020.

12 RABE, K. M.; AHN, C. H.; TRISCONE, J.-M. *Physics of ferroelectrics: a modern perspective*. [S.l.]: Springer Science & Business Media, 2007. v. 105.

13 RESTA, R. Quantum-Mechanical Position Operator in Extended Systems. *Phys. Rev. Lett.*, American Physical Society, v. 80, p. 1800–1803, Mar 1998. Disponível em: <https://link.aps.org/doi/10.1103/PhysRevLett.80.1800>.

14 BEENAKKER, C. Search for Majorana fermions in superconductors. *Annu. Rev. Condens. Matter Phys.*, Annual Reviews, v. 4, n. 1, p. 113–136, 2013.

15 LEIJNSE, M.; FLENSBERG, K. Introduction to topological superconductivity and Majorana fermions. *Semiconductor Science and Technology*, IOP Publishing, v. 27, n. 12, p. 124003, nov 2012. Disponível em: <https://dx.doi.org/10.1088/0268-1242/27/12/124003>.

16 FIDKOWSKI, L. et al. Universal transport signatures of Majorana fermions in superconductor-Luttinger liquid junctions. *Physical Review B*, APS, v. 85, n. 24, p. 245121, 2012.

17 NADJ-PERGE, S. et al. Observation of Majorana fermions in ferromagnetic atomic chains on a superconductor. *Science*, American Association for the Advancement of Science, v. 346, n. 6209, p. 602–607, 2014.

18 LAHTINEN, V. Interacting non-abelian anyons as majorana fermions in the honeycomb lattice model. *New Journal of Physics*, IOP Publishing, v. 13, n. 7, p. 075009, 2011.

19 SAU, J. et al. From anyons to majoranas. *Nature Reviews Physics*, Nature Publishing Group UK London, v. 2, n. 12, p. 667–668, 2020.

20 HYART, T. et al. Flux-controlled quantum computation with majorana fermions. *Physical Review B*, APS, v. 88, n. 3, p. 035121, 2013.

21 LIAN, B. et al. Topological quantum computation based on chiral majorana fermions. *Proceedings of the National Academy of Sciences*, National Acad Sciences, v. 115, n. 43, p. 10938–10942, 2018.

22 BRAVYI, S. B.; KITAEV, A. Y. Fermionic quantum computation. *Annals of Physics*, Elsevier, v. 298, n. 1, p. 210–226, 2002.

23 DEGOTTARDI, W.; SEN, D.; VISHVESHWARA, S. Topological phases, majorana modes and quench dynamics in a spin ladder system. *New Journal of Physics*, v. 13, n. 6, p. 065028, jun 2011. Disponível em: <https://dx.doi.org/10.1088/1367-2630/13/6/065028>.

24 HEGDE, S. et al. Quench dynamics and parity blocking in majorana wires. *New Journal of Physics*, IOP Publishing, v. 17, n. 5, p. 053036, may 2015. Disponível em: <https://dx.doi.org/10.1088/1367-2630/17/5/053036>.

25 HEGDE, S. S.; VISHVESHWARA, S. Majorana wave-function oscillations, fermion parity switches, and disorder in kitaev chains. *Physical Review B*, American Physical Society (APS), v. 94, n. 11, sep 2016. Disponível em: <https://doi.org/10.1103%2Fphysrevb.94.115166>.

26 VAL'KOV, V.; MITSKAN, V.; SHUSTIN, M. Ground-state fermion parity and caloric properties of a superconducting nanowire. *Journal of Experimental and Theoretical Physics*, Springer, v. 129, p. 426–437, 2019.

27 GRABSCH, A.; CHEIPESH, Y.; BEENAKKER, C. W. J. Pfaffian formula for fermion parity fluctuations in a superconductor and application to majorana fusion detection. *Annalen der Physik*, Wiley, v. 531, n. 10, p. 1900129, jun 2019. Disponível em: <https://doi.org/10.1002\%2Fandp.201900129>.

28 ALECCE, A.; DELL'ANNA, L. Extended Kitaev chain with longer-range hopping and pairing. *Physical Review B*, American Physical Society (APS), v. 95, n. 19, may 2017. Disponível em: <https://doi.org/10.1103\%2Fphysrevb.95.195160>.

29 MAITY, S.; BHATTACHARYA, U.; DUTTA, A. One-dimensional quantum many body systems with long-range interactions. *Journal of Physics A: Mathematical and Theoretical*, IOP Publishing, v. 53, n. 1, p. 013001, 2019.

30 VIYUELA, O. et al. Topological massive Dirac edge modes and long-range superconducting hamiltonians. *Physical Review B*, American Physical Society (APS), v. 94, n. 12, sep 2016. Disponível em: <https://doi.org/10.11032Fphysrevb.94.125121>.

31 JÄGER, S. B.; DELL'ANNA, L.; MORIGI, G. Edge states of the long-range Kitaev chain: An analytical study. *Physical Review B*, American Physical Society (APS), v. 102, n. 3, jul 2020. Disponível em: <https://doi.org/10.1103\%2Fphysrevb.102.035152>.

32 VODOLA, D. et al. Kitaev Chains with Long-Range Pairing. *Physical Review Letters*, American Physical Society (APS), v. 113, n. 15, oct 2014. Disponível em: <https://doi.org/10.1103\%2Fphysrevlett.113.156402>.

33 CATS, P. et al. Staircase to higher-order topological phase transitions. *Physical Review B*, American Physical Society (APS), v. 97, n. 12, mar 2018. Disponível em: <https://doi.org/10.1103%2Fphysrevb.97.121106>.

34 BERRY, M. V. Quantal phase factors accompanying adiabatic changes. *Proceedings of the Royal Society of London. A. Mathematical and Physical Sciences*, The Royal Society London, v. 392, n. 1802, p. 45–57, 1984.

35 BERNEVIG, B.; HUGHES, T. *Topological Insulators and Topological Superconductors*. Princeton University Press, 2013. ISBN 9780691151755. Disponível em: <https://books.google.com.br/books?id=wOn7JHSSxrsC>.

36 CAYSSOL, J.; FUCHS, J.-N. Topological and geometrical aspects of band theory. *Journal of Physics: Materials*, IOP Publishing, 2021.

37 XIAO, D.; CHANG, M.-C.; NIU, Q. Berry phase effects on electronic properties. *Reviews of Modern Physics*, APS, v. 82, n. 3, p. 1959, 2010.

38 SPALDIN, N. A. A beginner's guide to the modern theory of polarization. *Journal of Solid State Chemistry*, Elsevier, v. 195, p. 2–10, 2012.

39 SU, W. P.; SCHRIEFFER, J. R.; HEEGER, A. J. Solitons in polyacetylene. *Phys. Rev. Lett.*, American Physical Society, v. 42, p. 1698–1701, Jun 1979. Disponível em: <https://link.aps.org/doi/10.1103/PhysRevLett.42.1698>.

40 SU, W. P.; SCHRIEFFER, J. R.; HEEGER, A. J. Soliton excitations in polyacetylene. *Phys. Rev. B*, American Physical Society, v. 22, p. 2099–2111, Aug 1980. Disponível em: <https://link.aps.org/doi/10.1103/PhysRevB.22.2099>.

41 HEEGER, A. J. et al. (SSH) solitons in conducting polymers. *Reviews of Modern Physics*, APS, v. 60, n. 3, p. 781, 1988.

42 RYU, S. et al. Topological insulators and superconductors: tenfold way and dimensional hierarchy. *New Journal of Physics*, IOP Publishing, v. 12, n. 6, p. 065010, jun 2010. Disponível em: <https://doi.org/10.1088\%2F1367-2630\%2F12\%2F6\%2F065010>.

43 KITAEV, A. Periodic table for topological insulators and superconductors. In: AMERICAN INSTITUTE OF PHYSICS. *AIP conference proceedings*. [S.l.], 2009. v. 1134, n. 1, p. 22–30.

44 VELASCO, C. G.; PAREDES, B. Realizing and detecting a topological insulator in the AIII symmetry class. *Physical Review Letters*, American Physical Society (APS), v. 119, n. 11, sep 2017. Disponível em: <https://doi.org/10.1103%2Fphysrevlett.119.115301>.

45 MATVEEVA, P. et al. One-dimensional noninteracting topological insulators with chiral symmetry. *Physical Review B*, American Physical Society (APS), v. 107, n. 7, feb 2023. Disponível em: <https://doi.org/10.1103%2Fphysrevb.107.075422>.

46 RICE, M.; MELE, E. Elementary excitations of a linearly conjugated diatomic polymer. *Physical Review Letters*, APS, v. 49, n. 19, p. 1455, 1982.

47 SHEN, S. *Topological Insulators: Dirac Equation in Condensed Matters*. Springer Berlin Heidelberg, 2013. (Springer Series in Solid-State Sciences). ISBN 9783642328589. Disponível em: <https://books.google.com.br/books?id=ER9EAAAAQBAJ>.

48 FU, L. Topological crystalline insulators. *Physical Review Letters*, American Physical Society (APS), v. 106, n. 10, mar 2011. Disponível em: <https://doi.org/10.1103%2Fphysrevlett.106.106802>.

49 VOLOVIK, G. On edge states in superconductors with time inversion symmetry breaking. *Journal of Experimental and Theoretical Physics Letters*, Springer, v. 66, p. 522–527, 1997.

50 FISCHER, M. H. et al. Superconductivity and local inversion-symmetry breaking. *Annual Review of Condensed Matter Physics*, v. 14, n. 1, p. 153–172, 2023. Disponível em: <https://doi.org/10.1146/annurev-conmatphys-040521-042511>.

51 FRANCHINI, F. *An Introduction to Integrable Techniques for One-Dimensional Quantum Systems*. Springer International Publishing, 2017. Disponível em: <https://doi.org/10.1007\%2F978-3-319-48487-7>.

52 FRADKIN, E. *Quantum Field Theory: An Integrated Approach*. Princeton University Press, 2021. ISBN 9780691189550. Disponível em: <https://books.google.com.br/books?id=quEIEAAAQBAJ>.

53 FEDOSEEV, A. Size effects on the conditions of edge state formation in 1d systems. *Journal of Experimental and Theoretical Physics*, Springer, v. 128, p. 125–132, 2019.

54 ALTLAND, A.; SIMONS, B. D. *Condensed matter field theory*. [S.l.]: Cambridge University Press, 2010.

55 DEFENU, N. et al. *Long-range interacting quantum systems*. arXiv, 2021. Disponível em: <https://arxiv.org/abs/2109.01063>.

56 LIU, D.-P. Topological phase boundary in a generalized kitaev model*. *Chinese Physics B*, IOP Publishing, v. 25, n. 5, p. 057101, mar 2016. Disponível em: <https://dx.doi.org/10.1088/1674-1056/25/5/057101>.